Ville Telatie

Microgrid control optimization

Optimum frequency control strategy for a different generation- and load scenarios

School of Technology and Innovations
Master's thesis in Discipline
Smart Energy

Vaasa 2022

UNIVERSITY OF VAASA
School of innovation and technology
Author: Ville Telatie
Title of the Thesis: Microgrid control optimization : Optimum frequency control strategy for a different generation- and load scenarios
Degree: Master of Science in Technology
Programme: Smart Energy
Supervisors: Hannu Laaksonen & ATM Mustafizur Rahman
Year: 2022 **Pages:** 103

ABSTRACT:
Global warming forces the energy sector to move away from fossil fuels and towards renewable energy sources. The increasing number of inverter-based renewable energy resources decreases the amount of inertia coupled into power systems, affecting the power systems' ability to withstand the frequency deviations. This change has a more significant effect on microgrids than utility grids due to the already lower inertia connected to the power system. This thesis studies the change due to the decreasing inertia to help to optimize the frequency control for an islanded microgrid with high IBG penetration. It is done by studying the frequency behavior in three different microgrids. These microgrids differ from each other based on the share of synchronous and inverter-based generation. A simulation software called PSCAD is utilized to create the models and simulate different scenarios. The models are developed based on the IEEE 14 bus system, which is, in this case, considered a general microgrid. On the generation side, three generation patterns are considered. These patterns vary from each other based on the share of synchronous generation and inverter-based generation. All the simulation cases have a battery storage system implemented into the microgrid. The frequency behavior is observed by creating four different events. These events are recreated in four different conditions, including the ideal condition. Based on the results gained in this study, the inverter-based generation units can support the microgrid frequency almost at the same level as a synchronous generator. However, it is highly unpredictable and does require alternative generation units as a backup in case of absent renewable energy. This study is also used to create a modular tool for the Wärtsilä to utilize to analyze the frequency behavior in possible future and existing microgrids. However, this study shows that this model combined with the PSCAD is not suitable for business use due to the unnecessarily long simulation times.

KEYWORDS: Islanded microgrid, Frequency control, IEEE 14 bus system, Inertia

VAASAN YLIOPISTO
Tekniikan ja innovaatiojohtamisen yksikkö
Tekijä: Ville Telatie
Tutkielman nimi: Microgrid control optimization : Optimum frequency control strategy for a different generation- and load scenarios
Tutkinto: Diplomi-insinööri
Oppiaine: Smart Energy
Työn ohjaajat: Hannu Laaksonen & ATM Mustafizur Rahman
Valmistumisvuosi: 2022 **Sivumäärä:** 103

TIIVISTELMÄ:
Ilmaston lämpeneminen pakottaa energiasektorin siirtymään pois fossiilisista polttoaineista kohti uusiutuvia energialähteitä. Invertteripohjaisten uusiutuvien energiavarojen lisääntyminen vähentää sähköverkkoisin kytkeytyvän inertian määrää, mikä vaikuttaa niiden kykyyn sietää muutoksia taajuudessa. Tällä muutoksella on merkittävämpi vaikutus mikroverkkoihin kuin perinteisiin sähköverkkoihin jo ennestään pienemmän inertian vuoksi. Tässä diplomityössä tutkitaan inertian pienenemisestä johtuvaa muutosta, joka auttaa optimoimaan taajuuden säädön saarekekäytössä oleville mikroverkoille, jossa on korkea IBG-penetraatio. Se tehdään tutkimalla taajuuskäyttäytymistä kolmessa eri mikroverkossa. Nämä mikroverkot eroavat toisistaan tahtigeneraattoripohjaisen ja invertteripohjaisen tuotannon osuuden perusteella. Mallien luomiseen ja eri skenaarioiden simulointiin käytetään PSCAD-nimistä simulointiohjelmistoa. Mallit on kehitetty perustuen IEEE 14 -solmupisteenjärjestelmään, jota tässä tapauksessa pidetään yleisenä mikroverkkona. Tuotannon puolella tarkastellaan kolmea eriä tuotanto rakennetta. Nämä mallit eroavata toisistaan tahtigeneraattoripohjaisen tuotannon ja invertteripohjaisen tuotannon osuuden mukaan. Kaikissa simulaatiotapauksissa mikroverkkoon on liitettynä akkukäyttöinen energiavarasto. Taajuuskäyttäytymistä tarkkaillaan luomalla neljä erilaista tapahtumaa mikroverkkoon. Nämä tapahtumat luodaan uudelleen neljässä eri olosuhteissa, mukaan lukien ihanteellinen tilanne. Tässä diplomityössä saatujen tulosten perusteella invertteripohjaiset tuotantoyksiköt voivat tukea mikroverkon taajuutta lähes samalla tasolla kuin tahtigeneraattorit. Ne ovat kuitenkin erittäin arvaamattomia ja vaativat lisäksi vaihtoehtoisia tuotantoyksiköitä, jos uusiutuvaa energiaa ei ole saatavilla. Tämän diplomityön avulla luodaan myös Wärtsilälle modulaarinen työkalu, jonka avulla voidaan analysoida taajuuskäyttäytymistä mahdollisissa tulevissa ja olemassa olevissa mikroverkoissa. Tämä tutkimus kuitenkin osoittaa, että tämä PSCAD malli ei sovellu yrityskäyttöön tarpeettoman pitkien simulointiaikojen vuoksi.

AVAINSANAT: Islanded microgrid, Frequency control, IEEE 14 bus system, Inertia

Contents

Figures

Tables

Abbreviations

AC	Alternative Current
BESS	Battery Energy Storage System
DC	Direct Current
EPP	Engine Power Plant
EMT	Electromagnetic Transient
FESS	Flywheel Energy Storage System
FFR	Fast Frequency Response
GD	Generator Disconnected
IBG	Inverter-Based Generation
ID	Inverter Disconnected
LD	Load Disconnected
MFC	Master Frequency Control
MG	Microgrid
MPP	Maximum Power Point
MPPT	Maximum Power Point Tracking
ND	Network-Link Disconnected
OLTC	On-Load-Tap-Changer
PCC	Point of Common Coupling
PLL	Phase-Locked Loop
PV	Photovoltaic
PVPP	Photovoltaic Power Plant
PWM	Pulse Width Modulation
RES	Renewable Energy Sources
SOC	State of Charge
UFLS	Under-Frequency Load Shedding
VSC	Voltage Source Converter
VSI	Voltage Source Inverter
WT	Wind Turbine
WTPP	Wind Power Plant

List of symbols

E_{kin}	Kinetic Energy
P'_0	Rotated Component of Nominal Active Power
P_0	Nominal Active Power
P_m	Mechanical Power
Q'_0	Rotated Component of Nominal Reactive Power
Q_0	Nominal Reactive Power
S_r	Rated Apparent Power
T_a	Accelerating Torque
T_e	Electrical Torque
T_m	Mechanical Torque
V_0	Nominal Voltage
f_0	Nominal Frequency
k_{PV}	Voltage Sensitivity of Active Power Demand
k_{Pf}	Frequency Sensitivity of Active Power Demand
k_{QV}	Voltage Sensitivity of Reactive Power Demand
k_{Qf}	Frequency Sensitivity of Reactive Power Demand
k_p	Droop %
ω_r	Rotation Speed
ω_{r0}	Rated Rotation Speed
ΔP	Change in Active Power
ΔQ	Change in Reactive Power
ΔV	Change in Voltage
Δf	Change in Frequency
H	Inertia Constant
J	Moment Of Inertia
P'	Rotated Component of Active Power
Q'	Rotated Component of Reactive Power
R	Resistance
X	Reactance

Z	Impedance

1 Introduction

This chapter gives an overview of the thesis topic, discussing the research methods chosen for the study and outlining the structure. Also, an introduction to the basics of microgrid stability issues is discussed, giving the background for the thesis's importance.

Global warming forces the energy industry to move away from traditional fossil fuels and towards the renewable energy sources. Most renewable energy sources like, solar- and wind energy are connected to a grid using power converters. The electricity generated with solar energy (also known as photovoltaic energy) is in the form of direct current (DC). Since most transmission and distribution networks use alternative current (AC), the DC-power needs to be converted into AC-power using DC/AC-converters. In case of wind-energy, the wind speed can vary and for this reason the frequency of the generated energy also varies. To match the operating frequency of the electric system, which is normally 50 Hz or 60 Hz, an AC/AC- converter is needed.

For the electric system to be stable, generated power and consumed power always need to be in balance. In case of increased load in the electric system the frequency of the system will decrease and vice versa. Same principle applies to the amount of generated power. Since both, active power and frequency are tied together the term "Load-Frequency Control (LFC)" is used (Kundur, 1994, p. 582). To detect these changes in electric system, different metering devices are needed. The data gathered from the monitoring devices can be utilized to create control functions. These functions can then be implemented to the control systems to maintain the stable system frequency, by controlling the energy generation and load. Because of the different nature of synchronous generation and inverter-based generation, they need different kind of control systems. Due to the low inertia of renewable energy and the high unpredictable compared to the fossil fuels, the need for frequency control increases significantly. Other main stability issues in power systems are in voltage and angle stability, but this thesis only focuses on frequency stability (Kundur, 1994).

Microgrids are created to improve reliability, efficiency, and flexibility and help integrate distributed generation. A microgrid can be defined as a self-sufficient energy system on a specified geological location (Wood, 2020). An islanded microgrid is a microgrid that is not connected to a larger electric grid and has its own energy production and consumption. Permanently islanded microgrids are typically created because of their remote geographical location. Islanded microgrids suffer more from stability issues than grid-connected microgrids caused by a lack of support from the main grid and the absence of inertia created by large rotating masses. Lack of inertia causes more significant and faster variations in the grid frequency when the amount of generated power or load changes.

1.1 Thesis Motivation

The implementation of the inverter-based generation is decreasing the amount physical inertia in microgrid. This is expected to increase the frequency deviations in the microgrid during different events. This thesis studies this change in the frequency behavior and how to respond these changes with alternative control methods.

In addition to this the thesis aims to create a modular tool, which could be used to analyze, existing and future, microgrids for control concept design. Also, the suitability of the PSCAD as simulation tool for this kind of study is tested while doing the simulations for the thesis. This study is done for Wärtsilä Finland Oy.

1.2 Research methods

The study is started by studying the basics of the microgrid structure, in the form of a literature review, to develop a deeper understanding of the different characteristics of the microgrids. The same approach is also used to study the theory of frequency control. The main focus is on the different control strategies and their characteristics in frequency control.

IEEE 14 bus system is used as general presentation of a power system. It is commonly used for research purposes, and it can be configured to include different generations, loads, capacitor banks and transmission lines (PSCAD, 2018). Using the IEEE 14 bus system, a general AC microgrid is developed for each case study. The case studies differ from each other based on the share of synchronous generation and inverter-based generation in the microgrid–starting from a higher share of synchronous to a more significant share of inverter-based. For the first scenario, the configuration with only synchronous generation is chosen to set the baseline for the study. The second one consists of 60% synchronous generation and 40% inverter-based generation. In the third case, there is a higher share of 60% of inverter-based generation and only 40% of synchronous generation. In the third case, we can see how the microgrid behavior and need for frequency control changes when inverter-based generation is a more dominant form of power generation. As an inverter-based generation, wind and photovoltaic energy are considered. Also, the grid behavior is observed and analyzed when the following events and conditions are introduced to the microgrid:

- Events
    - Largest synchronous generation trip
    - Largest inverter-based generation trip
    - Largest load trip
    - Network link trip
- Conditions
    - Energy storage exhausted
    - Solar minimum/maximum
    - Wind Minimum/Maximum

These microgrid models are then developed in simulation software. The simulation software chosen for this study is PSCAD software. PSCAD is a simulation tool that can be used for accurate power system simulation (PSCAD, n.d.-a). When simulations are done to decide the best control strategy, it can also be seen how the microgrid frequency behavior and the nature of the control strategy changes when more inverter-based

generation is implemented to the system. Simulation results are imported into MATLAB for better analysis.

1.3 Thesis outline and structure

The thesis is structured in the following way. Chapter 2 discusses the stability problems caused by the low inertia in the microgrids. Chapter 3 gives theoretical look into microgrids and generation types. After that, in chapter 4, the different frequency control methods and strategies are discussed theoretically to create an understanding on the operation principles. The simulation models are developed in Chapter 5 for a different case studies using the PSCAD simulation software. In Chapter 6, the limits of the desired frequency stability are defined. After that the simulations results are analyzed. Finally, chapter 7 concludes the thesis, discussing the results and if the desired outcome was achieved. Also the possible future studies are discussed.

2 Frequency stability problems caused by low inertial microgrids

This chapter gives an understanding about the inertia as a phenomenon and discusses the challenges which the power systems, especially microgrids, are facing because of the inverter-based generation.

In a traditional power system there are rotating masses in the synchronous generators and the in the prime movers (Kundur, 1994), like diesel engines or gas turbines, which are used to rotate the generator rotor. To keep the certain frequency the synchronous generator always run at a constant speed, but in case of increased load in the system, the generators' rotational speed will decrease when it is trying to supply more power to the system. This is because it releases the power from the kinetic energy of its rotating masses. The same phenomenon also works in the opposite way. When the load in the power system decreases, the generator's rotational speed starts to increase. In this case, the generator stores the surplus energy from the system to its rotating masses in the form of kinetic energy. This phenomenon is called **inertia**. Usually, inertia is expressed in the form of inertia constant H.

$$H = \frac{E_{kin}}{S_r} = \frac{1}{2}\frac{J\omega_r^2}{S_r} \quad (1)$$

Where E_{kin} is kinetic energy, S_r apparent rated power, J moment of inertia, and ω_r rated rotational speed of the machine. This equation expresses the time interval in which the generator can supply its rated power by using kinetic energy (Fernández-Guillamón et al., 2020).

Change in load will cause instant change also in electrical torque. According to the equation of motion, it will cause accelerating torque T_a in the system (Kundur, 1994).

$$T_a = T_m - T_e \quad (2)$$

$$T_a = J\frac{d\omega_r}{dt} \tag{3}$$

Where ω_r is the rotor speed. By expressing the moment of inertia in terms of inertial constant, it is possible to rewrite the equation of motion in the following form (Kundur, 1994):

$$\frac{2H}{\omega_{r0}^2} S_r \frac{d\omega_r}{dt} = T_m - T_e \tag{4}$$

With some mathematical manipulation and considering $T_r = S_e/\omega_r$, the equation can be expressed by swing equation in per-unit form (Kundur, 1994):

$$2H\frac{d}{dt}\left(\frac{\omega_r}{\omega_{r0}}\right) = T_m - T_e \tag{5}$$

In an electric system the rapid changes in system frequency are effectively resisted by the inertia of connected rotating masses (Dudurych, 2021). In case of some disturbance in the microgrid the system with lower inertia will suffer from larger frequency deviation than a microgrid with high inertia.

3 Microgrids

This chapter will go through the structure and definition of a microgrid. Also, the characteristics of synchronous generation, inverter-based generation, energy storage systems, and different types of loads are studied and their impact on microgrid behavior.
Wood (2020) defines a microgrid well in her article, "A microgrid is a self-sufficient energy system that serves a discrete geographic footprint." By "self-sufficient," it is meant that the microgrid is capable of generating the amount of power to cover the demand in the microgrid area.

There are two types of microgrids (Hatziargyriou, 2014): grid-connected microgrid (**Figure 1**) and islanded microgrid (**Figure 2**). Islanded microgrids are typically used in geographically remote locations like remote islands, mines, or even space stations. In this case, the word "islanded" means that it is not connected to the national grid in any way. On the other hand, grid-connected, as the name implies, is connected to the grid. Nevertheless, as the definition of microgrid states, it can still generate the amount of power to feed all the loads (or at least critical loads) in the microgrid area. In case of disturbances in the grid, the grid-connected microgrid can be disconnected and operate in islanded mode. This increases the reliability of the power delivery, which is one of the main advantages of microgrids.

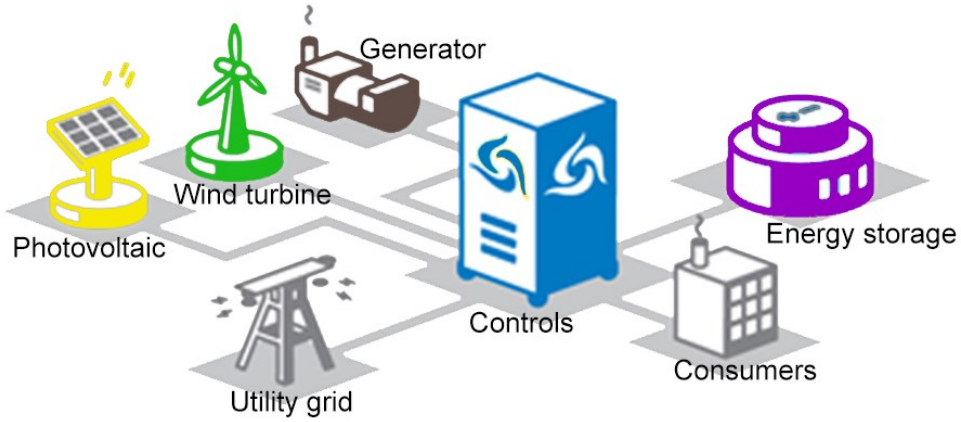

Figure 1. Grid-connected microgrid (Jenkins et al., 2020).

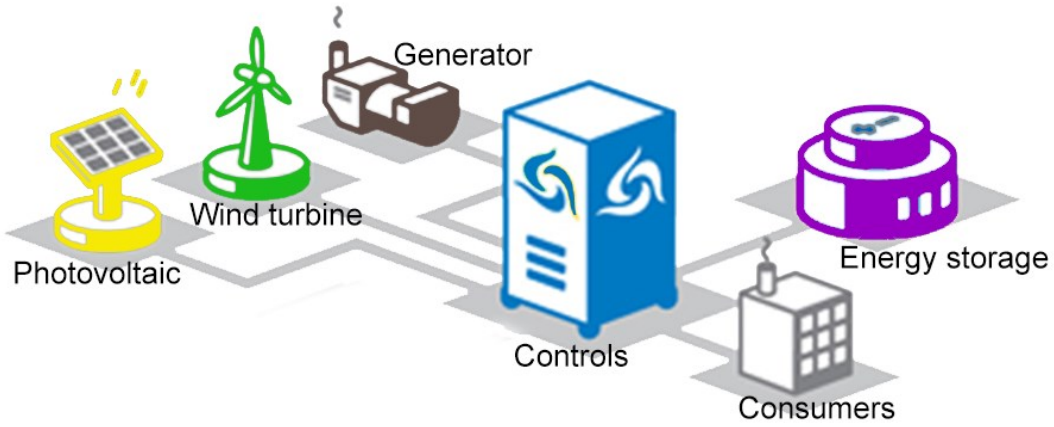

Figure 2. Islanded microgrid (Jenkins et al., 2020).

Structure-wise, a microgrid is similar to a standard electric grid but on a smaller scale. Power to the microgrid is generated with traditional synchronous generation and increasing numbers with the inverter-based distributed generation with renewable energy sources (RES). Different storage systems (batteries, flywheels, etc.) are also implemented to improve reliability and manage the loads and power generation.

Microgrids can use AC voltage, DC voltage, or a combination of both, but this thesis only focuses on AC microgrids. Microgrids usually operate on the medium or low voltage level (Abu-Rub et al., 2014). Typically, a high voltage level in an electric grid is used to minimize the transmission losses in the lines. Because of discrete geographical location, long transmission lines are not needed. However, losses are acceptable on medium or low voltage levels on a shorter distance. Load in MG typically consists of industrial-, commercial- and residential consumers.

3.1 Operation and Control of Microgrids

This chapter provides an understanding of microgrid operations and requirements of microgrid controllers based on the IEEE standard – IEEE Std 2030.7 (IEEE, 2017). This standard is created to ensure the interoperability of the different controllers and components.

For this reason, it is in this thesis considered as a base point for a microgrid control system. The standard also covers the requirement for grid-connected microgrid operations, but those are left out of this research.

As the standard states, "a key element of microgrid operation is the microgrid energy management system (MEMS)" (IEEE, 2017, p.10). MEMS handles the control functions, making it possible for the microgrid to operate autonomously in an islanded- or grid-connected mode and is responsible for connecting and disconnecting the microgrid from the main grid for power exchange and ancillary services. MEMS also ensures reliable and efficient operation by maintaining the short- and long-term power balance. Another main aspect of MEMS is to ensure economical operation by minimizing the daily operation costs by controlling the generation based on forecasted weather and load and electricity and fuel prices (Zahraoui et al., 2021).

Depending on the microgrid structure and location, the microgrid controls can be implemented in two ways: centralized and decentralized configuration. In a centralized control system, all the units are controlled by one microgrid control system, while in a decentralized model, the control functions are implemented into distributed microgrid components.

In the case of a permanently islanded microgrid, the microgrid control system's core function is dispatching MG's devices in specific operation mode and with specified set-points. In the standard, dispatch functions for the island operation mode have been defined in the following way:

- DER asset control/command, either individually or in a coordinated manner.
- Load management, curtailable loads.
- Dispatch control, either in the form of a look-up table or an optimization function (if applicable).

- Operation of breaker, switches, and other switching and control devices, as applicable.
- Voltage regulation, using appropriate methods, including capacitor switching, transformer tap changers, and the reactive power produced by inverter-based interfaces.
- Frequency control using a reference microgrid generator or storage resource.
- Maintaining power quality levels, ensuring continuous monitoring of power quality levels, and taking appropriate remedial actions.

The other main responsibility of the MG control system is to monitor the MG and notify the control system in case changes are required.

3.2 Synchronous Generation

Energy production using traditional rotating machines is called synchronous generation. Generators consist of two main parts – a rotor and a stator. The rotor is mechanically connected to the prime mover, for example, a diesel engine or gas turbine. When the prime mover is rotated, the rotor creates a rotating magnetic field with the excited rotor windings (Kundur, 1994). The rotating magnetic fields induce a voltage into the stators armature windings connected 120 degrees apart from each other. This will result in a 3-phase alternating voltage, whose frequency depends on the mechanical speed of the rotor—this is why the name "synchronous machine" (Kundur, 1994) is used. So, the generator is run at a constant speed to maintain the desired grid frequency of 50 Hz or 60 Hz in stable operation.

Synchronous generators can produce constant power to the grid due to the power generated using motors or steam turbines. For this reason, they are often used to generate the base power to the grid. Even though they can produce constant power, other stability issues can still occur. The synchronous generation's main issues are maintaining synchronism and voltage stability.

3.3 Inverter-Based Generation

The energy generation from renewable energy sources (RES) is called as an inverter-based generation. In this thesis, the main focus in RES will be on photovoltaic and wind energy. The use of RES introduces great variability of challenges into the power system, which need to be addressed utilizing various different operation and control modes.

Most renewable energy sources cannot produce stable AC power, so they need to be connected using a power electronic interface to the AC system. Even though it is possible to implement wind generation using gearing to connect directly, it is not used due to the inefficient power extraction, mechanical stress, and not meeting other current regulations (Abu-Rub et al., 2014). Depending on the energy source and generation method, AC/DC, AC/DC, or DC/AC-converters are used. Different configurations of AC/AC converters are used for more efficient operation. These AC/AC converters are often a combination of AC/DC and DC/AC converters with DC-link between them.

The use of a power electronic interface means that no rotating masses are directly connected to the microgrid, which means a lack of inertia in the system. Even though there are rotating masses in wind energy, they do not directly contribute to microgrid inertia because of the power converters. However, it is possible to artificially create virtual inertia by applying certain control functions to control the inverters (Fernández-Guillamón et al., 2020).

There are three main operation modes for inverters, which can be used to implement renewable energy sources and energy storage systems: grid forming, -feeding, and -supporting modes (Rocabert et al., 2012). The inverter type is chosen based on the use case. Normally the main factor in choosing the inverter type is based the microgrid operation mode; grid-connected or islanded.

In a **grid-following**, also known as grid feeding, mode, the inverter is acting as a current source and is following reference for active P^* and reactive power Q^* set by the high-

level controller (Bouzid et al., 2015; Unruh et al., 2020). The inverter adjusts its current output based on the voltage measurement. In **Figure 3** is a basic control structure for the grid feeding inverter, where can be seen the current control loop and power control loop can be seen, which are used to create the control signal for the PWM (pulse width modulation). Since grid feeding inverters do not actively control their output frequency, they are dependent on a synchronous generator, grid forming- or grid supporting inverter to act as a grid forming source. For this reason, grid feeding inverters are often only used in grid-connected microgrids. When considering higher penetration of grid feedings inverter-based generation, this is a limiting factor considering the grid stability. However, it is possible to support the grid frequency and voltage by adjusting the active and reactive power reference values.

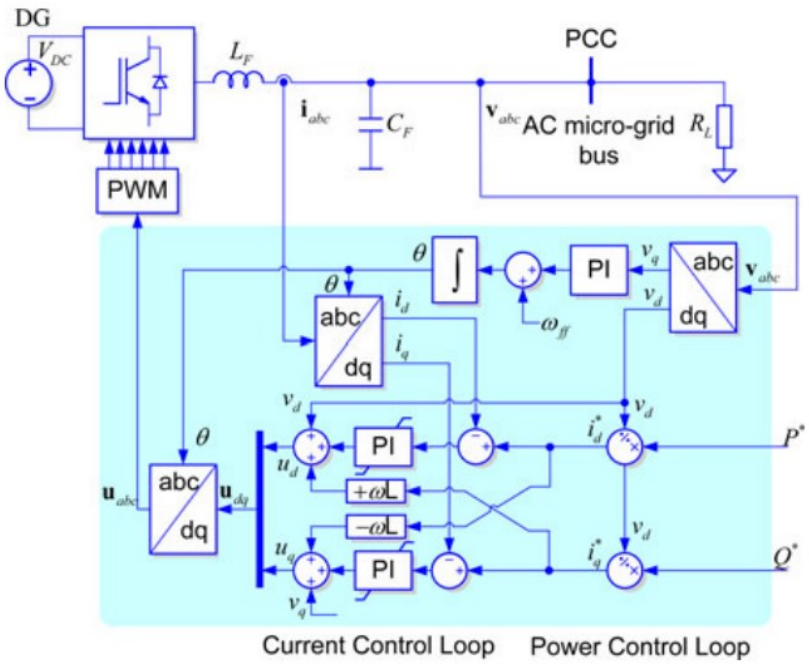

Figure 3. Basic control for grid feeding inverter (Rocabert et al., 2012).

In **grid forming** mode (Bouzid et al., 2015), the inverter acts as an ideal voltage source by actively controlling its frequency and voltage output based on a specific set point. These types of inverters are also referred to as voltage source inverters (VSI), voltage-forming inverters, and grid-voltage-forming inverters. (Rocabert et al., 2012; Unruh et al.,

2020). These inverters can be controlled in many different ways, but many of the control methods are based on the droop control. The inverter control is based on altering the DC-link voltage in the inverter, which can be achieved by controlling the PWM signal which controls the inverter legs. Various control methods are presented in the paper authored by Unruh et al. (2020), about grid-forming inverter control methods. By actively controlling the output frequency and voltage, voltage source inverters can be used to improve the grid stability. Due to its ability to act as an ideal AC voltage source, grid forming inverters do not need other voltage forming sources to be operated in parallel with them and are, for this reason, used in islanded microgrids. In **Figure 4** can be seen a basic control loop of the grid forming inverter. There the reference values for voltage amplitude v^* and frequency $\omega^*$are as an input for the control loop (Rocabert et al., 2012).

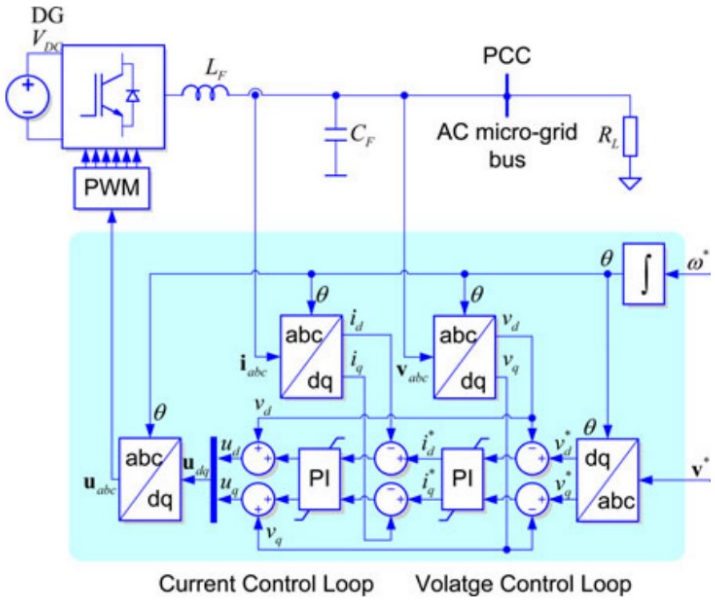

Figure 4. Basic grid-forming inverter control loop (Rocabert et al., 2012).

There are two main ways to control **grid-supporting** inverters: a current source and a voltage source (Bouzid et al., 2015). When an inverter is working as a current source, it regulates the active- and reactive power exchange and in this way keeps also regulates the voltage amplitude and frequency. As seen in **Figure 5**, the main supporting function

are based on the droop control. Like the grid-feeding inverter, the grid-supporting inverter, which is working as a current source, still needs at least one grid forming source to operate (Rocabert et al., 2012).

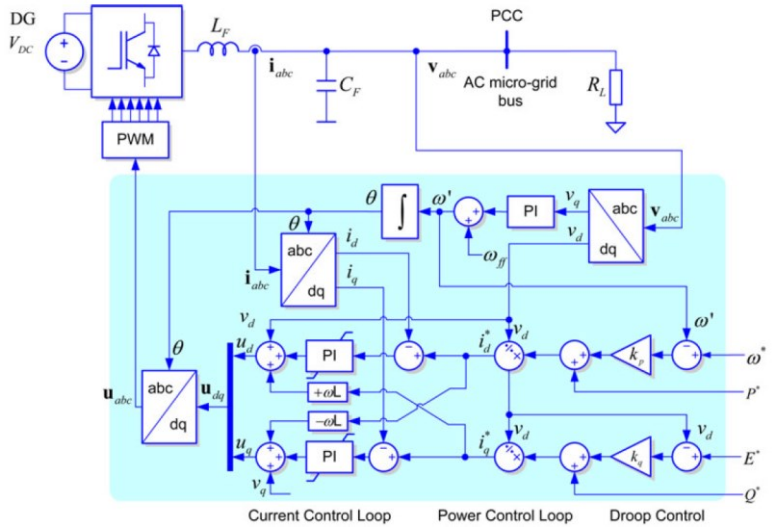

Figure 5. Grid-supporting inverter working as a current source (Rocabert et al., 2012).

On the other hand, a grid-supporting inverter working as a voltage source can act as a grid forming source and is not dependent on other grid-forming sources (Rocabert et al., 2012). Basic control structure is shown in **Figure 6**. Grid-supporting inverter working as a voltage source is controlled to emulate the behavior of synchronous generator (Bouzid et al., 2015). The inverter controls the voltage amplitude and frequency, while also supplies the connected load. In a grid forming inverter the voltage amplitude and frequency are fixed, but in grid-supporting inverter they are results from droop control function and based on the active and reactive power components.

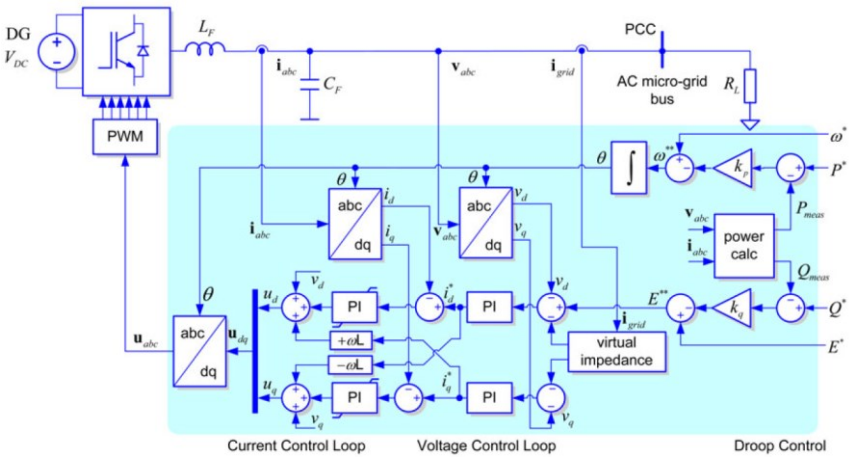

Figure 6. Grid-supporting inverter working as voltage source (Rocabert et al., 2012).

3.4 Energy storage systems

In a microgrid, especially in one with a high share of inverter-based generation, the amount of generated power fluctuates significantly during the day. Most renewable energy sources operate close to their maximum power limit, depending on the weather. For this reason, a power system with a high share of RES does not have a large spinning reserve. A spinning reserve is the available power of the generating units between their actual load and the maximum power rating (Machowski et al., 2008). These changes can be addressed by connecting energy storage systems into the microgrid, which acts as a spinning reserve and is capable of load leveling and peak shifting when acting as a load (Gao, 2015; Nazaripouya et al., 2019).

Energy storage systems can be split into two categories: Long- and short-term storage (Nemsi et al., 2016). The type of storage devices is divided based on the time they can provide energy. Systems categorized into short-term storage systems can provide energy for under 10 minutes, and long-term storage systems can provide energy for over 10 minutes.

Long-term storage can balance the generation fluctuation during the day (Nemsi et al., 2016). Typical long-term storage devices are battery energy storage systems (BESS) and

the use of water's potential energy. During the hours when there is over a generation in the microgrid, the surplus energy can be stored by charging the batteries or by pumping water into higher altitudes to store the energy in the form of potential energy. This energy can then be released into the microgrid during the hours when there is under generation, for example, during the night when photovoltage energy production is absent.

Typical short-term storages are flywheels and supercapacitors, but BESS can also act as short-term storage because of its fast dynamics. Short-term storage is used to react to more minor variations in power generation and load. These fluctuations constantly happen in a power system, and they need to be addressed immediately to maintain power and frequency balance in the system. Therefore, short-term storage devices need to be able to operate quickly. In a system with a high share of synchronous generation, short-term storage systems are not needed as much as in a system with a high share of inverter-based generation. This is because of the high amount of inertia in the system, which can balance out most of the more minor variations. A flywheel energy storage system (FESS) is also based on inertia. When there is overgeneration, a synchronous machine in FESS rotates the flywheel and stores the energy in the form of kinetic energy. In an event when there is under generation in the system, the flywheel starts to rotate the synchronous machine, which then acts as a generator and releases energy back to the microgrid (Nemsi et al., 2016).

3.5 Loads

A Load in a microgrid consists of different industrial, residential, and commercial loads. These loads consist of many different devices, including lamps, heaters, compressors, etc., but typically the highest share of the loads consists of induction motors (Kundur, 1994; Machowski et al., 2008). Depending on the characteristics of the load, the type of power demand can vary between active- and reactive power. They can consist of many different components to whole distribution networks, depending on the scale of the model. Loads can be divided into two main categories: Static loads and dynamic loads (Kundur, 1994). The complexity of the loads requires much simplification when it is

studied or modeled. These simplified load models are referred to as "composite loads" (Machowski et al., 2008, p. 104), and they can consist of a combination of both static and dynamic loads, as seen in **Figure 7**.

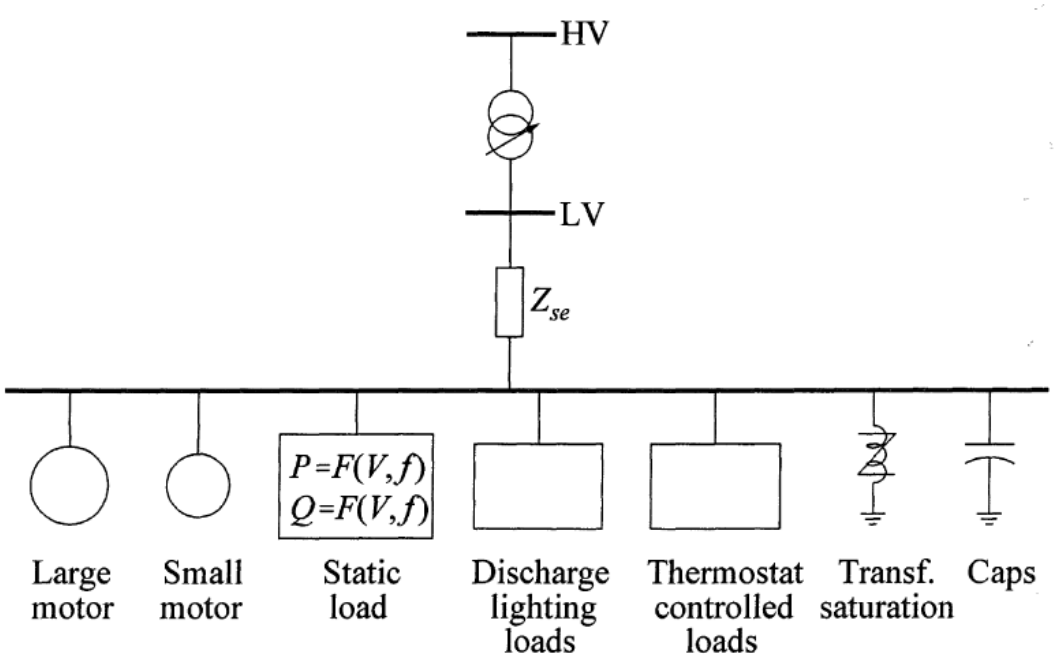

Figure 7. Example of composite load (Kundur, 1994).

Static load models can be used to describe loads where voltage and frequency changes are fast, but the steady-state is reached quickly. Static load models can be modeled using algebraic equations to describe the relationship between active and reactive power to voltage or frequency at any time (Kontis et al., 2017). By using static load characteristics, it is possible to describe the frequency and voltage dependency of active (*P(V, f)*) and reactive (*Q(V, f)*) power demand. Frequency- and voltage sensitivity describe the load's dependency on frequency and voltage. For example, if the frequency sensitivity of the load is high, small changes will cause significant changes in load demand. The following equations express frequency and voltage sensitivities (Machowski et al., 2008).

$$k_{PV} = \frac{\Delta P/P_0}{\Delta V/V_0} \tag{6}$$

$$k_{QV} = \frac{\Delta Q/Q_0}{\Delta V/V_0} \tag{7}$$

$$k_{Pf} = \frac{\Delta P/P_0}{\Delta f/f_0} \tag{8}$$

$$k_{Qf} = \frac{\Delta Q/Q_0}{\Delta f/f_0} \tag{9}$$

Usually, the frequency sensitivity of active power demand is higher than the voltage sensitivity and vice versa in reactive power demand.

As mentioned before, the highest share of loads in a power system consists of induction motors. Because of the dynamic nature of the motors, dynamic load models need to be considered for power system stability studies (Kundur, 1994). In addition to induction motors, other components like discharge lamps, protection relays, thermostatically controlled loads, capacitor banks, and loads connected to MG using on-load-tap-changer (OLTC) transformers need to be considered when modeling dynamic loads. When dynamic load models are modeled, the active and reactive power are presented as a function of time and voltage or frequency (Kontis et al., 2017). Load modeling is only an approximation and is constantly studied because of the constantly changing load due to the time variation, weather changes, and different dropout voltages and frequencies for a wide scale of different components. It is still one of the most challenging aspects of power system modeling.

4 Frequency Control

This chapter will go through the theory of frequency control and stability issues and define the acceptable limits of frequency variations and recovery time. Discussing the different control modes on the generation side. On the load side control, load scheduling and -shedding are considered.

4.1 Frequency Stability

"Stability is a condition of equilibrium between opposing forces" (Kundur, 1994, p. 22). Frequency stability in the power system is crucial for a stable operation. To be able to maintain the nominal frequency value in a power system, the generated active power has to match the load connected to the system. In a case where the frequency variation is too high, it can cause high magnetizing currents in the system and, in the worst case, even cause a system-wide blackout (Kundur, 1994).

However, how define frequency stability? When is the system frequency stable enough? The most important ones are frequency stability, frequency range limit, ROCOF (rate of change of frequency), and frequency response times. Frequency range defines the limits for acceptable over and under frequency in hertz (Hz). This can be divided into different levels, from normal operation frequency to the operating limits in case of some event or disturbance in the power system (Reliability Panel AEMC, 2020). ROCOF, on the other hand, measures how quickly the frequency changes after an imbalance have occurred in a system. It is measured in hertz per second (Hz/s) (Entso-E, 2020). In addition to ROCOF and frequency range, the settling time and recovery time are also important. Settling time defines the system's time to achieve a steady-state after the event. On the other hand, recovery time defines the time allowed to restore the nominal frequency of the system. These limits are defined in the grid code (European Union, 2017). Grid code often changes by the country or the continent, so there is not just one standard way to define it. Stability limits for this study will be defined in Chapter 6.1.

4.2 Hierarchical Control Structure

Power system frequency control is divided into three different levels: Primary- secondary- and tertiary control. The hierarchical control structure is shown in **Figure 8**.

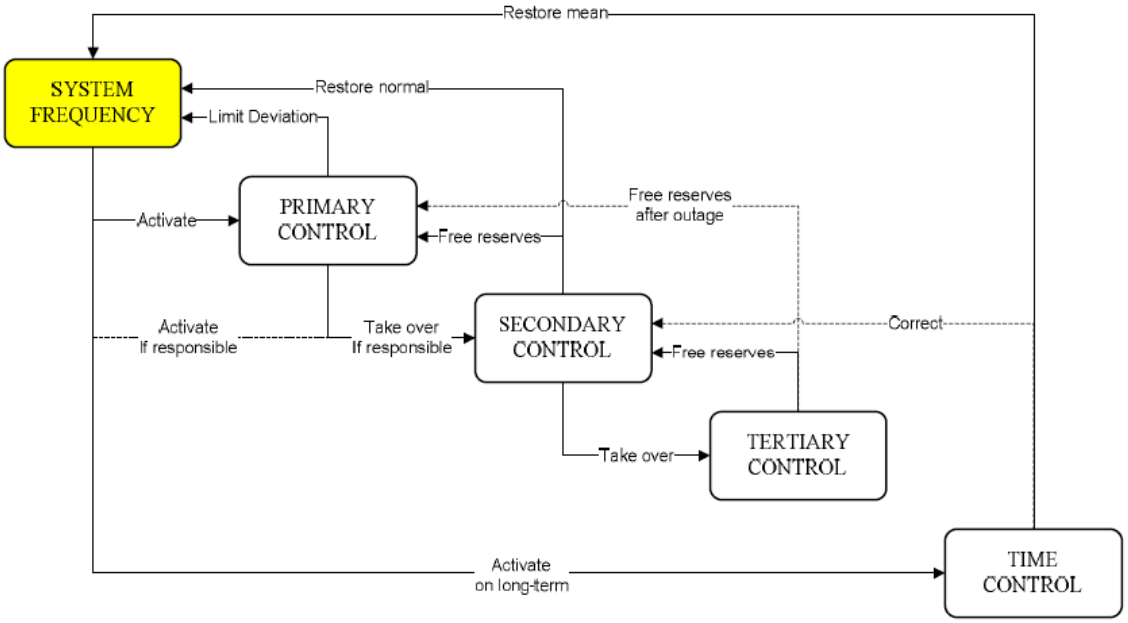

Figure 8. Hierarchical control structure (UCTE, 2014).

Smaller deviations constantly happen in a power system frequency. Primary control is used to limit this deviation and to achieve a steady-state by balancing the power output and load (UCTE, 2014). After the system has achieved the steady-state, the frequency differs from the nominal frequency. Droop control is typically used for primary control. Also, in more significant deviations, load shedding will be used as an emergency method to maintain interconnected operation.

When the system has reached a steady-state at a lower frequency than nominal, it must be increased back to the nominal value. It is handled by secondary control. See This will be done using spinning reserve/secondary control reserve. Secondary control will take action approximately after 15-30 seconds and can operate for several minutes (UCTE, 2014).

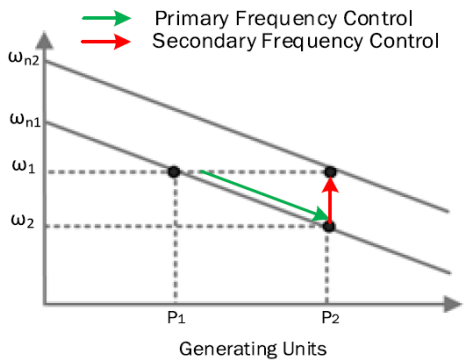

Figure 9. Example of primary and secondary control (Mohammadi et al., 2018)**.**

Secondary control is also used to ensure that the entire primary control reserve is available. See example of primary and secondary frequency control in **Figure 9**. Tertiary control is used to replace the reserve margin used in secondary control (UCTE, 2014). It is also responsible for importing and exporting power between the main grid and the microgrid in a grid-connected microgrid

4.3 Master-slave and Multi-Master Controls

In **master-slave control**, the control parameters are set by the supervisory control, and only a simple control algorithm is required on the component level. The system needs a good communication system to operate and distribute the control parameters from the supervisory control (master) to the generation units (slaves) (Hatziargyriou, 2014).
Master-slave control is challenging to adapt to microgrids because of the high communication requirements, extra cabling, and complex system expansion (Hatziargyriou, 2014).

In **multi-master control**, the generation units control their power output themselves, and supervisory control only sets the basic parameters, for example, nominal frequency, voltage, and droop control slopes. By using this method is possible to avoid excessive use of cabling for communication. The multi-master method also increases the possibility of system expansion later because of the simple supervisory control structure (Hatziargyriou, 2014).

4.4 Frequency control in traditional power systems with synchronous generation

The system frequency is typically controlled by generation side control on a normal operation state. This means the control of active power generated is adjusted to match the load to maintain the power balance.

4.4.1 Droop control

On traditional synchronous generation, small variations in the frequency can be adjusted by increasing or decreasing power input for the generator, which can be done by increasing the fuel flow or opening the steam valve. The generator's governor system senses these speed changes and controls the power output accordingly. This control method is called droop control (Kundur, 1994). It is the most traditional control method used for frequency and active power control with synchronous power generation.

The linear relationship between rotor speed and power output can be expressed with the following equation:

$$f - f_0 = -k_p(P - P_0) \tag{10}$$

Where f_0 is nominal frequency, f is frequency, P_0 is nominal power, P is power, and k_p is the droop %. This means that if a droop is, for example 3%, a 3% change in speed will cause a 100% change in power output. In **Figure 10** can be seen an illustration of a speed-droop slope. The droop % k_p, can be calculated by comparing the change in speed between no load (ω_{NL}) and full load (ω_{NL}) situations to nominal speed (ω_0).

$$k_p(\%) = \left(\frac{\omega_{NL} - \omega_{FL}}{\omega_0}\right) \times 100 \tag{11}$$

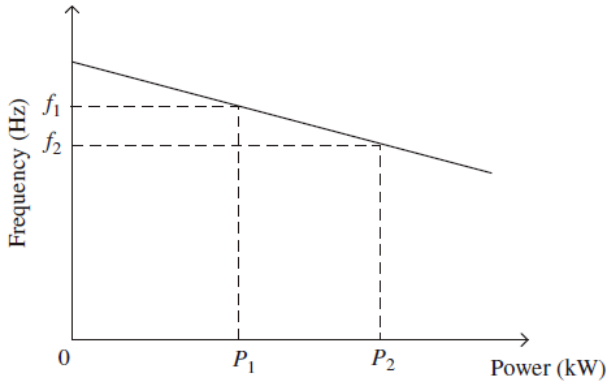

Figure 10. Speed-droop characteristics (Gao, 2015)**.**

From the **Figure 11** can be seen that after droop control response the system's frequency will achieve a steady state with a frequency which is lower than the nominal frequency.

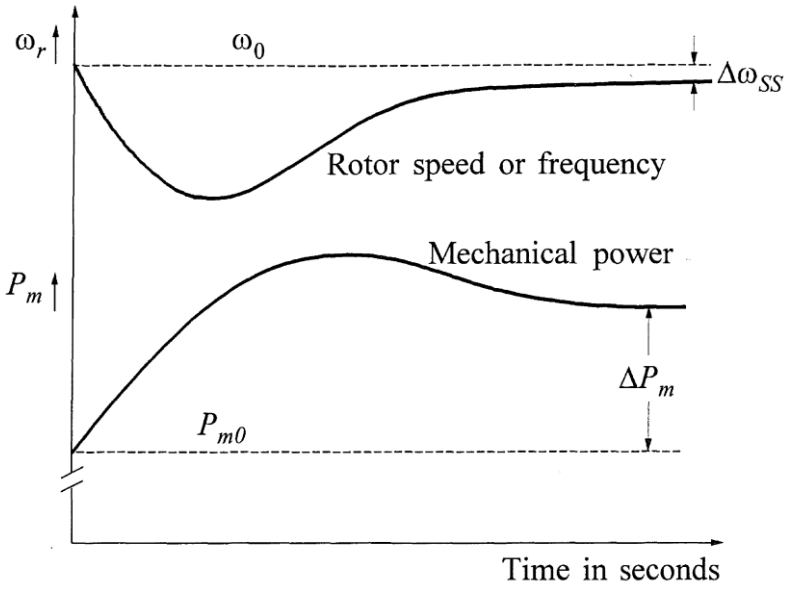

Figure 11. Generating units with speed-droop characteristics respond to system load increase (Kundur, 1994).

For the droop control to operate, the spinning reserve is needed. In case the generating unit is operating at its upper limit, it is not capable of increasing its power output to compensate for the frequency drop (Machowski et al., 2008). This can be seen in **Figure 12**.

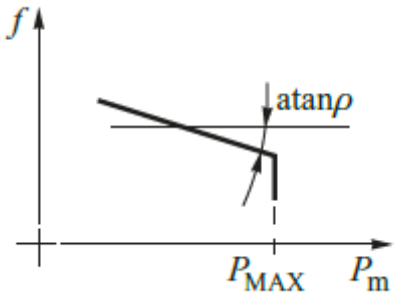

Figure 12. Speed-droop control with generating unit operating at its upper limit (Machowski et al., 2008).

Some of the generating units operate at their upper limit in a real system, and some are only party loaded to operate as a spinning reserve.

4.4.2 Isochronous control

Isochronous governor works by adjusting the prime mover's power output based on the frequency setpoint. The working principle is quite similar to droop control, but droop control works based on the change in frequency and isochronous based on the setpoint. System frequency is measured and then compared to the reference frequency value. Then gain is added to the error signal, which is then integrated to get the control signal (Ravikumar et al., 2017). An illustration of the isochronous control system can be seen in **Figure 13** below.

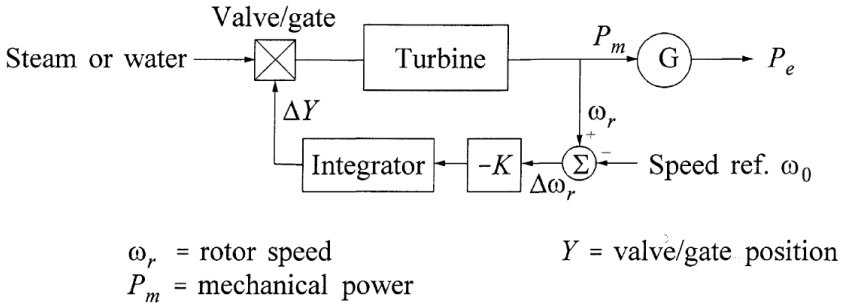

Figure 13. Isochronous governor block diagram (Kundur, 1994)**.**

Because the isochronous control system operates based on the frequency setpoint, the frequency will return to the reference value after disturbance seen in **Figure 14**.

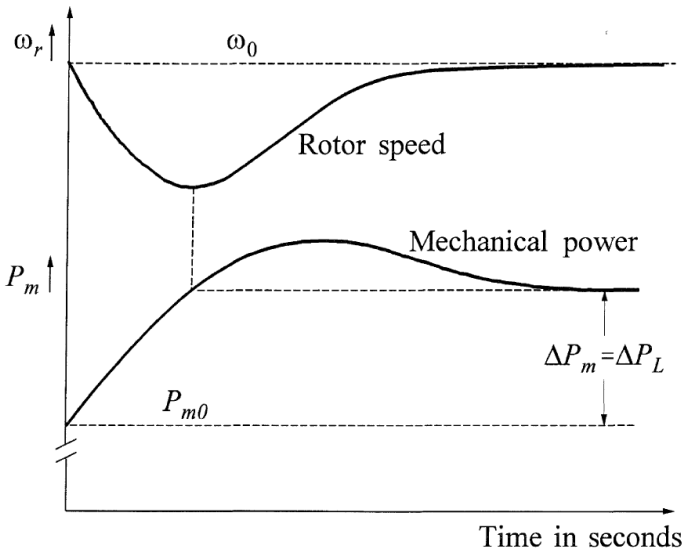

Figure 14. Isochronous control frequency response (Kundur, 1994)**.**

In a power system where, multiple generators are working in parallel using isochronous control can cause problems because the generators start to compete to response first to the frequency change. Because of this reason isochronous load sharing is introduced. In isochronous load sharing all the governors are operating in isochronous mode are connected to each other via a communication system. This way the controllers can exchange information and adjust their speed reference to achieve more balanced frequency response. The signal typically adjusted by adding or subtracting an analog bias signal into it (Ravikumar et al., 2017).

4.4.3 Fixed Active Power Control

The generator can be used to output constant active power. This control method can also be called true kW-, fixed kW-, base loading or constant output (Ravikumar et al., 2017). As the name "base loading" implies this control is often used when the generator is acting as a base load in the power system. It is often used then the generator is running parallel with the utility grid, but it can also be used in larger microgrids. Typically, in when generators are running in fixed active power mode they do not participate in frequency control, and it is handled by other generators running in droop- or isochronous control

mode. However, these generator can be utilized in secondary control to bring the frequency back to the nominal value, by altering the active power set point.

4.5 Frequency Control of Low-Inertia Inverter-Based Power Systems

This chapter discusses different control methods, which can be utilized to control to control inverter-based generation. These methods will cover different control methods for short- and long-term frequency control.

4.5.1 Virtual Inertia

With inverter-based power generation, there are no rotating masses directly connected to the grid, which means they do not naturally contribute any inertia to the power system. However, it is possible to create control strategies for inverters to replicate the behavior of the inertia of synchronous generators and release more active power to the system. Nevertheless, artificially created control functions need measurements from the system. Because these measurements take time, they cannot operate as fast as inertia created by rotating masses, which is a natural phenomenon. Some RESs have rotational inertia, like wind turbines. However, it is called hidden inertia since they are not directly connected to the grid and cannot directly contribute to the system inertia (Fernández-Guillamón et al., 2020). Virtual inertia is also often referred to as fast frequency response (FFR) (Rahmann & Castillo, 2014).

Since photovoltaic energy does not have any rotating masses to contribute to system inertia, energy storage systems are needed. In addition to ESS, it is possible to use a deloading control strategy, where the PV plant is operated under its maximum power point (MPP), so there is some power reserve to use for FFR. The more common solution is to utilize BESS to supply active power in case of decreased generation or increased load (Rahmann & Castillo, 2014).

De-loading strategy can also be implemented into wind power plants in two ways, by using pitch control or over-speed control. In pitch control, the pitch of turbine blades is adjusted so that the wind turbine operates under the MPP. In the case where additional power needs to be supplied, the pitch is adjusted for higher power generation. On the other hand, in over-speed control, the WT is driven on over speed when it is generating less power than in MPP. To generate additional power for the inertial response, the speed of the rotor is decreased to release the kinetic energy from the blades (Fernández-Guillamón et al., 2020).

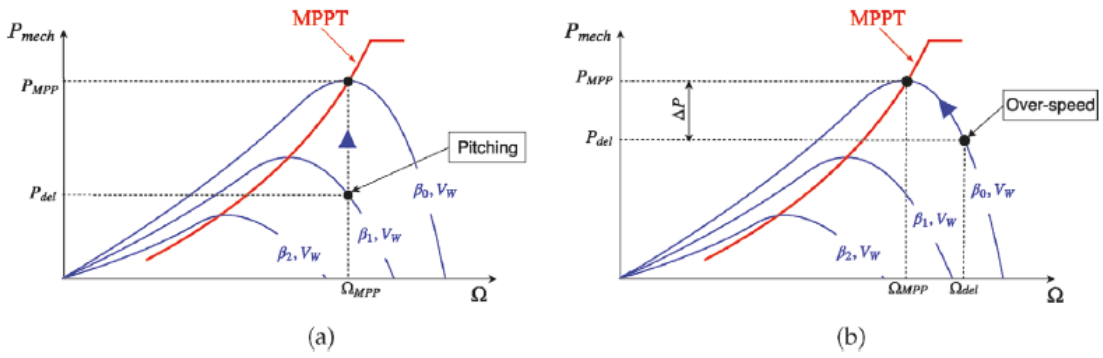

Figure 15. De-loading controls for wind turbines. (a) Pitch control. (b) Over-speed control.

4.5.2 VSI Droop

In the inverter-based system, it is possible to emulate the behavior of synchronous machines to implement droop control. Using a phase-locked loop (PLL), the system frequency is measured from three-phase terminal voltage for frequency regulation using a phase-locked loop (PLL). In a real-world system, accurate readings of the system frequency are difficult to obtain. Therefore, active power measurements are preferred (Hatziargyriou, 2014).

When using the VSI droop control, the droop characteristics vary between primarily inductive high voltage microgrid and mostly resistive low voltage microgrid. In their book, Bevrani et al. (2017) prove that in an inductive microgrid, the active power controls the

frequency, and reactive power controls the voltage independently so that the droop control can be written in the following form (Bevrani et al., 2017):

$$f - f_0 = -k_p(P - P_0) \tag{12}$$

On the other hand, Bevrani et al. (2017) prove a high linkage between reactive power, active power, frequency, and voltage in a highly resistive microgrid. Therefore, the frequency droop control is expressed in the following way:

$$f - f_0 = -k_p(Q - Q_0) \tag{13}$$

In a general grid, both inductive and resistive components should be considered as in the following equation:

$$f - f_0 = -k_p(P' - P_0') = -k_p \frac{X}{Z}(P - P_0) + k_q \frac{R}{Z}(Q - Q_0) \tag{14}$$

4.5.3 Frequency-Watt Control

Frequency-watt control can be used to support the grid frequency by altering the active power output of the inverters. In an under-frequency situation, the inverter power output is increased to support the frequency, and in an over-frequency situation, the power output is decreased. An illustration of the frequency-watt droop curve can be seen in **Figure 16** (Pattabiraman et al., 2018).

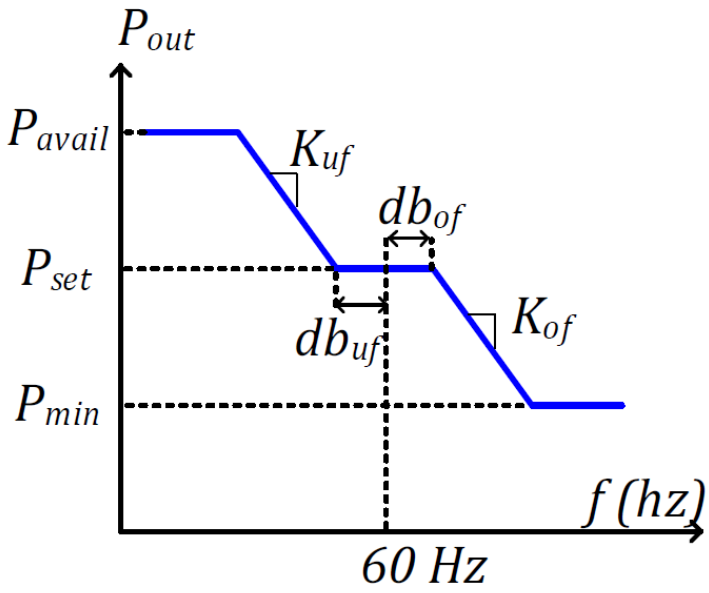

Figure 16. Frequency-watt droop curve with power reserve (Pattabiraman et al., 2018).

According to (Pattabiraman et al., 2018), most photovoltaic inverters operate at their maximum power point and hence cannot support system frequency in an under-frequency event. For the under-frequency response to work, inverters must work under their maximum power point. In **Figure 17** can be seen the frequency-watt droop curve for a system operating without a power reserve.

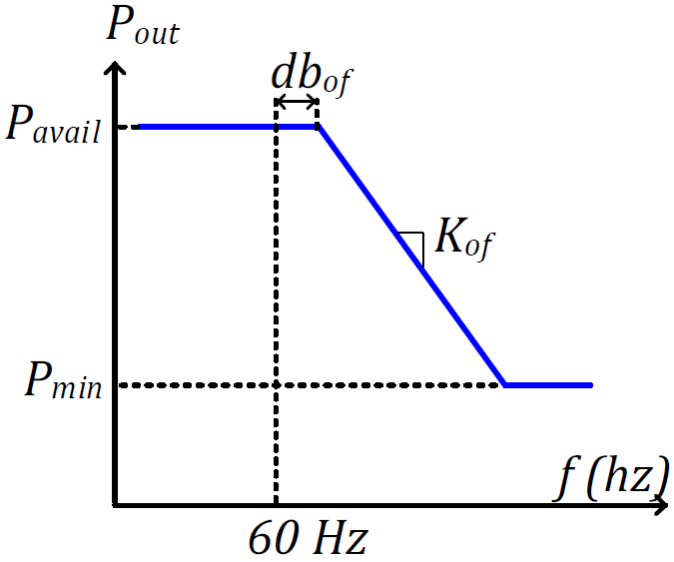

Figure 17. Frequency-watt droop curve for inverter without a power reserve(Pattabiraman et al., 2018).

4.5.4 Role of Forecasting in Frequency Control

During the day, the load and generated power from RES vary greatly. The RES generations vary due to their weather-dependent nature, primarily based on the wind speed and amount of available sunlight in the wind and photovoltaic energy. Load, on the other hand, vary based on multiple factors. Due to the people's habits and working hours, the demand can vary significantly from day to night (Sharma et al., 2018). One other key factor is also the weather. Based on the temperature, the needed power for heating and cooling changes. Due to these reasons, forecasting techniques need to be implemented. These factors can be considered by using historical data on load and weather, combined with current and forecasted weather. In a microgrid, the aim is always to maximize renewable generation. This is done to optimize power generation from controllable power resources, like gas turbines, diesel engines, and energy storage systems (Dutta et al., 2017).

Forecasting can be divided into three main categories: short-term -, medium-term-, and long-term forecasting. From the frequency control side, short-term forecasting is the most relevant. Its forecasting period varies from one hour to one week. Renewable energy generation forecasting typically belongs to short-term forecasting because the weather is almost impossible to accurately predict for an extended period of time accurately (Sharma et al., 2018).

4.6 Load Shedding Schemes for Frequency Support in a Power System

The load can also be controlled in a power system to maintain the balance between generation and demand. Load side control is based on connecting and disconnecting the loads to the power system at desired times.

Load scheduling, also known as energy consumption scheduling, has been introduced to even out variations in power consumption during the day. The highest consumption

hours are during the day when most people are working and then decreasing towards the nighttime. Load scheduling, also known as energy consumption scheduling, has been introduced to even out these variations. The basic working principle in load scheduling is to encourage consumers to shift their heavy loads to off-peak hours (Bevrani et al., 2017).

Load shedding can be used as an emergency control strategy if the power system's power plants cannot generate the necessary power to meet the demand. By disconnecting some loads load from the microgrid, the balance can be maintained. Load shedding plan can be based on the frequency or voltage measurements or a combination of both. In this thesis, the focus will be on frequency-based load shedding, which is also known as under-frequency load shedding (UFLS) (Bevrani et al., 2017).

Load shedding is only utilized in an event where the frequency change is significant, and the frequency exceeds a certain threshold. In addition to frequency measurements, ROCOF can also be used in load shedding to improve accuracy. Significant changes in frequency can be due to a significant increase in load or tripping of a line or a generator. The load shedding process is typically started by disconnecting the non-critical loads, but this process is also highly influenced by economic, political, and social reasons (Bevrani et al., 2017).

5 Development of Simulation Models

This chapter develops the simulation models for different configurations of the microgrid and different frequency control methods. The configurations vary based on the share of the synchronous- and inverter-based generation connected to the microgrid. The study has been separated into three main cases. The first cases consist of only synchronous generation, and the following two cases consist of a mix of synchronous generation and inverter-based generation in 60 % to 40 % split in both ways. An engine power plant (EPP) is used as the synchronous generation and for the inverter-based generation, photovoltaic power plant (PVPP) and wind turbine power plant (WPP) are used. Also, a 20 MW BESS is included in all the cases. In all these cases, variable combined loads are considered. **Table 1** summarizes the configurations of each case study.

Table 1. Configuration of different case studies.

	Case 1	**Case 2**	**Case 3**
Microgrid Voltage	33kV	33kV	33kV
Total load	100 MW	100 MW	100 MW
BESS	20MW	20MW	20MW
Gen Unit 1	EPP	EPP	EPP
Gen Unit 2	EPP	EPP	EPP
Gen Unit 3	EPP	EPP	PVPP
Gen Unit 4	EPP	PVPP	PVPP
Gen Unit 5	EPP	WPP	WPP

The IEEE 14 bus system is created to implement new ideas and concepts, creating a comprehensive electric grid for the researchers (PSCAD, 2018). For this reason, it is also chosen for this study. In this study, the IEEE 14 bus system model provided on the PSCAD website is used as a base for the simulation models (**Figure 18**). This microgrid model consists of transmission lines, 14 buses, ten loads, capacitor bank and five generators. Simulation models are configured to match the desired generation and mixes.

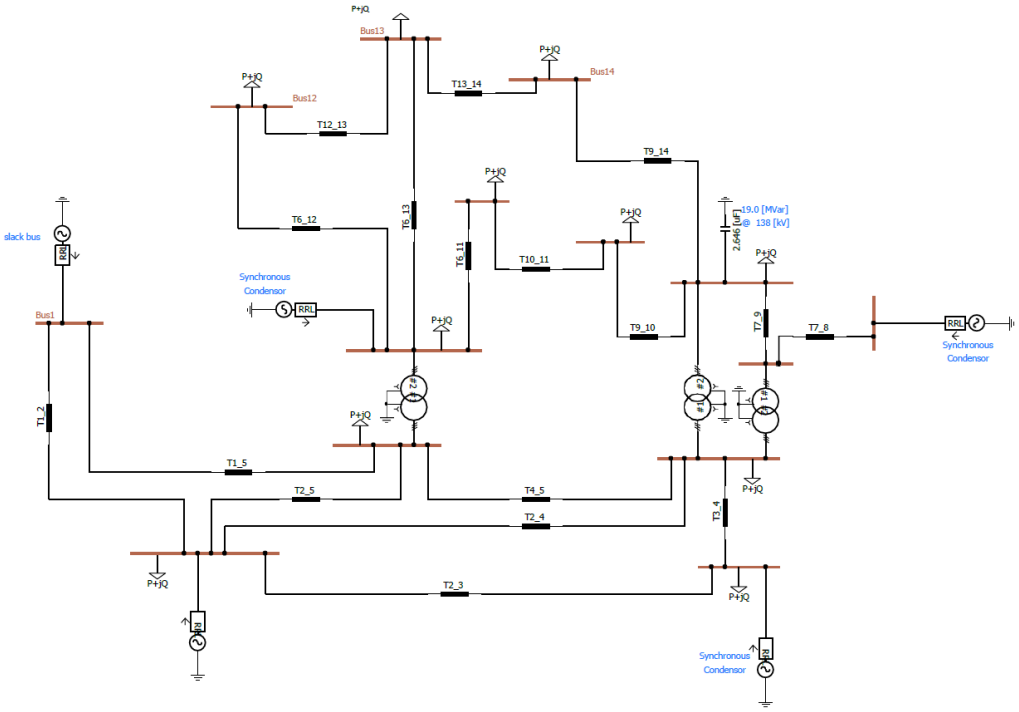

Figure 18. General IEEE 14 bus system used as a template (PSCAD, 2018a).

The 14-bus system configured for this study does not represent any specific real-life microgrid. For this reason, the values are chosen only to create a possible example of a microgrid. The system frequency for this study is 50 Hz. Each 14-bus system operates on a 33kV medium voltage level. This voltage level is chosen for this study to be a good base point for the model regarding future use as a tool to analyze existing and future microgrids. The system frequency is monitored from the bus 14 in all the simulations cases. Since the object of this thesis is to observe the system's frequency behavior, the decision not to model the distribution lines was made to speed up the long simulation times in such a large model with over 250 nodes.

In the IEEE 14 bus model, there are also three distribution transformers. Each of these transformers is rated at 110 MVA. Since the voltage level on the whole microgrid is kept at a 33 kV voltage level, both transformer windings are 33 kV. These transformers do not server any specific purpose in the model and are only included because they are part of the model.

As a load in the microgrids, total of 100 MW of composite loads connected to 10 different buses are used. The power factor of connected loads is approximately 0,95 inductive (lagging)—more specific details concerning each load are specified in following **Table 2**.

Table 2. Connected loads.

Loads				
BUS	**S [MVA]**	**P [MW]**	**Q [MVAR]**	**p.f.**
Bus 2	**8,6**	**7,5**	**4,3**	**0,87**
Bus 3	**20,5**	**20**	**4,5**	**0,98**
Bus 4	**16,1**	**16**	**2**	**0,99**
Bus 5	**2,5**	**2,5**	**0,5**	**0,98**
Bus 6	**9,1**	**8,4**	**3,4**	**0,93**
Bus 9	**11,4**	**10**	**5,5**	**0,88**
Bus 10	**3,6**	**3**	**1,9**	**0,84**
Bus 11	**4,1**	**4**	**0,8**	**0,98**
Bus 12	**14,2**	**14**	**2,5**	**0,98**
Bus 13	**4,9**	**4,5**	**1,9**	**0,92**
Bus 14	**10,8**	**10,1**	**3,7**	**0,94**
Total	**105,8**	**100**	**31**	**0,95**

Loads in the models are modeled using three-phase fixed load components seen in **Figure 19**. Some loads are connected using breakers to help with the system's initialization and disconnect a load in a load tripping event.

Figure 19. Load and breaker model.

5.1 Generation units

This chapter introduces the different generation unit models and their features used for these simulations. Some of the models are not described in detail because of confidentiality reasons. However, the essential functions and how they are operated and controlled are described to understand the models.

5.1.1 Engine power plant

For the synchronous generation unit, an engine power plant (EPP) is used. The power plant model is provided by the Wärtsilä with their W18V50DF engines producing 16,5 MW of active power. Overview of the model is shown in the **Figure 20** and **Figure 21**. This model is possible to scale from one engine to four engines. In these simulations, these power plants are run with 2 engines, with a maximum combined power output of 33 MW. So, the maximum active power output of the model is 66 MW. For these simulations at EPP active power set-point is set to 20 MW.

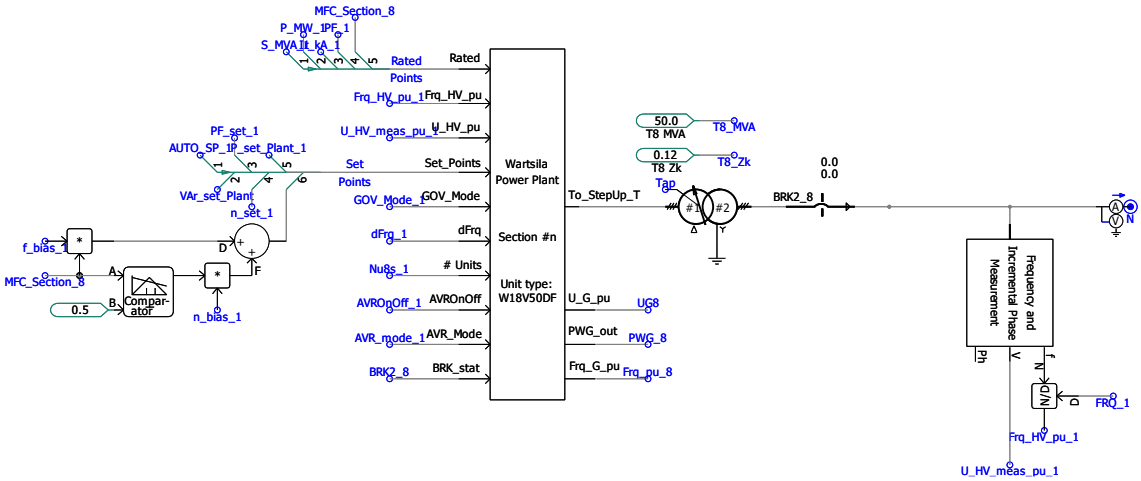

Figure 20. Overview of the engine power plant PSCAD model.

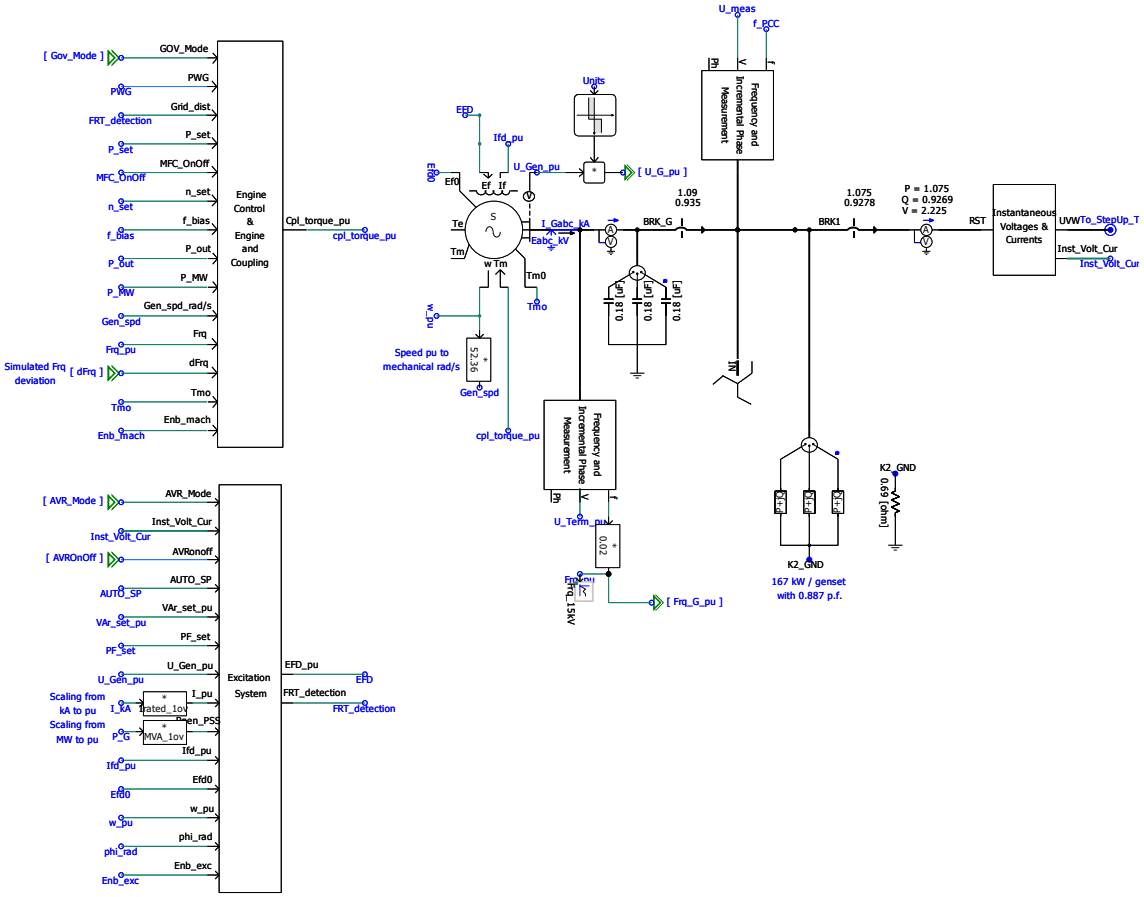

Figure 21. Overview of the engine power plant PSCAD model inside the Wärtsilä power plant block.

These gensets are connected to the microgrid using step-up transformers to increase the voltage from generated 15 kV to the microgrids nominal voltage of 33 kV. All of the transformers are rated at 50 MVA nominal apparent power. After the transformer is a medium voltage circuit breaker which is used to connect the power plant to the microgrid and, in some simulation cases, to disconnect it from the MG.

These engine power plants can be run in three different control modes: Droop control, isochronous control, and true kW control. In addition to these three primary control modes, secondary control mode called "master frequency control" (MFC) will be used to bring the system frequency back to the nominal value after variation. MFC is a slower control, which speed is dependent on the controller gain and ramp rate limiter. It also has a dead band of 10 mHz where the MFC will be disabled.

Since the object of the thesis is to find the best frequency control strategy for the microgrid. For this reason, the engine power plants are controlled using droop or isochronous control method, leaving out the true kW control mode. True kW control mode does not offer any fast-acting frequency support for the system and is not considered for this reason, even though it could be used in a real-life microgrid. Although the power plant can offer slower frequency support in true kW mode by adjusting the active power set-point.

Since the EPP model is in active use it has the default protection functions included. Exceeding these limits will cause the EPP to trip. The default protection parameters are shown in **Table 3** and **Table 4**.

Table 3. EPP's frequency protection parameters.

Frequency Protection	Limit (Hz)	Tripping Time Delay (s)
Over-frequency Protection, HV	51,1	120
Over-frequency Protection, HV	50,6	600
Under-frequency Protection, HV	49,4	600
Under-frequency Protection, HV	47	120
Over-frequency Protection, MV	52,1	3
Over-frequency Protection, MV	50,7	30
Under-frequency Protection, MV	49,3	30
Under-frequency Protection, MV	46,9	3

Table 4. EPP's voltage protection parameters.

Voltage Protection	Limit (pu)	Tripping Time Delay (s)
Over-voltage Protection, HV	**1,3**	**0,04**
Over-voltage Protection, HV	**1,25**	**0,2**
Over-voltage Protection, HV	**1,2**	**2**
Over-voltage Protection, HV	**1,15**	**20**
Over-voltage Protection, HV	**1,1**	**1200**
Under-voltage Protection, HV	**0,9**	**10**
Under-voltage Protection, HV	**0,8**	**2**
Over-voltage Protection, MV	**1,35**	**2**
Over-voltage Protection, MV	**1,25**	**3**
Over-voltage Protection, MV	**1,21**	**22**
Over-voltage Protection, MV	**1,11**	**1320**
Over-voltage Protection, MV	**1,05**	**30**
Under-voltage Protection, MV	**0,95**	**10**
Under-voltage Protection, MV	**0,86**	**11**
Under-voltage Protection, MV	**0,78**	**10**

The amount of moment of inertia on one of these gensets is J = 21644,7 kgm^2. The inertial constant of the genset can be calculated using the equation (1) from this the *H* is 1,349 kWs/KVA.

5.1.2 Photovoltaic Power Plant

The photovoltaic power plant (PVPP) used in this study is based on the PSCAD simple solar farm model, which can be found from their website (PSCAD, 2021). Main structure of the model is shown in **Figure 22** and **Figure 23**. PV arrays used in this model generate in maximum of 250 kW of power. By using the scaling component, the model scaled to be 25 MW with 100 units but is operated on the 20 MW set-point. But in reality, the output active power varies depending on the load balancing. Which means that each PVPP has 5 MW spinning reserve in ideal conditions.

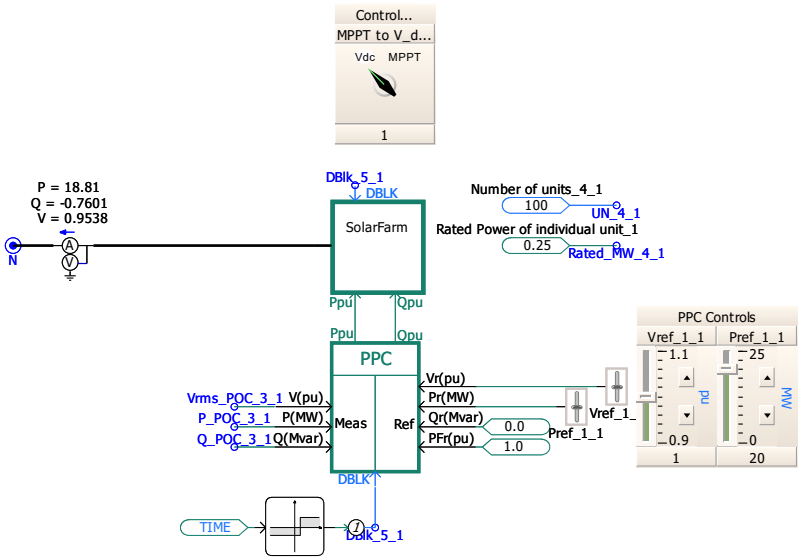

Figure 22. Overview PSCAD Simple solar farm model.

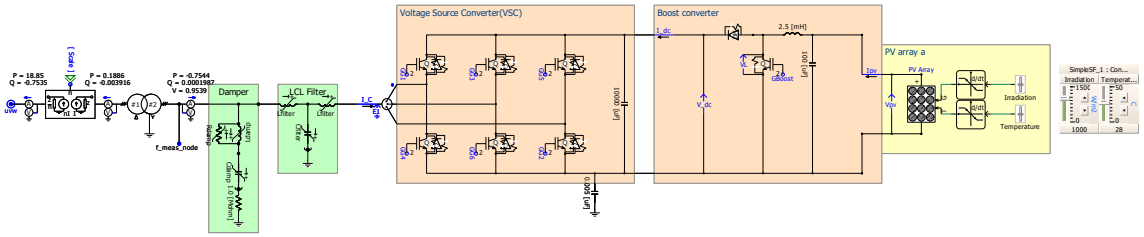

Figure 23. PSCAD Simple solar farm detailed model.

In the model it is also possible to change the ambient temperature and irradiation so simulate different conditions which effect amount of available power. For this study these are kept at the default value of 1000 W/m^2 irradiation and the ambient temperature at 28 °C.

The model can be operated in MPPT mode and in so called “V_dc” mode in which it operates under the MPPT and be used to support the microgrid frequency. The frequency control circuit is shown in **Figure 24**. The power output is altered by adjusting the inverter DC voltage in the inverter. Inverter droop can be adjusted to optimize the frequency support function using the frequency-watt control with the dead band of 0,4 Hz and ramp rate of 0,45 pu/Hz as shown in following **Figure 25**. The PVPP is expected to run on 0,8 pu active power point set-point.

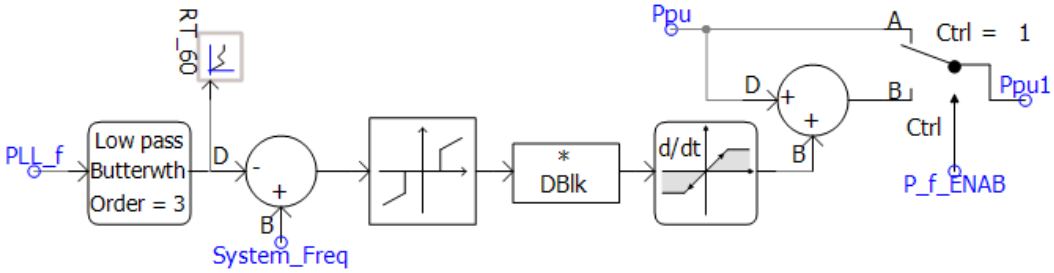

Figure 24. PSCAD Simple solar farm P(f) control circuit.

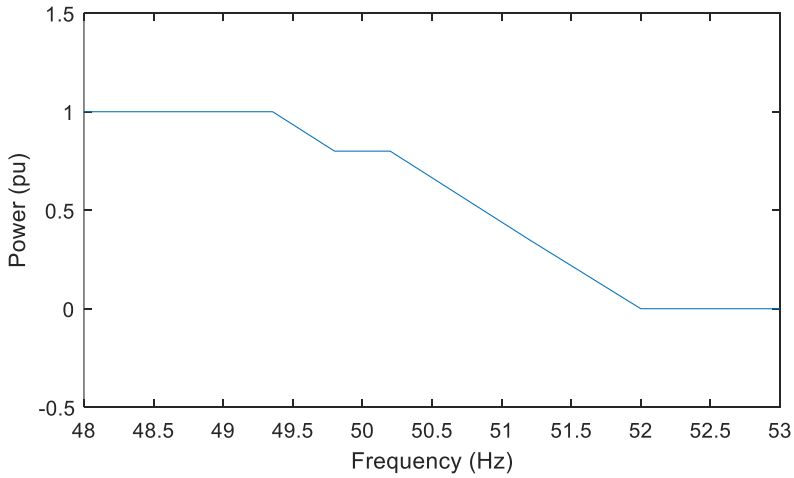

Figure 25. Visualization of photovoltaic power plant frequency-watt response curve on 0,8 pu power set-point.

5.1.3 Wind Power Plant

For the wind power plant model, the "Type -4 Wind Turbine Model", which can be found from the PSCAD website, is used for this study (PSCAD, 2018b). Overview of the WT is shown in **Figure 26**. WT is connected to the grid using AC-AC converter with DC-link. The WPP model is operated in MPPT mode to output the maximum available wind energy into the microgrid.

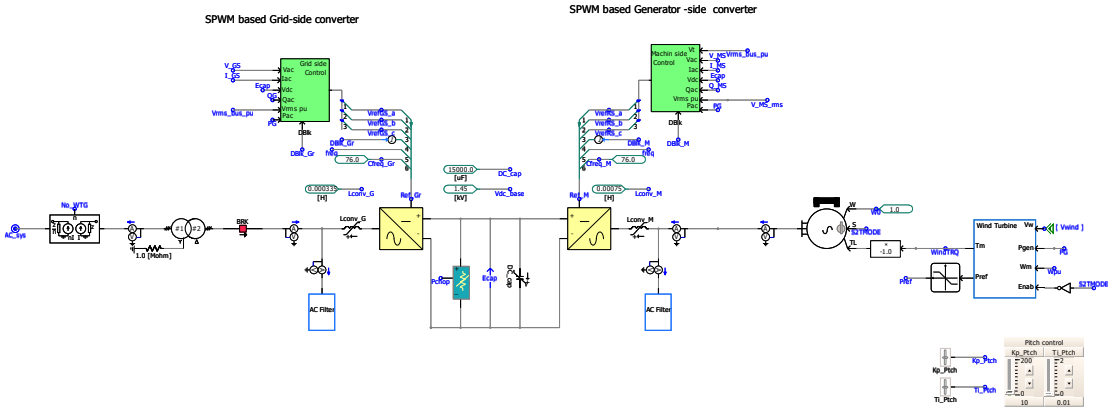

Figure 26. Type-4 wind turbine model (PSCAD, 2018b).

The model is scalable and is used in this study as an 20 MW wind power plant. The wind speed can be changed from 3 m/s to 25 m/s. But for these simulations the wind speed is kept at the default value of 10 m/s, excluding the cases where wind speed is considered to be minimal. In those case the WPP is disabled completely to bring down the simulation time.

5.1.4 Battery Energy Storage System

The battery energy storage system (BESS) used in this model is rated at 20 MW. A well-known inverter manufacturer provides the inverter model. Overview of the model is shown in **Figure 27**, but this thesis does not describe the model's design in detail due to the confidentiality reasons. The same BESS model is used in all the models, and it is connected to the bus number 14.

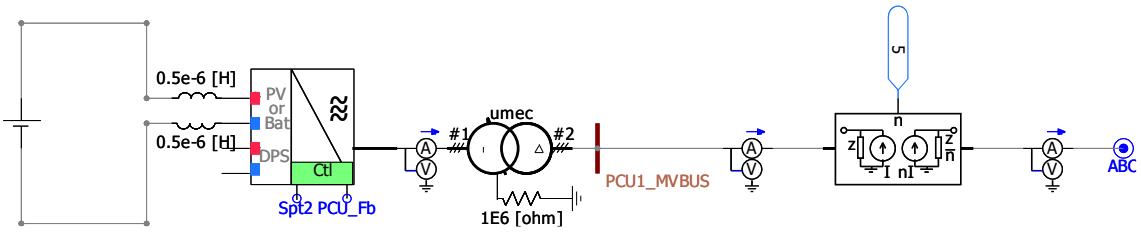

Figure 27. BESS model.

It operates in grid-forming mode and actively supports the frequency in under and over-frequency events using the frequency-watt control. Frequency support functions are activated if the frequency deviation is more than ±0,2 Hz. The frequency response curve is shown in the **Figure 28**.

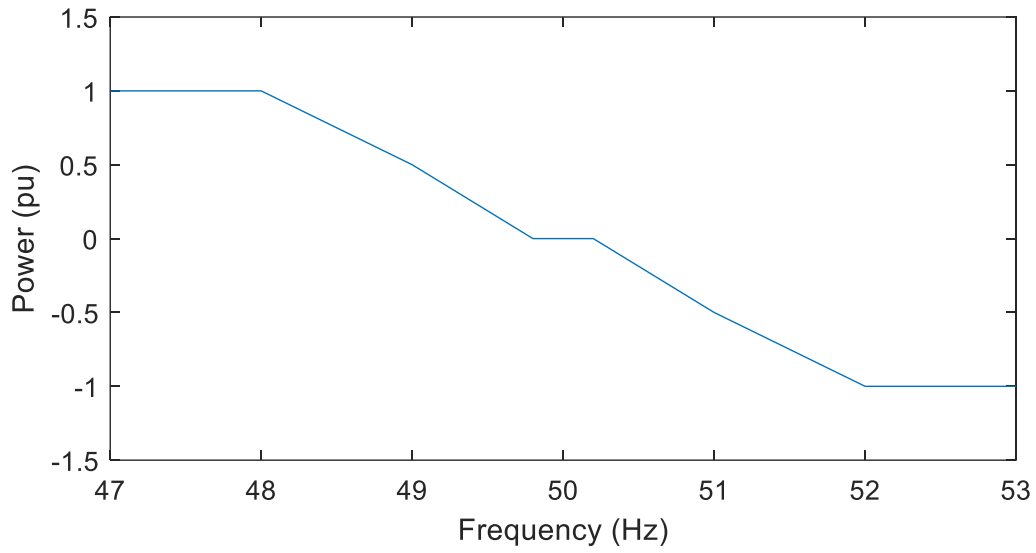

Figure 28. BESS frequency-watt response curve.

In addition to frequency measurement, the BESS inverter actively monitors the system ROCOF. Frequency support is activated if ROCOF exceeds the 1,5 Hz/s value.

The batteries are modeled using the shepherd model. As BESS's batteries initial state of charge (SOC) 60% is used to optimal performance in both, under- and over-frequency situations. This thesis does not focus on maintaining the BESS SOC on the desired level for a longer period.

5.2 Study Cases

This chapter introduces the different study cases. Going through the basic structure of the model, and the type, capacity, and the location of the generation units. Also, the total generation capacity and the amount of spinning reserve are discussed.

5.2.1 Case 1: Only Synchronous Generation

This chapter discusses the configuration of the model in Case 1. To set the base point for the study, Case 1 consists of only synchronous generation. It gives a good understanding of change in frequency behavior due to the power system's lower inertia in cases where inverter-based generation is added. Engine power plants are connected to bus numbers; 1, 2, 3, 6, and 8, as shown in **Figure 29**. In total the installed generation capacity is 165 MW of synchronous generation and 20 MW BESS. In total the model has 85 MW (85%) spinning reserve under ideal conditions. The model is shown in **Figure 29**.

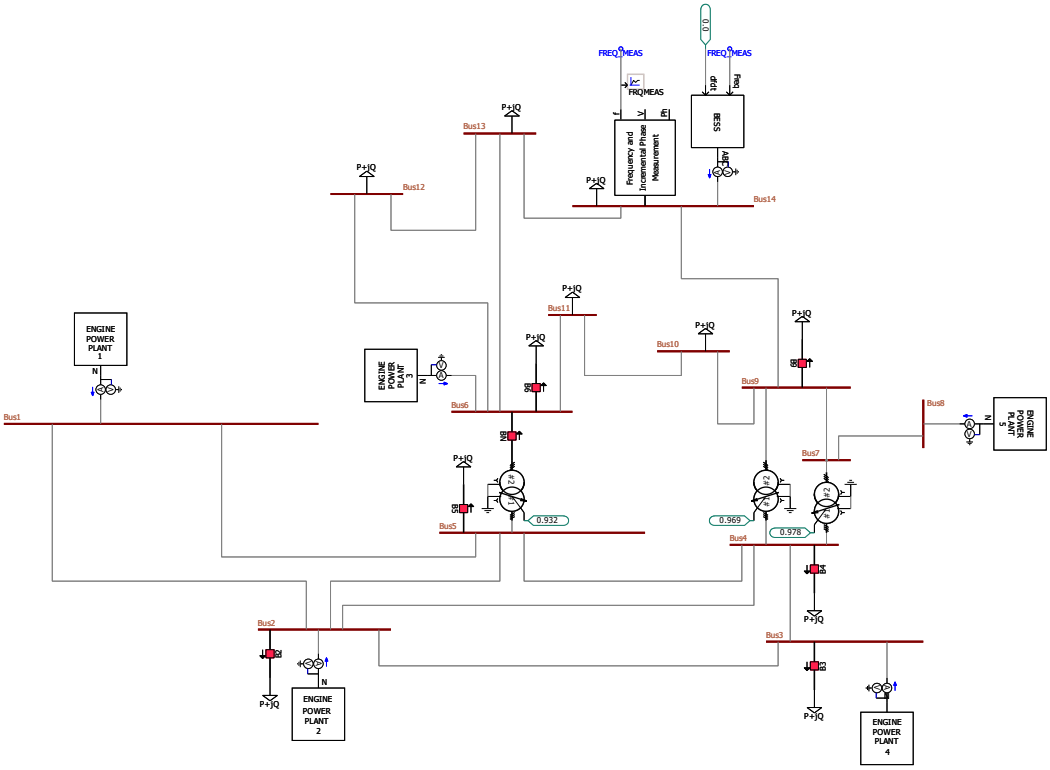

Figure 29. Case 1 PSCAD model.

5.2.2 Case 2: 60 % Synchronous Generation

In the second case study, inverted-based generation is connected to the power system. Configuration consists of 60% share of synchronous generation and 40% share of inverter-based generation. This configuration consists of three 33 MW engine power plants, a 20 MW wind power plant, a 25MW photovoltaic power plant, and a 20 MW BESS. In total the amount of connected generation is 164 MW. EPPs are connected to the busses number 1, 3 and 6, PVPP is connected to the bus number 2 and WPP is connected to the bus number 8. In case of under-frequency situation this model has 64 MW (64%) spinning reserve under ideal conditions. The model is shown in **Figure 30**.

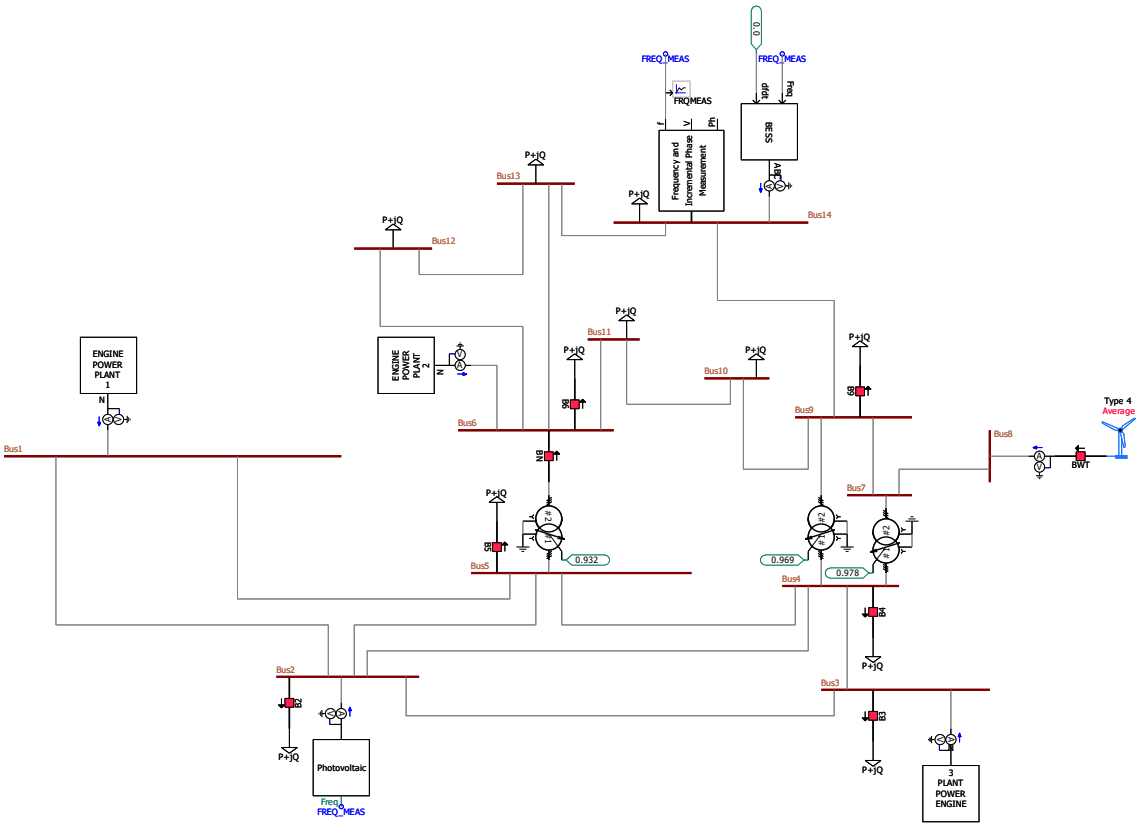

Figure 30. Case 2 PSCAD model.

5.2.3 Case 3: 60 % Inverter-Based Generation

The third case study consists of a 60% share of inverter-based generation and a 40% share of synchronous generation. This configuration consists of two 33 MW engine power plants, two 25 MW photovoltaic power plants, a 20 MW wind power plant, and a 20 MW BESS. In total the amount of connected generation is 156 MW. EPPs are connected to the busses number 1, and 3, PVPPs are connected to the buses number 2 and 6, and WPP is connected to the bus number 8. In case of under-frequency situation this model has 56 MW (56%) spinning reserve under ideal conditions. The model is shown in **Figure 31**.

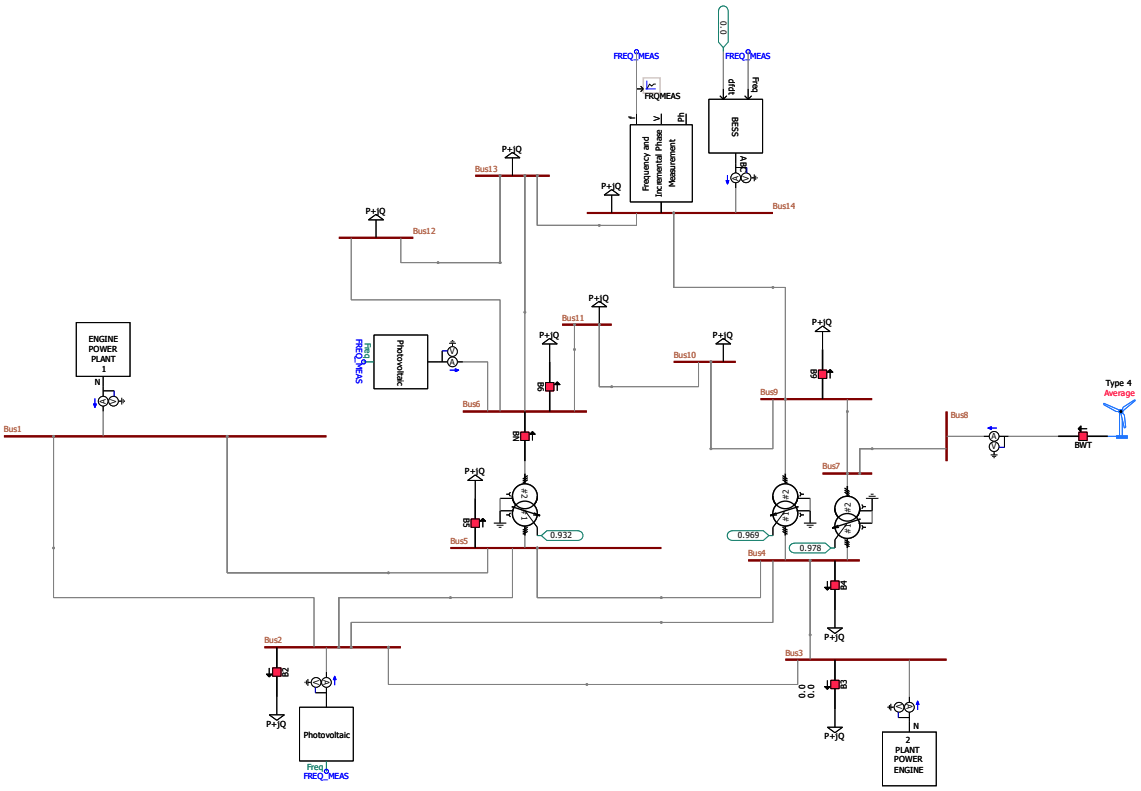

Figure 31. Case 3 PSCAD model.

6 Simulations Results and Analysis

This chapter goes through and analyzes the results of simulations. Since the studied microgrids do not represent any existing microgrid, the acceptable operational frequency range limits are defined based on existing grid codes.

There are four main events simulated to create an understanding of the grid behavior. All the events are timed to happen 120s after the simulation has started. This moment is chosen, so the grid can reach its nominal frequency before the event. All the simulation scenarios for the different study cases are shown in the **Table 5**, **Table 6** and **Table 7**.

Table 5. Case 1: Simulations scenarios.

CASE	EVENT	EPP CONTROL	CONDITION
Case 1	Load trip	Droop	Ideal
Case 1	Load trip	Droop	No BESS
Case 1	Load trip	Isochronous	Ideal
Case 1	Load trip	Isochronous	No BESS
Case 1	Synch. generation trip	Droop	Ideal
Case 1	Synch. generation trip	Droop	No BESS
Case 1	Synch. generation trip	Isochronous	Ideal
Case 1	Synch. generation trip	Isochronous	No BESS
Case 1	Network-link trip	Droop	Ideal
Case 1	Network-link trip	Droop	No BESS

Table 6. Case 2: Simulations scenarios.

CASE	EVENT	EPP CONTROL	CONDITION
Case 2	Load trip	Droop	Ideal
Case 2	Load trip	Droop	No BESS
Case 2	Load trip	Droop	No PV
Case 2	Load trip	Droop	No WT
Case 2	Load trip	Isochronous	Ideal
Case 2	Synch. generation trip	Droop	Ideal
Case 2	Synch. generation trip	Droop	No BESS
Case 2	Synch. generation trip	Droop	No PV
Case 2	Synch. generation trip	Droop	No WT
Case 2	IBG trip	Droop	Ideal
Case 2	IBG trip	Droop	No BESS
Case 2	IBG trip	Droop	No PV
Case 2	IBG trip (PV)	Droop	No WT
Case 2	Network-link trip	Droop	Ideal
Case 2	Network-link trip	Droop	No BESS
Case 2	Network-link trip	Droop	No PV
Case 2	Network-link trip	Droop	No WT

Table 7. Case 3: Simulations scenarios.

CASE	EVENT	EPP CONTROL	CONDITION
Case 3	Load trip	Droop	Ideal
Case 3	Load trip	Droop	No BESS
Case 3	Load trip	Droop	No PV
Case 3	Load trip	Droop	No WT
Case 3	Load trip	Isochronous	Ideal
Case 3	Synch. generation trip	Droop	Ideal
Case 3	Synch. generation trip	Droop	No BESS
Case 3	Synch. generation trip	Droop	No PV
Case 3	Synch. generation trip	Droop	No WT
Case 3	IBG trip	Droop	Ideal
Case 3	IBG trip	Droop	No BESS
Case 3	IBG trip	Droop	No PV
Case 3	IBG trip (PV)	Droop	No WT
Case 3	Network-link trip	Droop	Ideal
Case 3	Network-link trip	Droop	No BESS
Case 3	Network-link trip	Droop	No PV
Case 3	Network-link trip	Droop	No WT

The first event is the largest load trip to create an over-frequency situation in the microgrid. It is achieved by disconnecting the 20 MW load connected to bus number 3. This

creates a 20% load step into the system in which the generation units are expected to decrease their output to maintain the power balance.

The second event is the largest synchronous generation trip. It is done by opening the outgoing breaker from the engine power plant. It creates an under-frequency situation for the microgrid, which needs to be compensated by increasing the power output from other generation units.

The third event is the largest inverter-based generation trip. It is done by disconnecting the wind power plant from the microgrid. The wind power plant is considered the largest inverter-based generation in the microgrid because it operates with MPPT, and photovoltaic power plants operate under their MPP and generate less power than the WPP. In the Cases 2 and 3, a photovoltaic power plant is tripped under the condition of no wind energy.

The last event is a network link trip. This scenario is executed by opening a breaker between the distribution transformers and bus number 6. It is done to change the power flow in the microgrid to create a temporary unbalance in the power system.

These events are also simulated in different conditions, which were mentioned before. As an ideal condition, a condition where photovoltaic and wind energy are available at the maximum capacity is considered. Also, other conditions where either photovoltaic or wind energy is not available are considered. In addition to these, a condition where BESS is exhausted is considered. In the event in which the BESS is exhausted, the whole BESS model is disabled in the simulation model to speed up the simulations. Even though exhausted BESS can offer frequency support in over-frequency situations, it does not differ from where BESS has a 60% state of charge.

Also, the different engine control methods are considered to achieve the best control strategy for the microgrid. However, simulating all the possible configurations with

different control combinations in this model is impossible; considering the schedule for a master's thesis, the number of different scenarios is limited to cover the most relevant configurations based on previous knowledge. In all the cases, master frequency control is used with the engines running in droop mode to bring the frequency back to the nominal value.

From the results of the following simulation, it can be noticed that not all the controllers are optimized for this specific power system and can, for this reason, have small oscillation after the event. Most of this oscillation is caused by the master frequency control on engine power plants. It can be minimized by tuning the controllers, but these models are not suitable for this kind of work due to the reason that some simulations can take over 48 hours for 240 seconds simulation time (Kundur, 1994). In cases 2 and 3, some high-frequency harmonics are caused by inverter-based generation units. They could be minimized with AC-filter tuning on the generation units, but it is left out of the scope of this thesis (Abu-Rub et al., 2014).

The results from the simulations are shown using graphs and tables, summarizing the frequency nadir, maximum frequency deviations, and time when the maximum value is reached to visualize them for the reader easily. Following acronyms are used to describe the events when reporting the simulation results:

- LD = Load disconnected
- GD = Generator disconnected
- ND = Network link disconnected
- ID = Inverter disconnected

In some cases, it is necessary to disable the protection functions (frequency and voltage protection) from the EPPs. These configurations are marked with the symbol * in the tables.

6.1 Stability Limits

As mentioned before, the microgrid does not represent any real-life microgrid and, for this reason, is not under any specific grid code. For this reason, it is decided to use the frequency limits defined in the grid code from FINGRID (2018) and Entso-E frequency stability evaluation criteria for the synchronous zone of continental Europe (2016).

A limit for the normal operating frequency is considered to be between 49 Hz – 51 Hz, meaning that the system must be able to operate in this frequency range for an unlimited time period. In an over-frequency situation, the frequency limit of 51,5 Hz is considered. While in under-frequency situations, the frequency limit of 47,5 Hz is considered. Other frequency limits are shown in **Table 8** but do not affect the simulation result analysis considering the short simulation times. Everything exceeding these limits is considered unsuccessful. As the ROCOF limit, 2 Hz/s is considered.

Table 8. The power system's operation frequency range based on existing grid codes (Entso-E, 2016; FINGRID, 2018).

Frequency range	The time period for operation
51,0 Hz-51,5 Hz	30 min
49,0 Hz-51,0 Hz	Unlimited
48,5 Hz-49,0 Hz	30 min
47,5 Hz-48,5 Hz	30 min

The stabilization limits are based on the frequency operating standards set by the Reliability Panel AEMC (2020). Based on this, the system is considered stabilized when the frequency is within 49 Hz-51 Hz. This frequency range needs to be achieved within 2 minutes.

6.2 Case 1 Only Synchronous Generation

Case 1 is simulated and analyzed first to create a baseline because of high inertia synchronous generation units. Since, in this case, the microgrid has only synchronous generation, simulations are done only under two different conditions: ideal and with the exhausted BESS. These events include the largest synchronous generation trip, largest

load trip, and network-link trip. In addition to these, the simulations are done with droop and isochronous control to compare these two control methods.

These simulations show the benefits of the BESS for the microgrid frequency response, even in a high inertia system. It shows significant improvement in the frequency response in both, under- and over-frequency situations.

6.2.1 Case 1 The Largest Load Trip

In the first simulation case, the largest load trip event is simulated. This simulation has four configurations. In the first two cases, all the engines are running in droop mode with BESS connected and the second one without BESS. The other two configurations are similar, with the difference that one engine is operated in isochronous mode. Droop is set to 5% in these simulation runs. The frequency response of each configuration can be seen in **Figure 32** and **Table 9**.

Table 9. Case 1 the largest load tripped.

Configuration	Freq. peak (Hz)	Max freq. deviation (Hz)	Freq. peak reached (s)
Droop, Ideal	50,97	0,97	121,04
Droop, no BESS	51,47	1,47	121,38
Isochronous, Ideal	51,03	1,03	121,05
Isochronous, no BESS	51,70	1,70	121,71

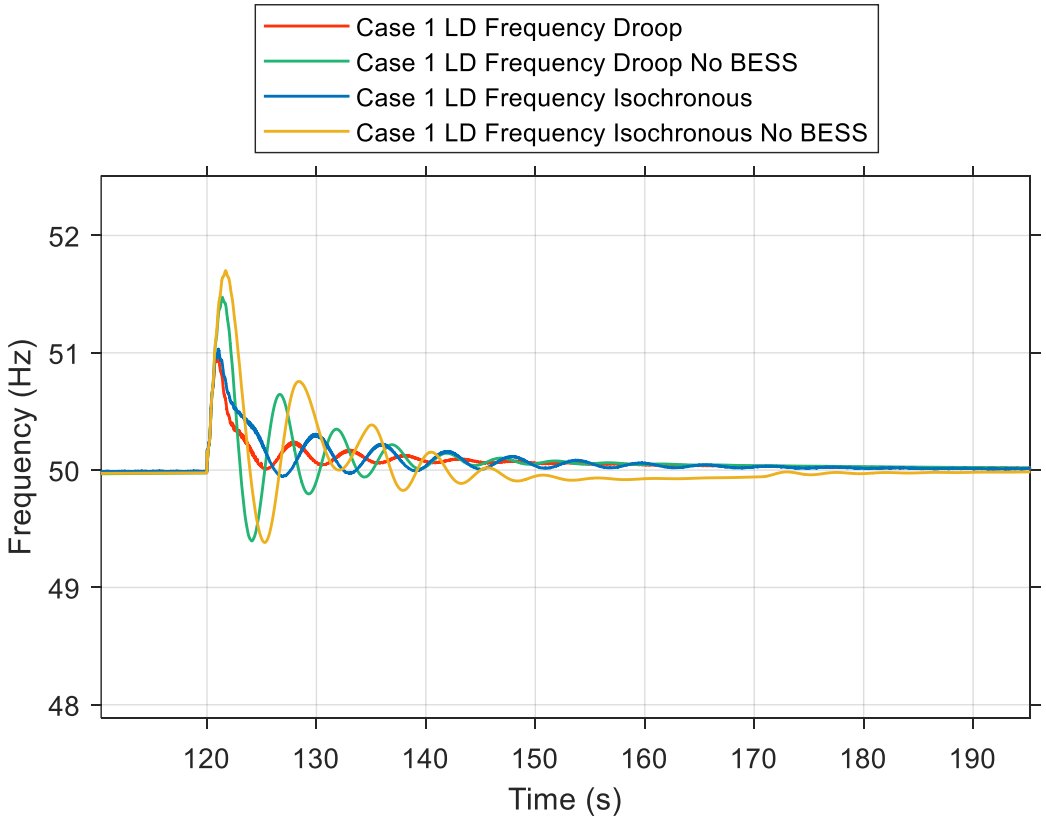

Figure 32. Case 1 the largest load tripped.

The results show that the droop control combined with BESS can offer a slightly better frequency response in the over-frequency situation due to the load tripping than isochronous control with BESS. The configuration with droop control and BESS reaches its highest frequency value of 50,97 Hz, 1,042 s after the event. The configuration with isochronous control reaches its highest value of 51,03 Hz, 1,05 s after the event. The maximum frequency deviation with droop control is 6,2 % lower than with isochronous control. Both of the configurations have some oscillation before reaching the steady state.

When the configurations without BESS are observed, it can be seen how significant support BESS can offer in over-frequency situations by acting as a load when charging the batteries. With droop control mode, the maximum frequency deviation is 51,5% larger in the case without BESS than in configuration with BESS. The same difference between

the configurations with Isochronous control is 65,0%. **Figure 32** also shows that the frequency does not overshoot after response when the BESS is included in the system.

When observing the results from the simulation with the isochronous control mode without BESS, it is shown that frequency exceeds 51,5 Hz over the frequency limit and is, for this reason, considered unsuccessful.

6.2.2 Case 1 The Largest Synchronous Power Plant Trip

The second event simulated is the tripping of the largest synchronous generator. It is done by opening the outgoing breaker from the engine power plant number 4. Disconnecting the generation unit creates an under-frequency situation, which needs to be compensated by increasing the power output from the other engine power plants. Results from this simulation can be seen in **Table 10** and **Figure 33**.

Table 10. Case 1 the largest synchronous generation trip.

Configuration	Freq. nadir (Hz)	Max freq. deviation (Hz)	Freq. nadir reached (s)
Droop, Ideal	48,95	-1,05	120,75
Droop, no BESS	48,31	-1,69	121,38
Isochronous, Ideal	48,90	-1,10	120,76
Isochronous, no BESS	47,85	-2,15	121,69

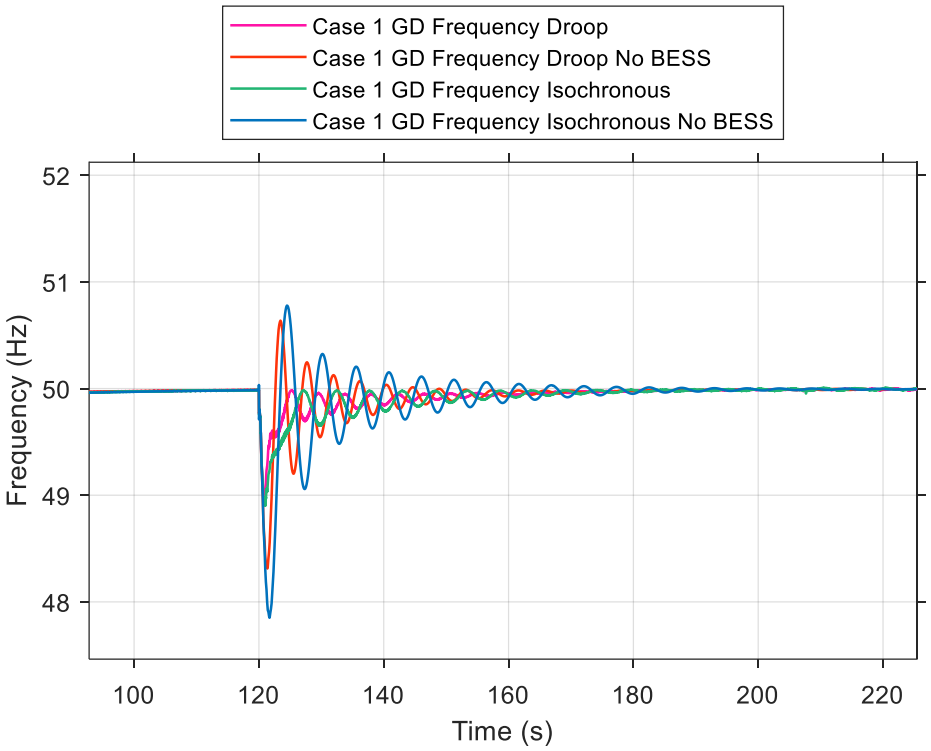

Figure 33. Case 1 the largest synchronous generation trip.

In this event, the same trend continues as in the event where the largest load was tripped. The best frequency response is achieved with droop control combined with BESS, which had a 4,5 % smaller maximum frequency deviation than the configuration with isochronous control mode and BESS.

Like in the load tripping event, the BESS brings significant frequency support to the system. In the case with droop control without the BESS, the maximum frequency deviation is 60,9 % higher than in the case with BESS. With the isochronous control, the maximum frequency deviation is almost double, compared to the one with BESS, with a 95,5 % difference, between the configurations with and without the BESS. Even though frequency deviation is higher without the battery storage system, none of these configurations exceed the 47,5 Hz under-frequency limit and are considered acceptable in terms of frequency stability.

6.2.3 Case 1 Network Link Tripped

The third event is tripping the network link inside the microgrid. In **Table 11** and **Figure 34**, it can be seen that the network link tripping in the microgrid has a negligible effect on the system frequency since 50,01 Hz is considered normal frequency oscillation. In these simulations, having the BESS in the microgrid does not make any difference because the frequency deviation stays within the limits of the dead band in the BESS control system and therefore is not activated. Due to the reason that frequency deviation is so minimal, it is decided that there is no reason to study the frequency response in this network tripping event any further with different control methods.

Table 11. Case 1 network link trip.

Configuration	Freq. peak (Hz)	Max freq. deviation (Hz)	Freq. peak reached (s)
Droop, Ideal	50,01	0,01	121,41
Droop, no BESS	50,01	0,01	121,42

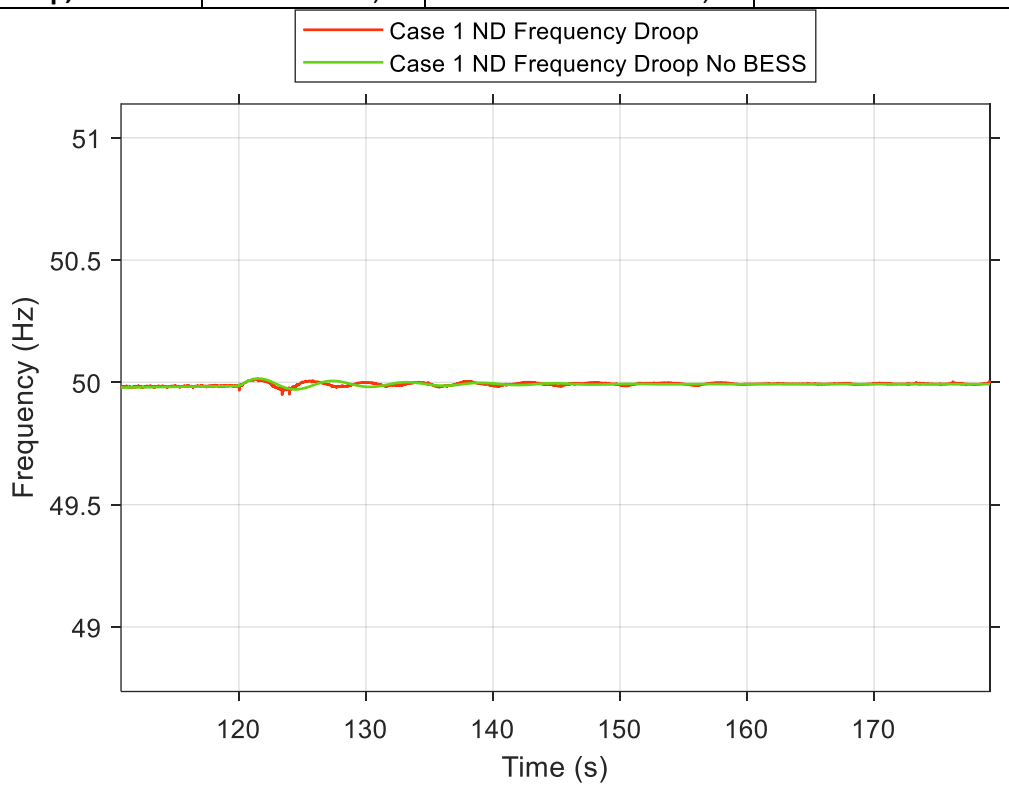

Figure 34. Case 1 Network link trip.

6.3 Case 2 More Significant Share of Synchronous Generation

This chapter covers the results gained from the simulations of Case 2. Because of the addition of IBG in Case 2, the event of the largest inverter-based generation tripping is also simulated. It also adds the possibility of simulating the frequency behavior in these events under the conditions when either photovoltaic or wind energy is unavailable. In the case of wind energy, it also simulates the situation when the wind speed exceeds the upper cutoff limit on the wind turbines.

Based on the results gained from the following load tripping event simulation in this case and the results from Case 1, the droop control method is chosen as the most suitable control method for the engine power plants and is, for this reason, used to control the EPPs in Case 2 simulations.

The implementation of IBG also introduces the importance of spinning reserve to operate the microgrid reliably under conditions where either wind, solar, or both are not available. Without sufficient spinning reserve, a blackout is to be expected. Load shedding can be implemented as an emergency measure, but it cannot be utilized for a more extended period. Also, it is not a desirable solution from an economic point of view, and it, for this reason, is not considered in this study.

6.3.1 Case 1 The Largest Load Tripped

Simulations in Case 2 are started with the load tripping event. First, the first simulation runs are done in ideal conditions, operating the EPP's speed control in both; droop and isochronous mode. It is done to define the control method for the rest of the simulation cases. The results from these simulations are shown in **Table 12** and **Figure 35**. When comparing the results with each other, it can be said that the difference is almost negligible. The configuration with droop control mode has more oscillation before reaching the stabilizing, which could be decreased with proper controller tuning. Since the difference between these control methods is minor, the droop control is chosen to be used

for the rest of the simulations. With this choice, the simulation configurations are more consistent and easier to compare.

Table 12. Case 2 the largest load trip.

Configuration	Freq. peak (Hz)	Max freq. deviation (Hz)	Freq. peak reached (s)
Droop, Ideal	51,38	1,38	121,05
Droop, no BESS	52,06	2,06	121,30
Droop, no PV	51,46	1,46	121,04
Droop, no WT	51,14	1,14	120,75
Isochronous, Ideal	51,39	1,39	121,03

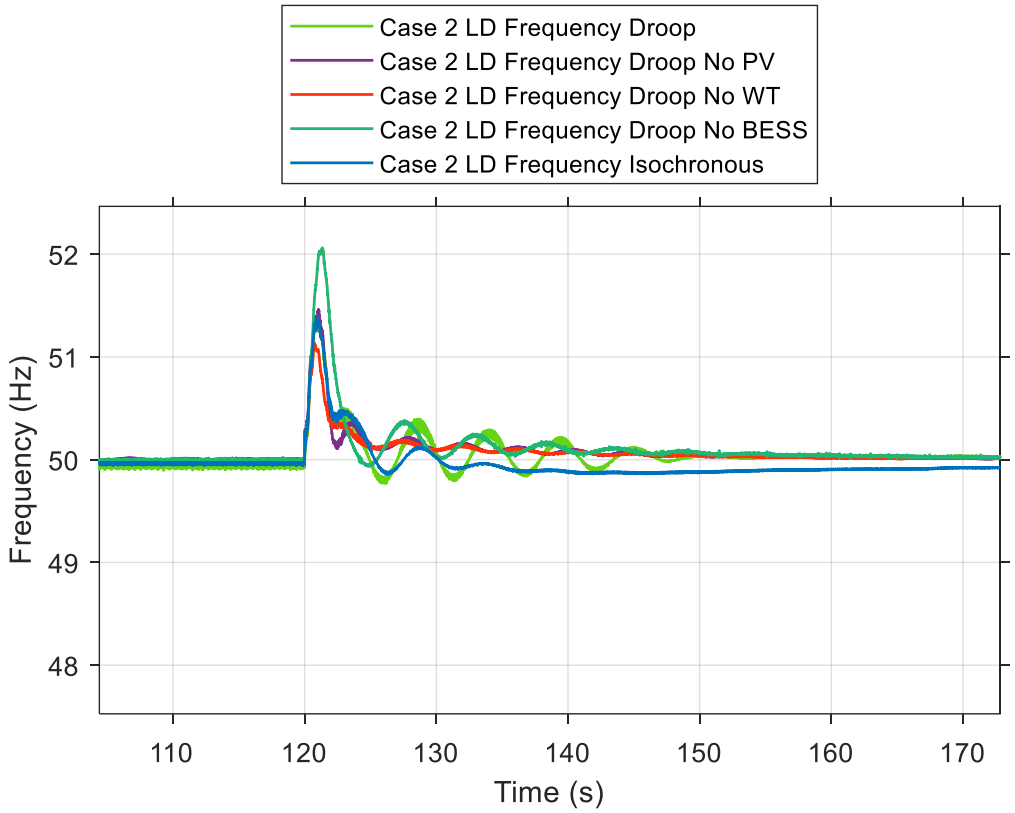

Figure 35. Case 2 the largest load trip.

6.3.2 Case 2 The Largest Synchronous Generation Trip

The results from the event of the largest synchronous generation tripping in Case 2 are shown in **Table 13** and **Figure 36**. Without wind or photovoltaic energy, the microgrid frequency became unstable due to the EPP's under-voltage protection tripping. Due to this reason, the protection functions are disabled.

Under the ideal conditions with droop control, the frequency drops by -1,26 Hz, which is within acceptable limits. This situation changes if the microgrid does not have frequency support from the BESS. In that case, the maximum deviation is over double (113,5 %) with a -2,69 Hz drop in frequency. This significant deviation is not acceptable according to the limits set.

Table 13. Case 2 the largest synchronous generation trip.

Configuration	Freq. nadir (Hz)	Max freq. deviation (Hz)	Freq. nadir reached (s)
Droop, Ideal	48,74	-1,26	120,70
Droop, no BESS	47,31	-2,69	121,39
Droop, no PV*	47,89	-2,11	121,01
Droop, no WT*	48,84	-1,16	120,72

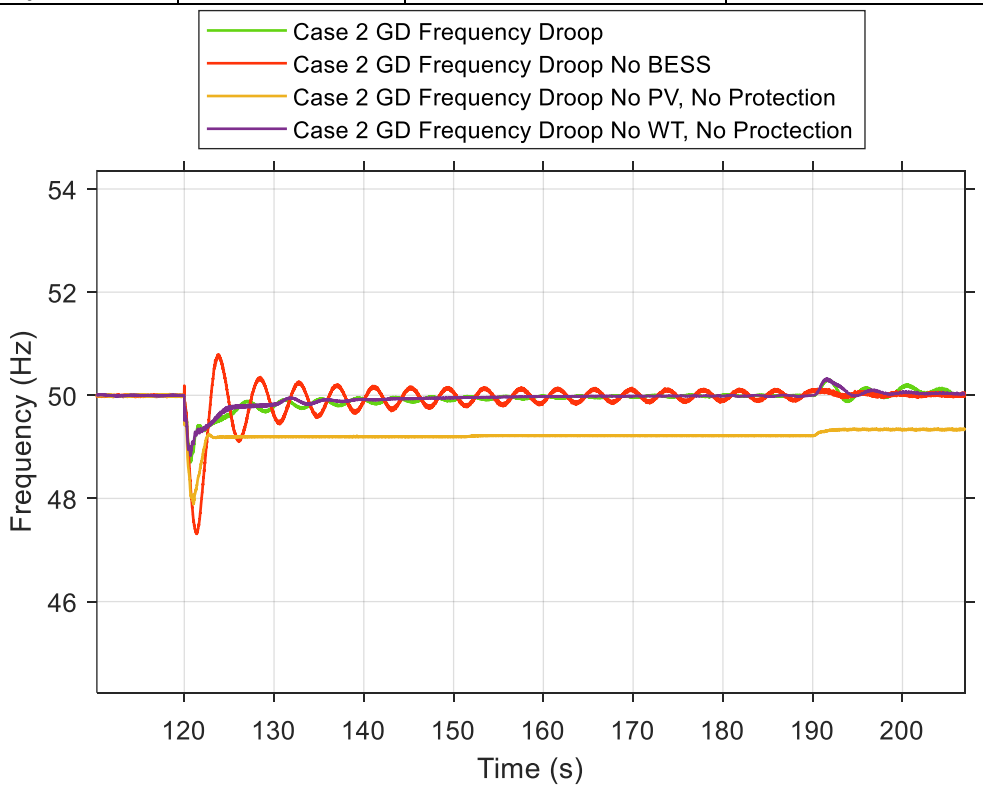

Figure 36. Case 2 the largest synchronous generation trip.

The best frequency response in this event is achieved under the condition of no wind energy with the voltage protection disabled. It is possible because all the remaining generation units contribute to the frequency support under this condition.

Under the condition of unavailable photovoltaic energy, the frequency drops to the value of 47,89 Hz. After the initial frequency response, the frequency stabilizes to 49,2 Hz. The microgrid frequency cannot be brought back to the nominal frequency of 50 Hz due to

the insufficient spinning reserve. However, 49,2 Hz is still within the normal operating frequency, so this result is considered acceptable. In this kind of situation, the frequency can be brought back to nominal by increasing the synchronous generation by activating one of the additional generators in one of the EPPs.

6.3.3 Case 2 The Largest Inverter-Based Generation Trip

In the event of the largest IBG trip in Case 2, all the simulation runs are within the acceptable limits. These results are shown in **Table 14** and **Figure 37**. The simulation run without wind energy was done by opening the outgoing breaker from the PVPP. The best frequency response was achieved, as expected, in the ideal conditions. In this case, the maximum frequency deviation was 67,3 % larger in the case without BESS than with BESS.

The condition without PV or WT is similar in terms of available spinning reserve after the event since only synchronous generation and BESS are left. The configuration without PV has a 28,8 % larger frequency peak value than in ideal conditions, and the configuration without WT has a 19,2 % larger maximum frequency deviation. Since the frequency response should be identical based on the available generation units, the different connection points can explain this change in frequency.

Table 14. Case 2 the largest inverter-based generation trip.

Configuration	Freq. nadir (Hz)	Max freq. deviation (Hz)	Freq. nadir reached (s)
Droop, Ideal	48,96	-1,04	120,75
Droop, no BESS	48,26	-1,74	121,33
Droop, no PV	48,66	-1,34	120,76
Droop, no WT	48,80	-1,20	120,73

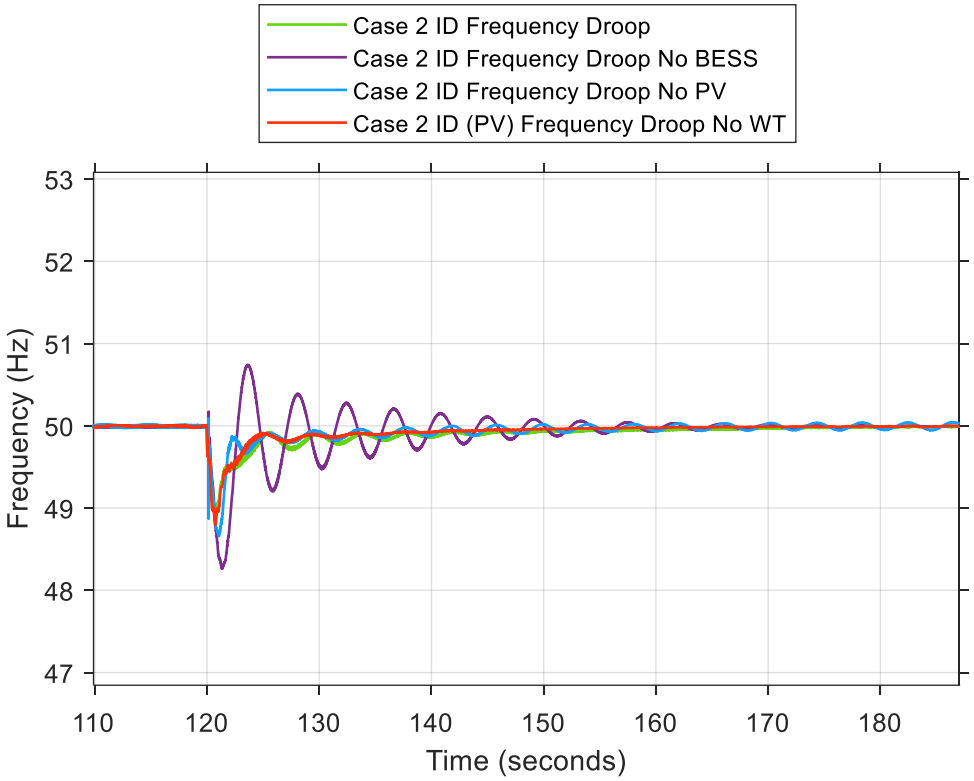

Figure 37. Case 2 the largest inverter-based generation trip.

6.3.4 Case 2 Network-Link Tripped

The results of network-link tripping on Case 2 are shown in **Table 15** and **Figure 38**. From these results, an observation can be made that the best frequency response is achieved under the conditions where wind energy is absent. When the wind energy is absent, the load is shared between the remaining generation units, which are all capable of active frequency control. In all the cases, the frequency deviation is so minimal that most of the frequency response is handled by the EPP droop because IBG control systems do not react until the deviation exceeds their dead band.

Table 15. Case 2 network-link trip.

Configuration	Freq. nadir (Hz)	Max freq. deviation (Hz)	Freq. nadir reached (s)
Droop, Ideal	49,75	-0,25	121,52
Droop, no BESS	49,76	-0,24	121,60
Droop, no PV	49,82	-0,18	121,91
Droop, no WT	49,95	-0,05	120,94

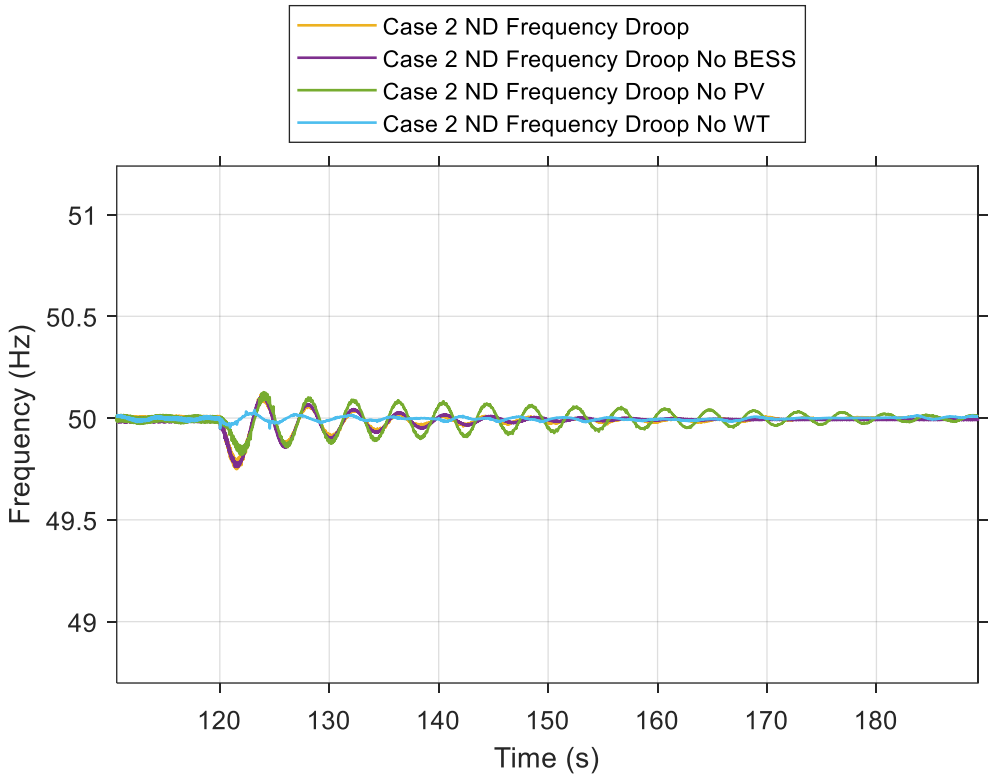

Figure 38. Case 2 network-link trip.

6.4 Case 3 More Significant Share of Inverter-Based Generation

In this chapter, the results from Case 3 are discussed and analyzed. The results from these simulations present the challenges we come across when the share of IBG in power generation passes the share of synchronous generation. In Case 2, some events in the microgrid caused significant instabilities because of the insufficient spinning reserve. However, from this case's results, the importance of the spinning reserve does become evident. The absence of photovoltaic energy in Case 3 means the absence of 50 MW power generation. It will cause the simulations to become unstable before they reach the time when the event happens in the microgrid.

6.4.1 Case 3 The Largest Load Trip

Simulations in Case 3, load tripping events, were started with a comparison between the EPP droop and isochronous control to decide the control method for the rest of the configurations. The results for this event are shown in **Table 16** and **Figure 39**. The results

show that droop control offers a better frequency response from these two, with a maximum frequency deviation of 1,34 Hz. However, the difference between these two control methods is minimal since the maximum frequency deviation with isochronous control is only 1,5 % larger than with the droop control. For this reason, it is chosen for the other three simulations.

The condition with no wind energy shows us a good example of the possibilities the grid-forming inverters bring for frequency support since the best frequency response is achieved under these conditions. More specifically, the highest frequency deviation in this condition is only 0,94 Hz. This difference can be explained because all the generation units offer active frequency support in this condition. This result also shows the importance of frequency support functions in the microgrid.

Table 16. Case 3 the largest load trip.

Configuration	Freq. peak (Hz)	Max freq. deviation (Hz)	Freq. peak reached (s)
Droop, Ideal	51,34	1,34	120,69
Droop, no BESS*	52,42	2,42	121,14
Droop, no PV*	48,66	-1,34	120,47
Droop, no WT	50,94	0,94	120,45
Isochronous	51,36	1,36	120,72

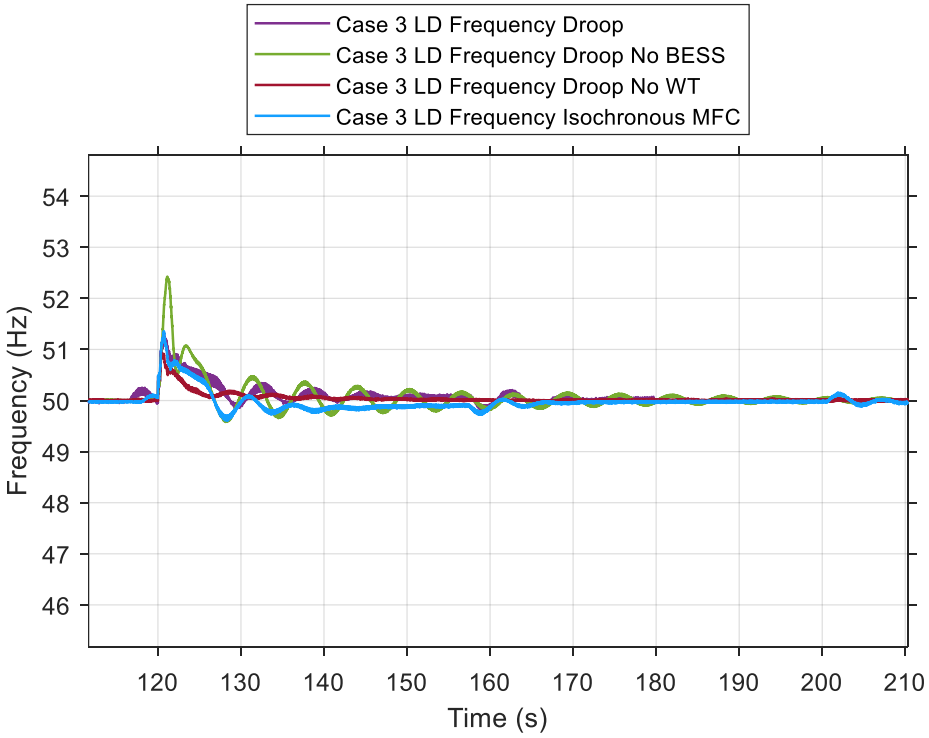

Figure 39. Case 3 the largest load trip.

Under the condition of unavailable photovoltaic energy, the microgrid will trip after 90 s due to the microgrid voltage dropping under the 0.9 pu for 10 seconds. Since this study does not focus on voltage stability, voltage protection can be disabled. With the voltage protection turned off, the system is stable but does not have enough generation, and the frequency cannot reach the nominal frequency of 50 Hz before the event, but it stabilizes to 47,5 Hz. After the event, the frequency peak goes to 48,66 Hz, but it is too large for the microgrid and becomes unstable. **Figure 40** shows the frequency curve from the case with unavailable photovoltaic energy.

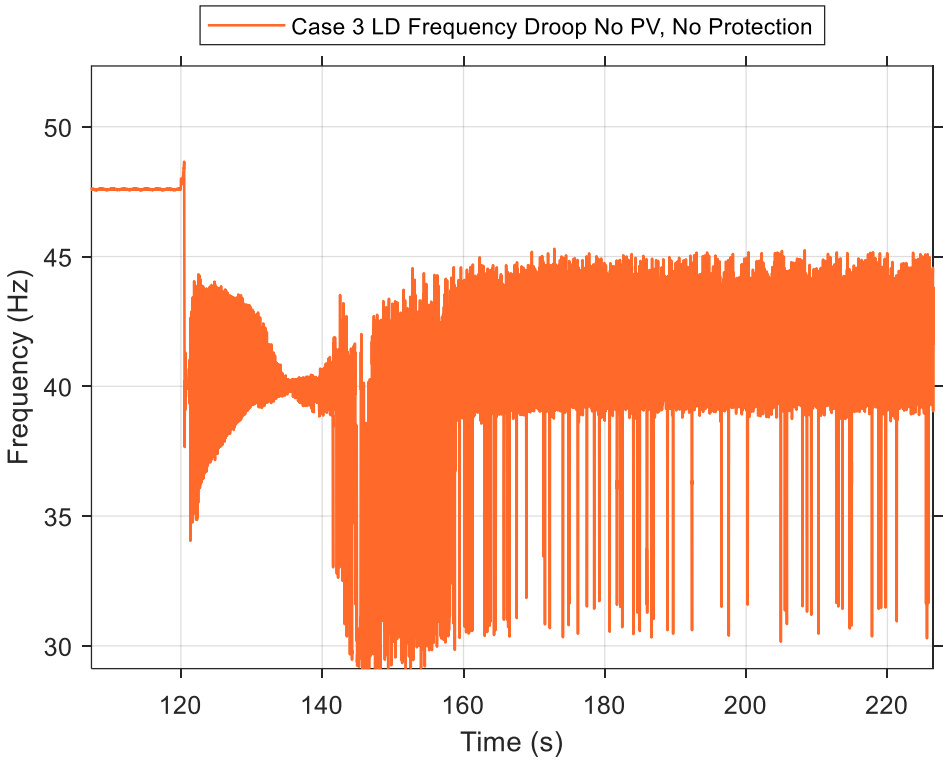

Figure 40. Case 3 the largest load trip – Without photovoltaic energy

6.4.2 Case 3 The Largest Synchronous Generation Trip

The largest synchronous generation trip event results are shown in **Table 17**, **Figure 41**, and **Figure 42**. The best frequency response, and only acceptable, was achieved under the ideal condition in this event. In this condition, the system's frequency deviation was only 0,99 Hz. The frequency support provided by the BESS is significant. The frequency deviation without the BESS is 206 % larger than under the ideal conditions.

Table 17. Case 3 the largest synchronous generation trip.

Configuration	Freq. nadir (Hz)	Max freq. deviation (Hz)	Freq. nadir reached (s)
Droop, Ideal	49,01	-0,99	120,87
Droop, no BESS*	46,97	-3,03	121,53
Droop, no PV*	**UNSTABLE**		
Droop, no WT*	48,97	-1,03	120,42

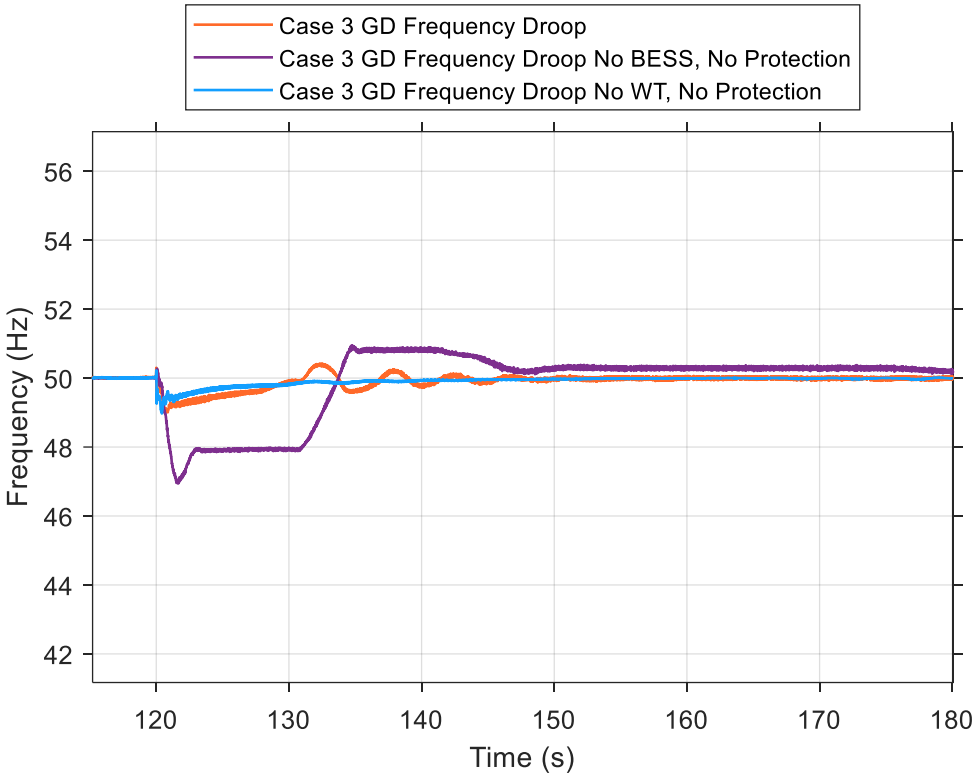

Figure 41. Case 3 the largest synchronous generation trip.

Without the photovoltaic energy the unbalance between generation and demand becomes too large and the system becomes unstable. Under the condition of no wind energy available, the system can bring the frequency back to the nominal value, and the maximum frequency deviation is only 4 % larger than under ideal conditions. However, the RoCoF of 2,45 Hz/s exceeds the acceptable limit of 2 Hz/s.

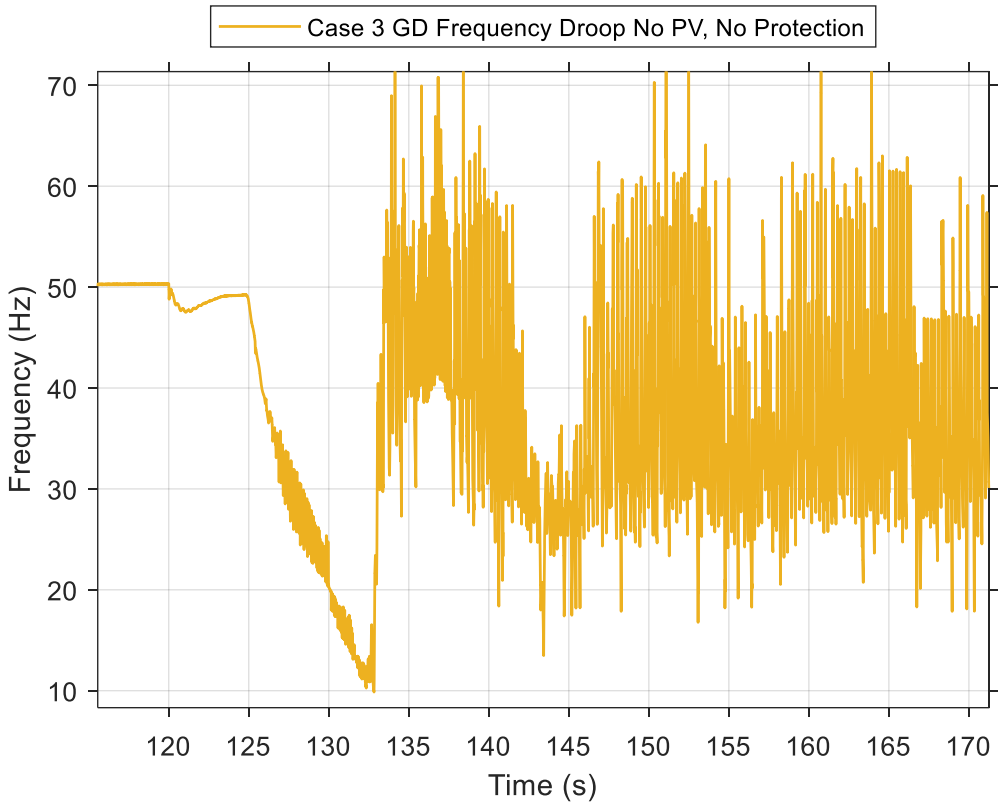

Figure 42. Case 3 the largest synchronous generation trip – photovoltaic energy unavailable.

6.4.3 Case 3 The Largest Inverter-Based Generation Trip

In the following simulations of the largest IBG tripping event, the EPPs were controlled in the droop control mode based on the previous Case 1 and Case 3 load trip event results. All the results from these simulations are shown in **Table 18** and **Figure 43**.

In the simulation where wind energy is not available, one of the PVPP was tripped. Again, in the condition of no photovoltaic energy, the EPP voltage protection is tripped and becomes unstable after 90 s. For this reason, the protection functions are disabled.

The best frequency response was achieved under the ideal conditions, where the system was able to limit the frequency drop to 0,75 Hz. Compared to the synchronous generation trip event, the frequency response was 24,2 % better in the IGB tripping event. In this event, the BESS improves the frequency response by 13%. In terms of hertz, it only

means 0,12 Hz since the frequency deviation is relatively small in the first place, and BESS's frequency support function does not activate for an extended period.

Without wind energy, the frequency deviation is 54,7 % larger than in the ideal condition with the frequency nadir of 48,84 Hz. Even though this frequency value is still well within the stability limits, the RoCoF of 2,63 Hz/s is over the limit. For this reason, this simulation is considered unsuccessful.

When the photovoltaic energy is unavailable, the system cannot bring the frequency to the nominal value of 50 Hz before the event but stabilizes to 49,1 Hz. After the event, the unbalance between generation and demand becomes too large, and the system becomes unstable.

Table 18. Case 3 the largest inverter-based generation trip.

Configuration	Freq. nadir (Hz)	Max freq. deviation (Hz)	Freq. nadir reached (s)
Droop, Ideal	49,25	-0,75	120,99
Droop, no BESS	49,13	-0,87	121,60
Droop, no PV*	**UNSTABLE**		
Droop, no WT	48,84	-1,16	120,44

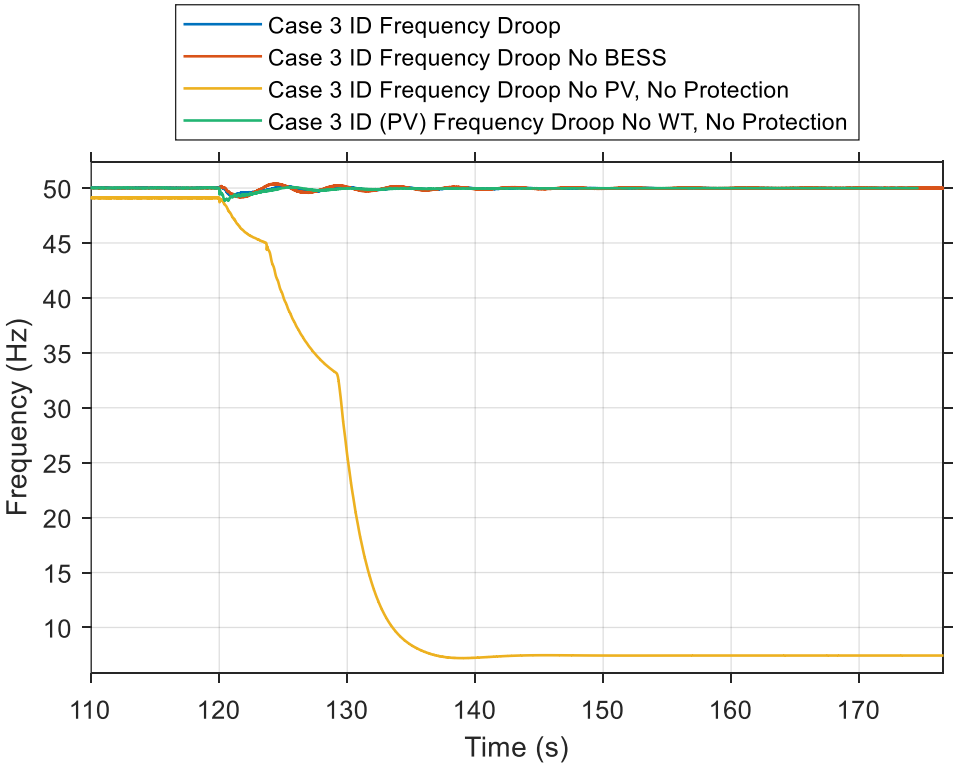

Figure 43. Case 3 the largest inverter-based generation trip.

6.4.4 Case 3 Network-Link Trip

The Case 3 network-link trip event results are shown in **Table 19** and **Figure 44**.

The configuration without PV will again trip due to the under-voltage after the 90 seconds simulation time. For this reason, the protection functions in the EPP models need to be disabled again.

Table 19. Case 3 network-link trip.

Configuration	Freq. peak (Hz)	Max freq. deviation (Hz)	Freq. peak reached (s)
Droop, Ideal	50,39	0,39	121,01
Droop, no BESS	50,48	0,48	121,43
Droop, no PV*	47,51	0,09	120,02
Droop, no WT	50,13	0,13	121,04

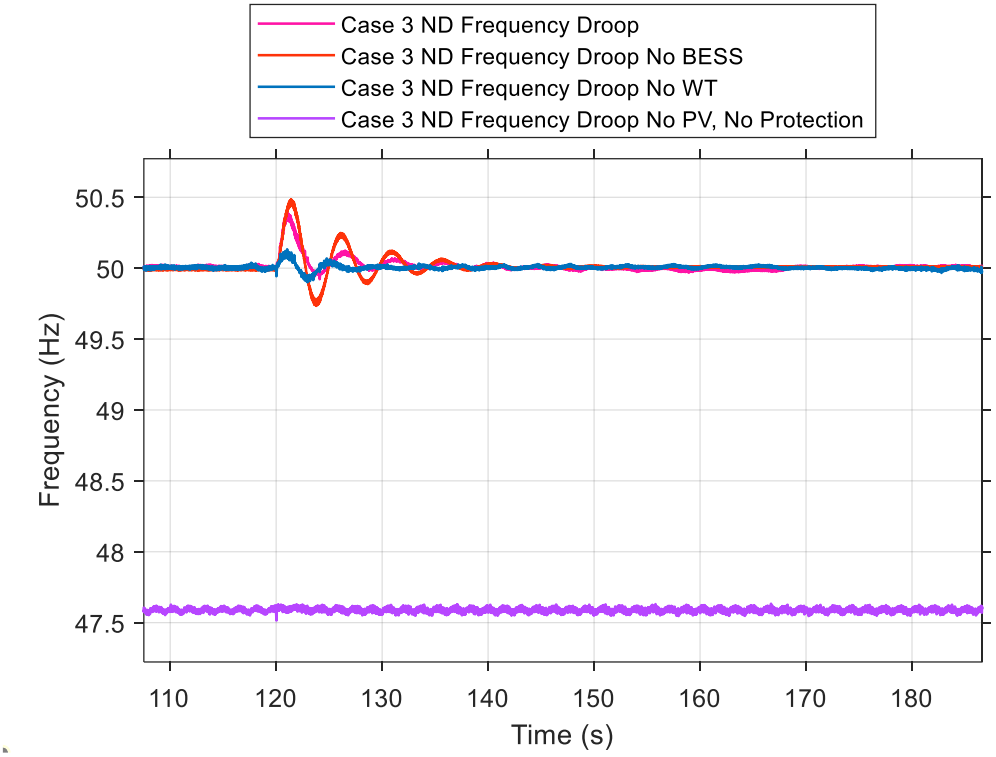

Figure 44. Case 3 network-link trip.

In this event, the most minor frequency deviation was achieved in the case without PV with only 0,09 Hz deviation. However, the system frequency cannot reach the nominal value of 50 Hz before the event due to insufficient generation. The frequency stabilizes to 47,6 Hz, which is unacceptable already before the event.

Under all other conditions, the frequency deviation stays within ±0,5 Hz. The most minor deviation from these is seen in the case without wind energy with only a 0,13 Hz deviation. This happens because the EPPs contribute more to the energy generation and minimize the frequency deviation in this situation. Also, the location of the generation units concerning the network topology change affects this situation. The most significant deviation is seen in the case without BESS, but it is still well within limits with only 0,09 Hz (23,1 %) higher peak value than in the ideal case.

6.5 Comparison between the cases to determine the effect of lower inertia on frequency stability

In this chapter, simulation cases are compared with each other to create an understanding of the effect that lower inertia has on the microgrid. Differences are studied by comparing the maximum frequency deviation in different events. As the control methods for this comparison, the following control methods are chosen to limit the number of comparisons to a reasonable amount:

- Engine power plants: Droop control
- Photovoltaic power plant: Frequency-watt
- Wind power plant: MPPT
- BESS: Frequency-watt

In these comparisons, the active power curves from each generation unit are added to give better visualization and understanding of their contribution to the frequency support.

6.5.1 The Largest Load Tripped Comparison

First, an event is studied where the largest load is tripped on bus 3 of the microgrid. In the following **Table 20** and **Figure 45**, the frequency behavior of each case is compared with each other. As expected, the best frequency response is achieved in Case 1. The

frequency peak value of 50,97 Hz in Case 1 is 0,37 Hz lower than in Case 2 and 0,41 Hz lower than in Case 3.

The 40 % decrease in inertia from Case 1 to Case 2 caused a 42,2% increase in maximum frequency deviation compared to Case 1. Furthermore, in the case of Case 3, the decrease in inertia is 60 %, but the change in maximum frequency deviation is smaller, with only a 38,1 % increase compared to Case 1. From these results can be seen that the control systems implemented in PV and BESS systems are acting fast, bringing almost physical inertia level frequency support for the microgrid.

Table 20. Comparison between each case in the largest load trip event.

Configuration	Freq. peak (Hz)	Max freq. deviation (Hz)	Freq. peak reached (s)
Case 1	50,97	0,97	121,03
Case 2	51,38	1,38	121,05
Case 3	51,34	1,34	120,69

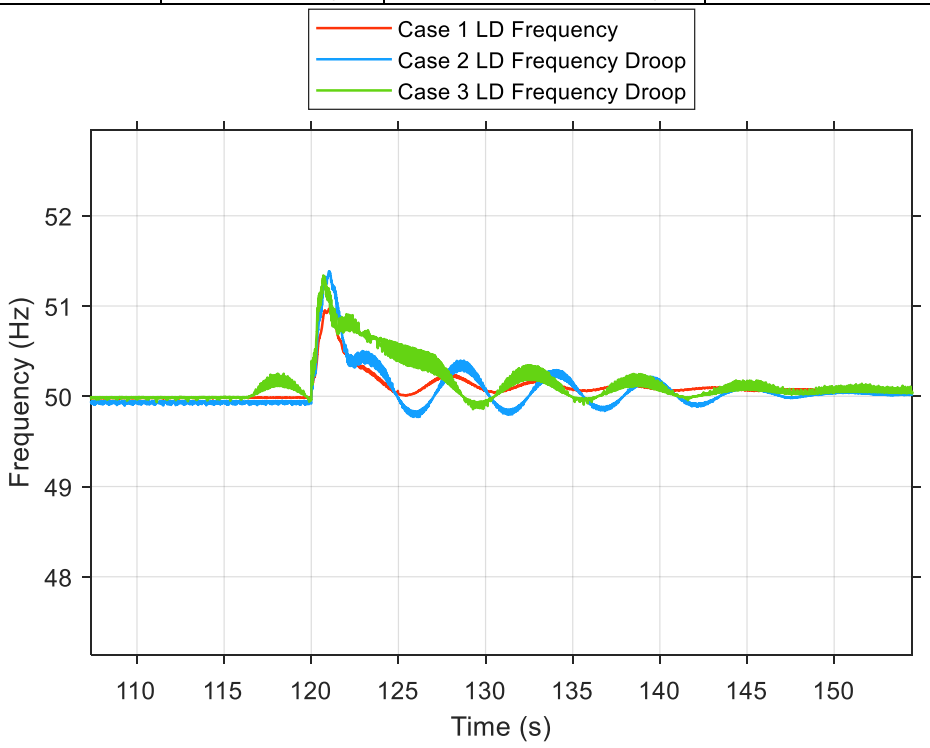

Figure 45. Comparison between each case in the largest load trip event.

In **Figure 46**, **Figure 47**, and **Figure 48** is shown the active power curves from each generation unit. The graphs show how the BESS supports the frequency by acting as load. In

Case 3, the BESS consumes almost 15 MW of active power to replace the tripped load and to resist the frequency deviation. After the event, the EPPs will decrease their output to regain the balance in the system. The active power output of the IBG-units stays close to the same as before the event.

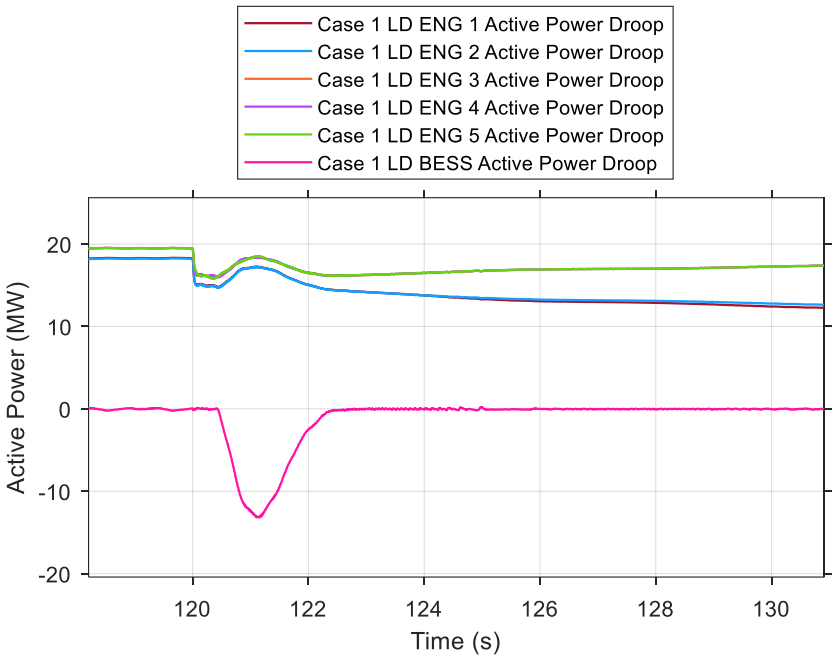

Figure 46. Case 1 active power curve in the largest load trip event.

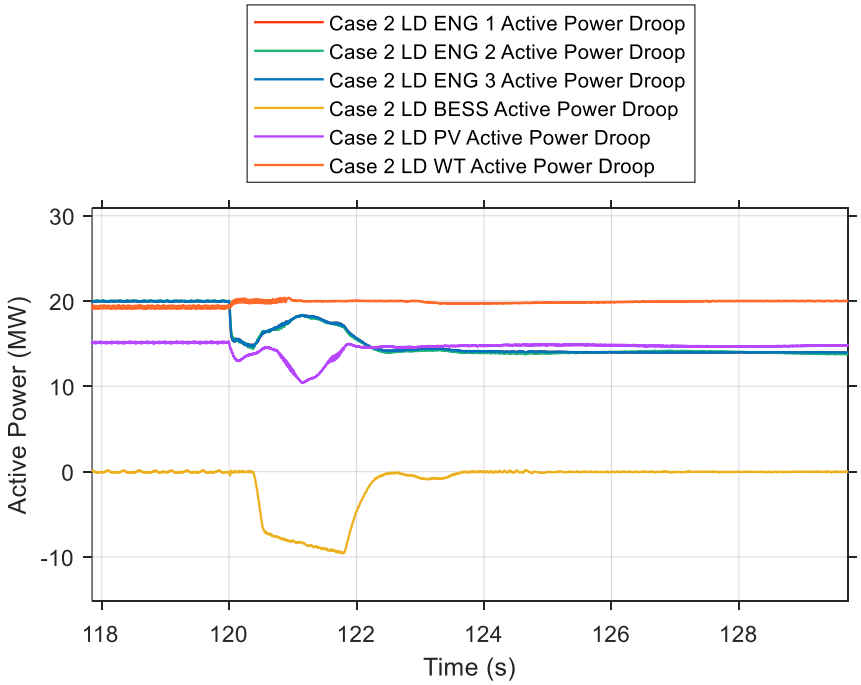

Figure 47. Case 2 active power curve in the largest load trip event.

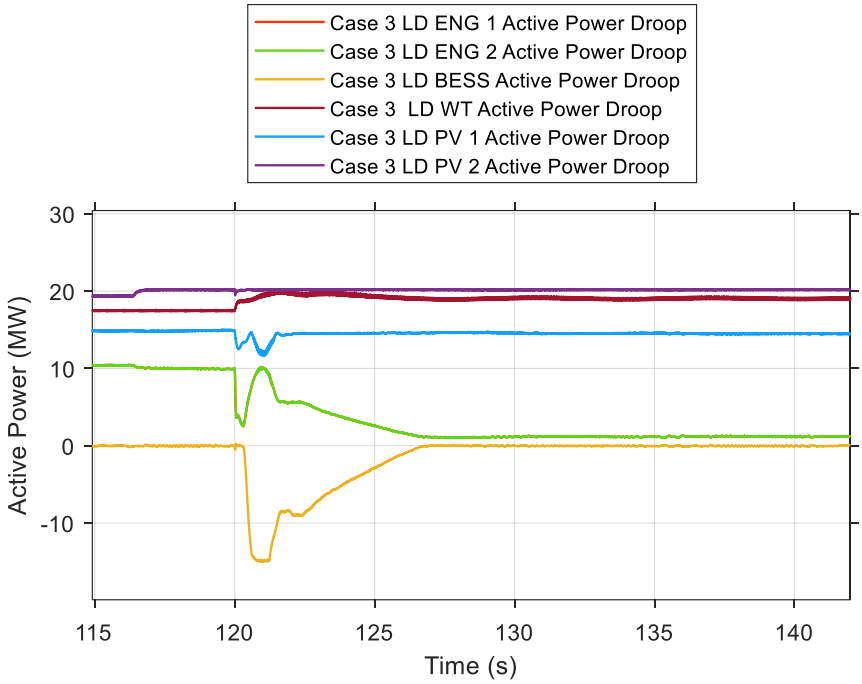

Figure 48. Case 3 active power curve in the largest load trip event.

That to be said, even though the difference in maximum frequency deviation between Case 2 and 3 is almost negligible, Case 3 has a higher ROCOF than Case2. The higher inertia in Case 2 can explain this difference. Even though the droop control system implemented in PV and BESS inverters is fast, they cannot release power instantly to the physical inertia created by the kinetic energy in synchronous machines.

6.5.2 The Largest Synchronous Generation Trip Comparison

This chapter compares the frequency response between Cases 1, 2, and 3 to study the effect of lower inertia in the under-frequency situation. These results are shown in **Table 21** and **Figure 49**. In this simulation scenario, the EPP connected to Bus 3 of the microgrid is tripped at the 120 s mark. Active powers from each generation unit in each case are shown in **Figure 50**, **Figure 51**, and **Figure 52**.

Table 21. Comparison between each case in the largest synchronous generation trip event.

Configuration	Freq. nadir (Hz)	Max freq. deviation (Hz)	Freq. nadir reached (s)
Case 1	48,95	-1,05	120,75
Case 2	48,74	-1,26	120,71
Case 3	49,01	-0,99	120,85

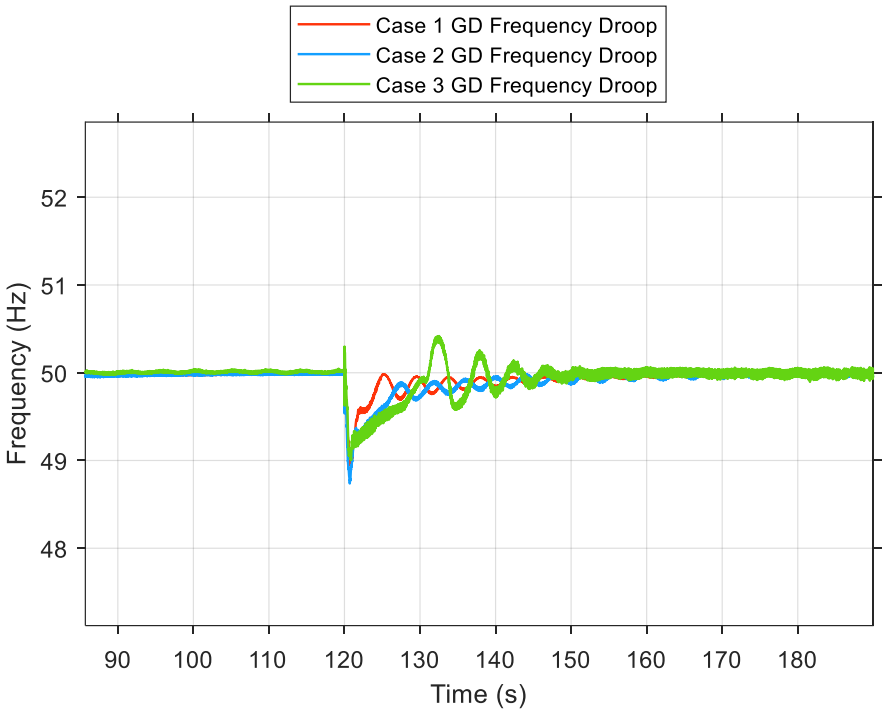

Figure 49. Comparison between each case in the largest synchronous generation trip event.

In all cases, the frequency stayed within the set under-frequency limits. However, Case 1 is expected to give the best frequency response, but surprisingly the best frequency response is achieved in Case 3 with only a 0,99 Hz deviation. The frequency nadir value of 49,01 Hz is reached 0,85 seconds after the event. After the governor response, the frequency overshoots slightly, but this oscillation can be minimized with proper primary controller tuning. This result is a prime example of the frequency support achieved with the grid-forming inverters in the ideal conditions. In Case 1, the frequency deviation was 6,1 % higher than in Case 3. The most significant frequency drop happened in Case 2, which had a 27,3 % larger deviation than Case 3. The active power curve shows that the BESS contributes to the frequency support by increasing its active power output significantly. In Case 2, the active power output from the BESS is the highest because of the most significant frequency deviation. After the frequency has reached the nominal value, the BESS does not release any active power to the microgrid. From these curves can also be seen that the remaining EPPs will increase their active power output to meet the demand in the steady-state after one of the EPPs has tripped in addition to the initial frequency response.

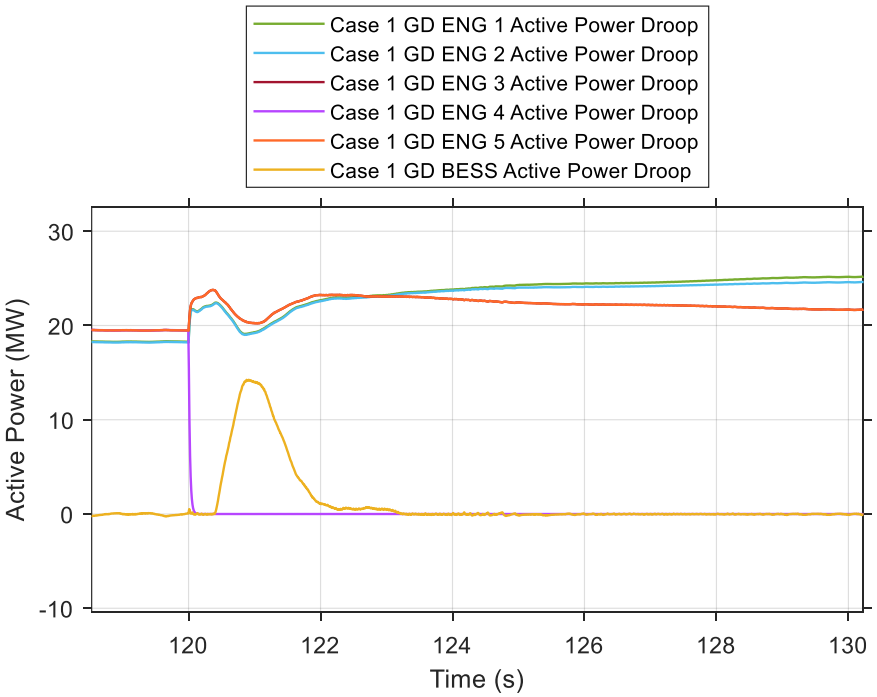

Figure 50. Case 1 active power curve in the largest synchronous generation trip event.

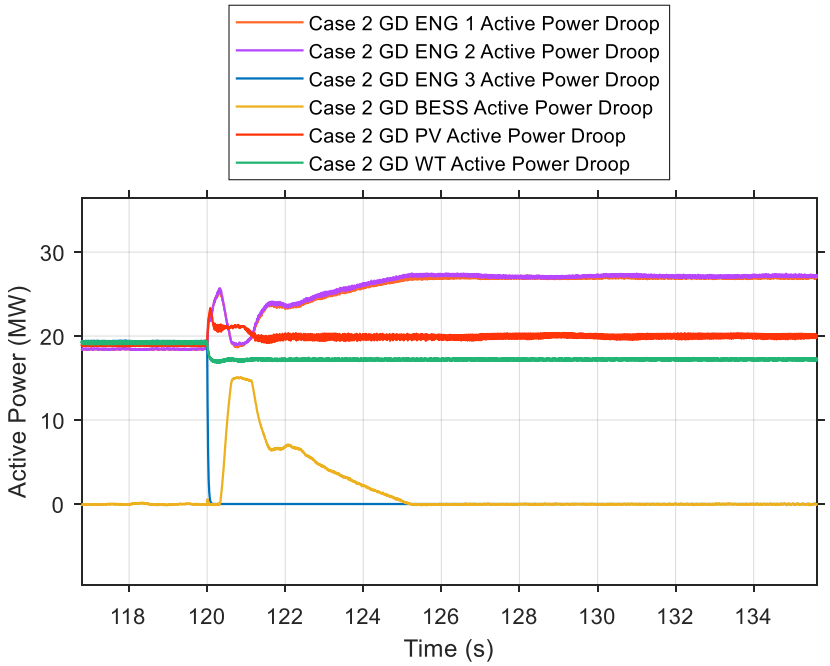

Figure 51. Case 2 active power curve in the largest synchronous generation trip event.

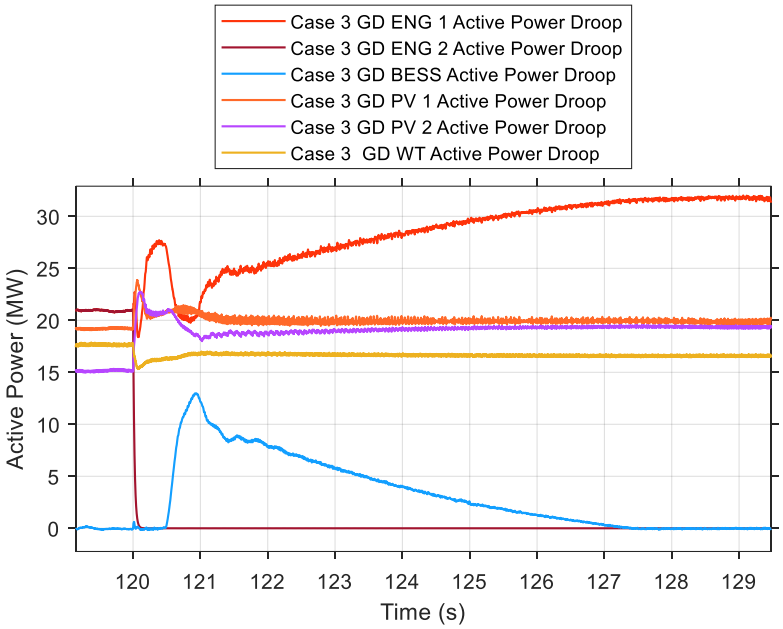

Figure 52. Case 3 active power curve in the largest synchronous generation trip event.

6.5.3 The Largest Inverter-Based Generation Trip Comparison

The largest IGB tripping event can only be compared between Case 2 and Case 3 because Case 1 does not have any inverter-based generation implemented into the system. Both of these cases managed to stay within the frequency limits set for this study. These results from the comparison are shown in **Table 22** and **Figure 53**. From these results can be seen that even though Case 3 has 50 % less inertia coupled into the microgrid, it still manages to limit the frequency drop more than in Case 2. After the event, Case 2 has three EPPS, one PVPP, and one BESS contributing to the frequency support, while in Case 3, there is only 2 EPPS with 2 PVPP and one BESS. This shows that the PVPP can provide even better frequency support than an EPP in these ideal conditions.

Table 22. Comparison between each case in the largest inverter-based generation trip event.

Configuration	Freq. nadir (Hz)	Max freq. deviation (Hz)	Freq. nadir reached (s)
Case 2	48,96	-1,04	120,75
Case 3	49,25	-0,75	120,99

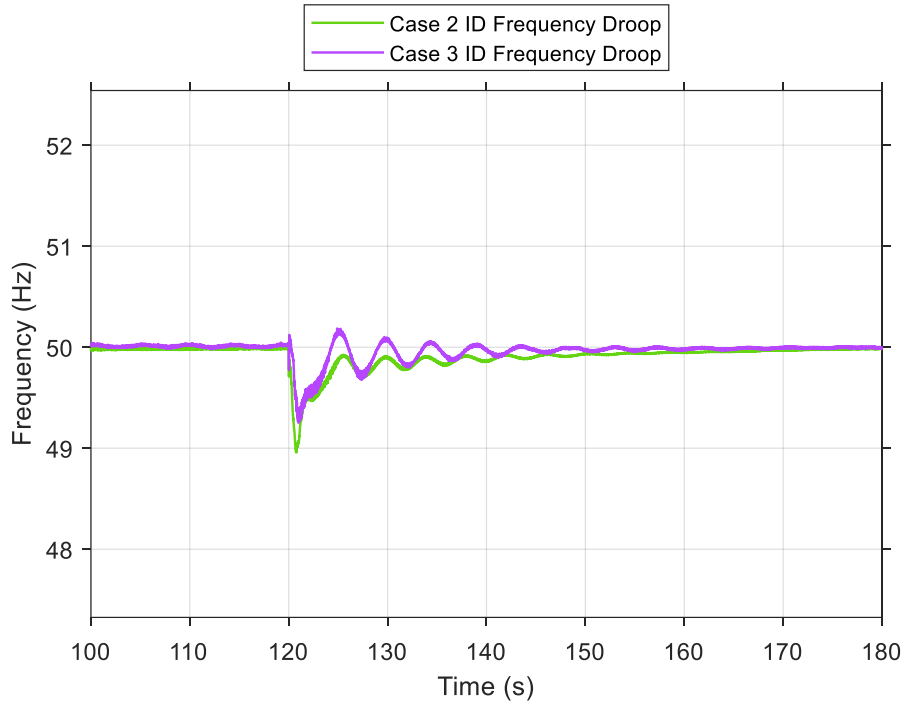

Figure 53. Comparison between each case in the largest inverter-based generation trip event.

The active power output of each generation unit from Case 2 is shown in **Figure 54** and from Case 3 in **Figure 55**. In Case 2, the frequency support from BESS is approximately double compared to Case 3. From Case 3, the almost instantaneous frequency response from the PVPP can also be seen.

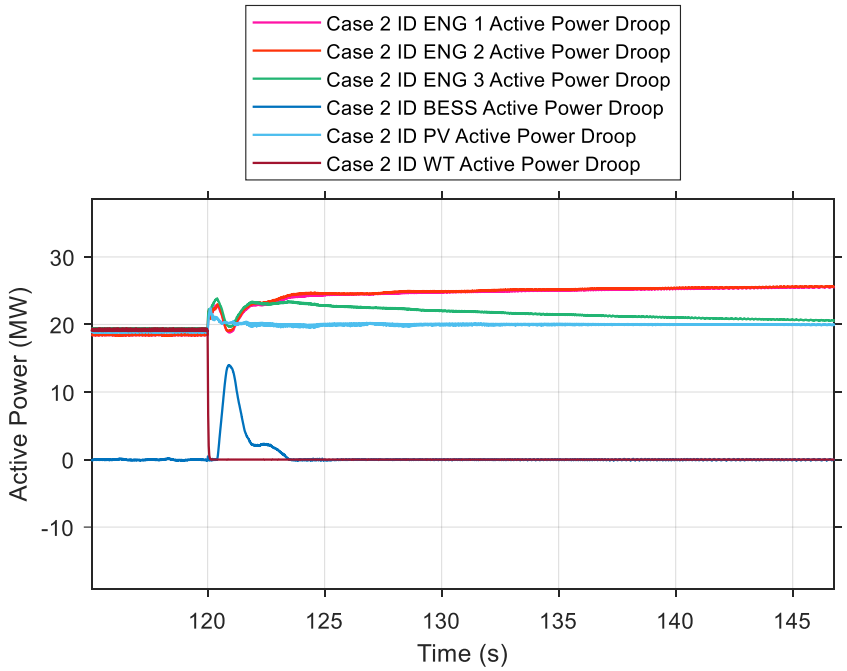

Figure 54. Case 2 active power curve in the largest inverter-based generation trip event.

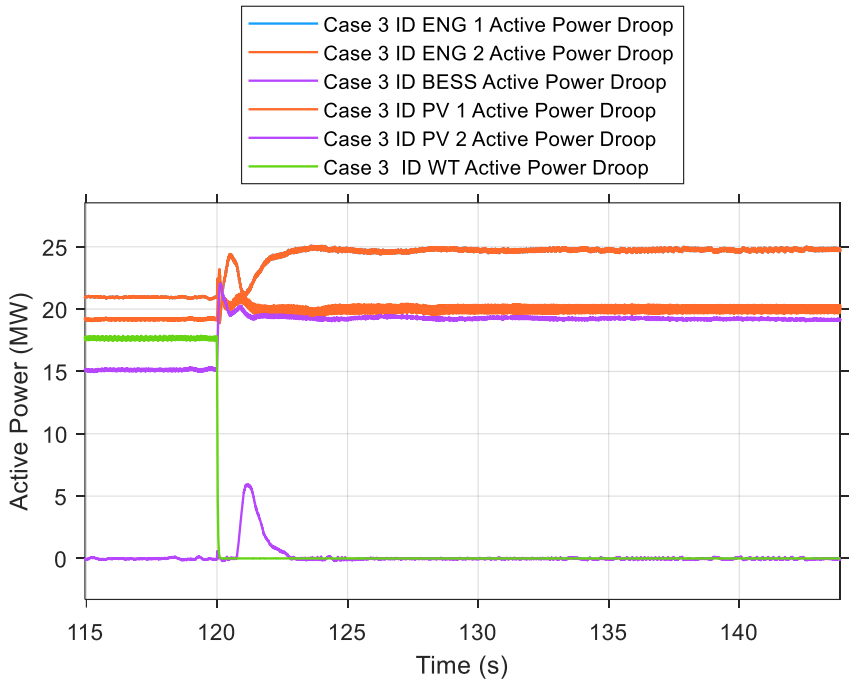

Figure 55. Case 3 active power curve in the largest inverter-based generation trip event.

6.5.4 Network Link Trip Comparison

The network-link trip event comparison results are shown in **Table 23** and **Figure 56**. In the network-link tripping event, the results follow the initial hypothesis that the frequency deviation will increase when inertia is decreased. However, all the simulations are well within the frequency limits.

Table 23. Comparison between each case in the network-link trip event.

Configuration	Freq. peak/nadir (Hz)	Max freq. deviation (Hz)	Freq. nadir reached (s)
Case 1	50,01	0,01	121,15
Case 2	49,75	-0,25	121,52
Case 3	50,39	0,39	121,01

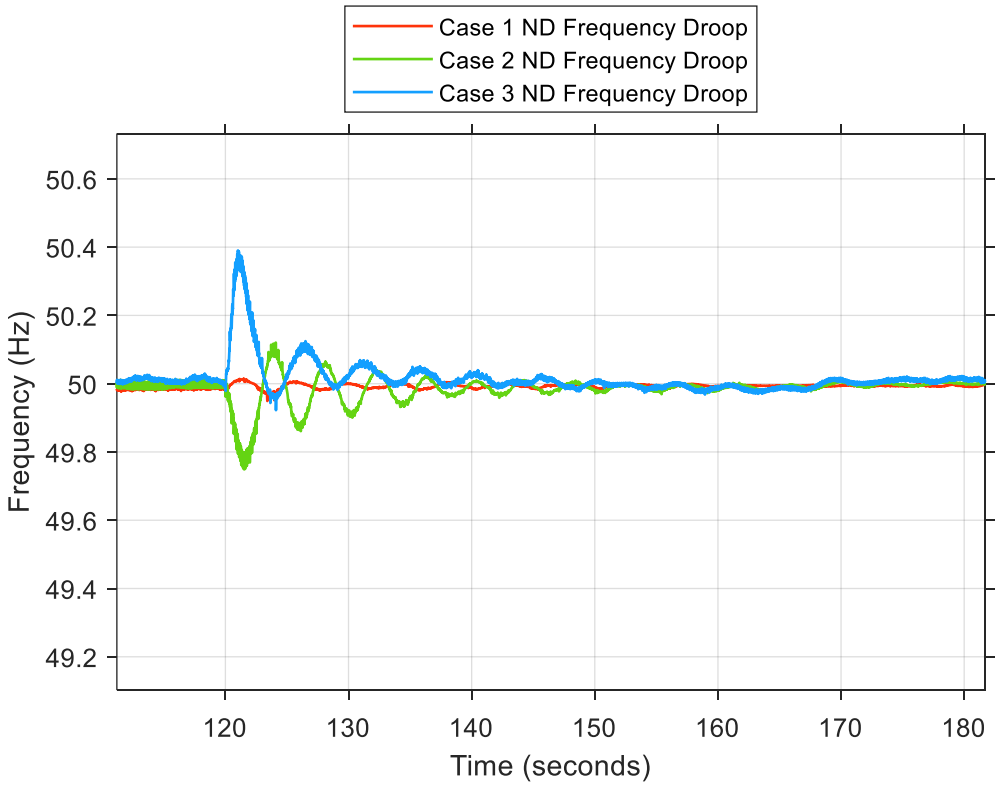

Figure 56. Comparison between each case in network trip event.

Surprisingly, the results show that in Case 2, the network link tripping caused an under-frequency situation, while in Case 3, it caused an over-frequency situation. This shows us that the power flow was more significant through tripped network-link in Case 2 than in Case 3 from the frequency measurement point of view. In Case 1, the deviation is negligible, which shows us the capability of the synchronous generators to resist the frequency deviation.

The active power output from each case and generation unit are shown in **Figure 57**, **Figure 58**, and **Figure 59**. From these graphs can be seen that in Cases 1 and 2, the frequency deviation is so minor that BESS is not activated. However, in Case 3, the over-frequency exceeds the frequency-watt control dead band, and the BESS is acting as a load.

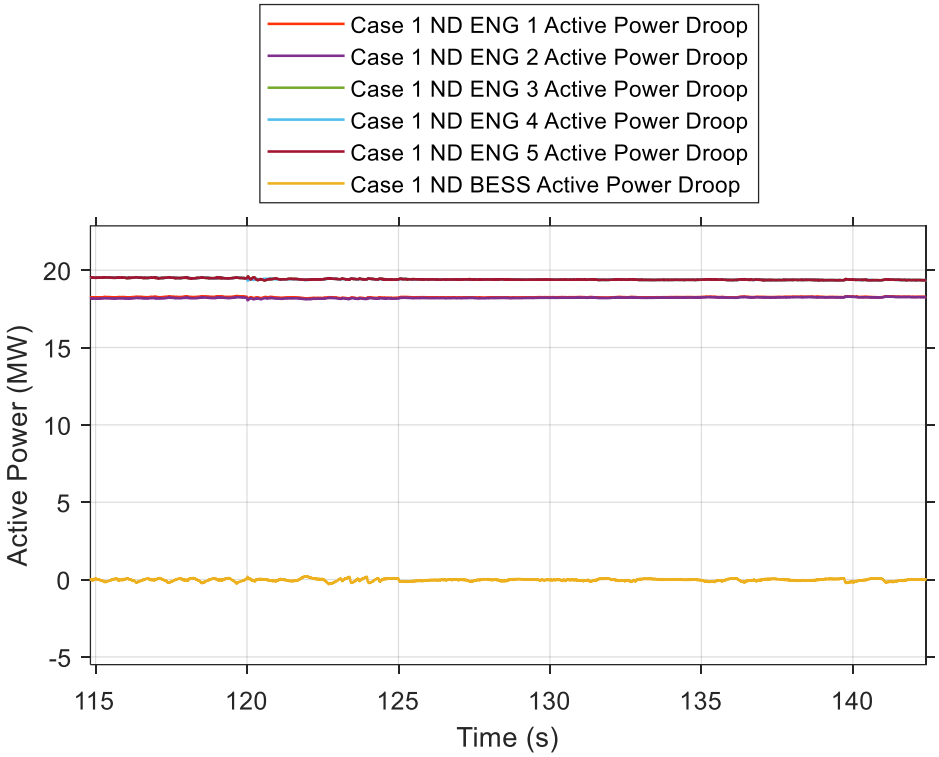

Figure 57. Case 1 active power curve in the network-link trip event.

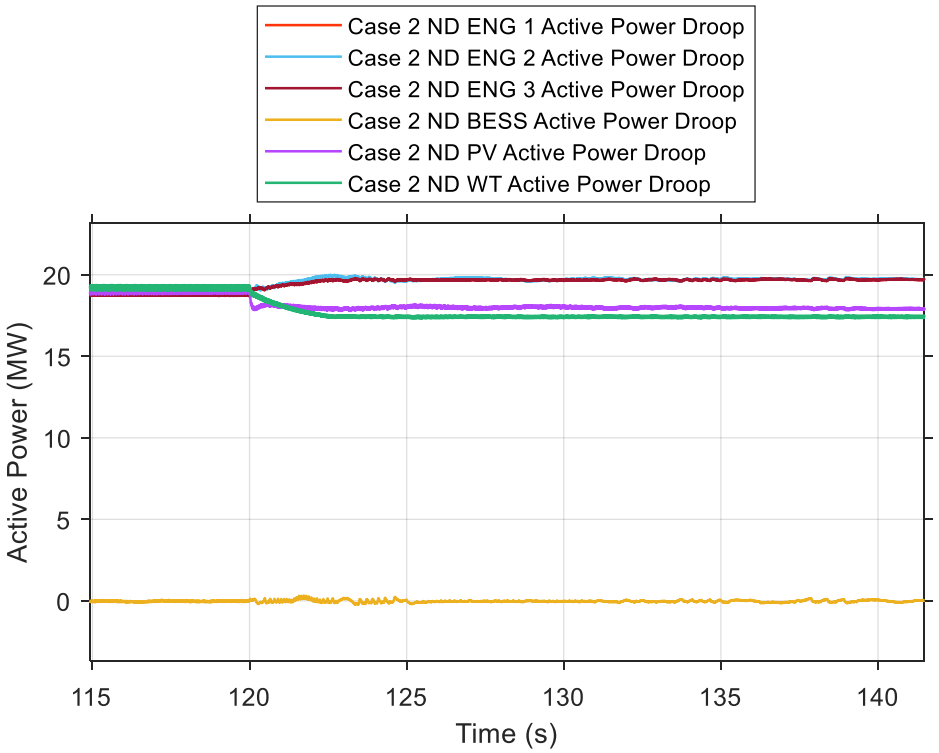

Figure 58. Case 2 active power curve in the network-link trip event.

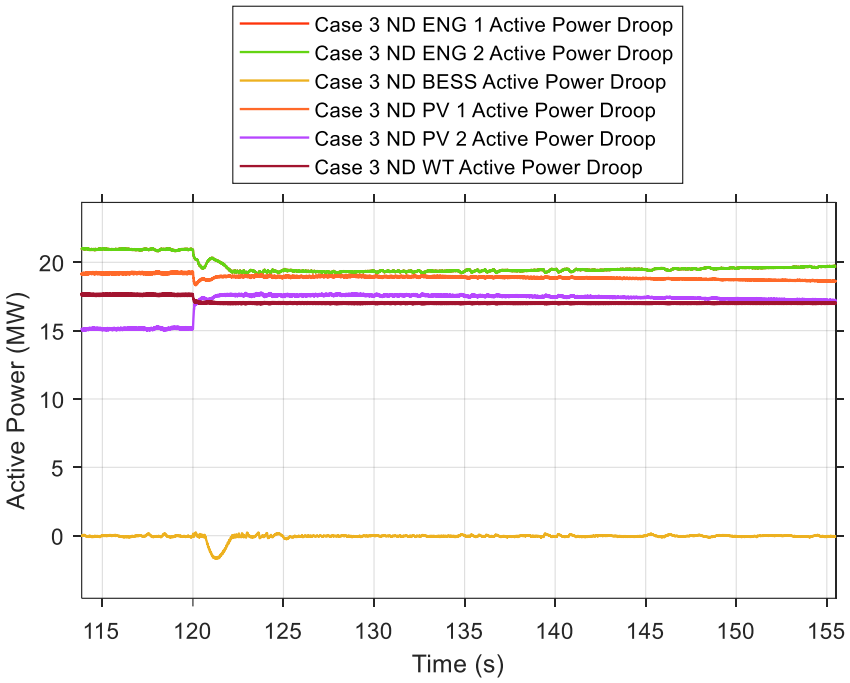

Figure 59. Case 3 active power curve in the network-link trip event.

6.6 PSCAD: Fixed Load Component Problem

An unexpected phenomenon appeared concerning the fixed load component in the simulation models during the result analysis. The loads are not configured to be voltage- or frequency-dependent in these models. However, when analyzing the results, it became evident that the loads are voltage-dependent, as seen in **Figure 60**.

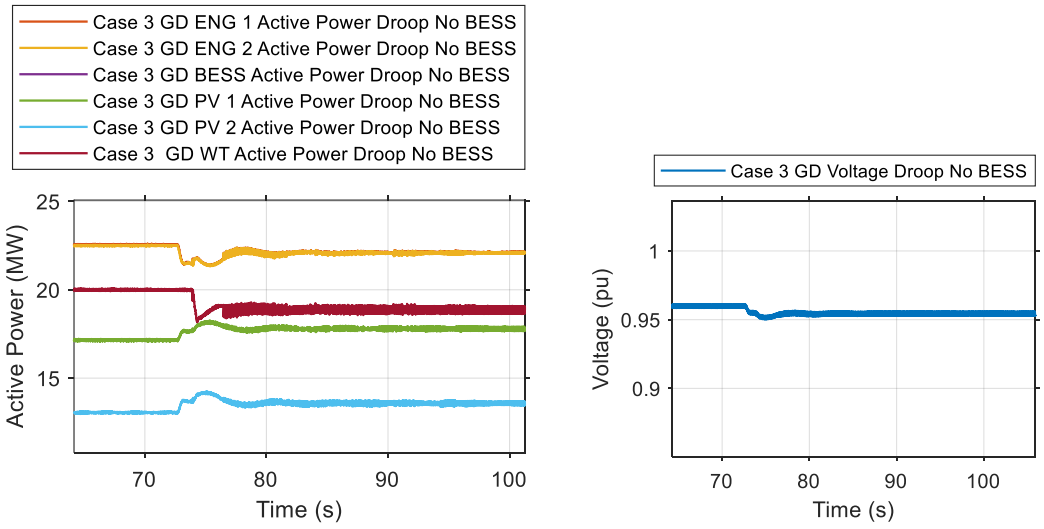

Figure 60. Case 3 active power & voltage.

In the fixed load model, the active power characteristics follow the following equation (PSCAD, n.d.):

$$P = Scale * P_0(1 + K_{PF} * dF) * \left(K_A \left(\frac{V}{V_0}\right)^{NPA} + K_B \left(\frac{V}{V_0}\right)^{NPB} + K_C \left(\frac{V}{V_0}\right)^{NPC}\right) \quad (15)$$

Where NPA, NPB, and NPC are the voltage indices, in which the letters A, B, and C mark the parts of the composite load. A more detailed description of the model characteristics can be found in Appendix 4. **Figure 61** is added as an example to show the load parameters used in the load connected to Bus 3. Here, under coefficients and indices, indices are set to the value of 0, and the number of parts in the composite load is 1. It means that only part A active in the load. According to these settings, the equation should take the following form:

$$P = 1 * P_0(1 + 0 * dF) * \left(1 \left(\frac{V}{V_0}\right)^{0}\right) \quad (16)$$

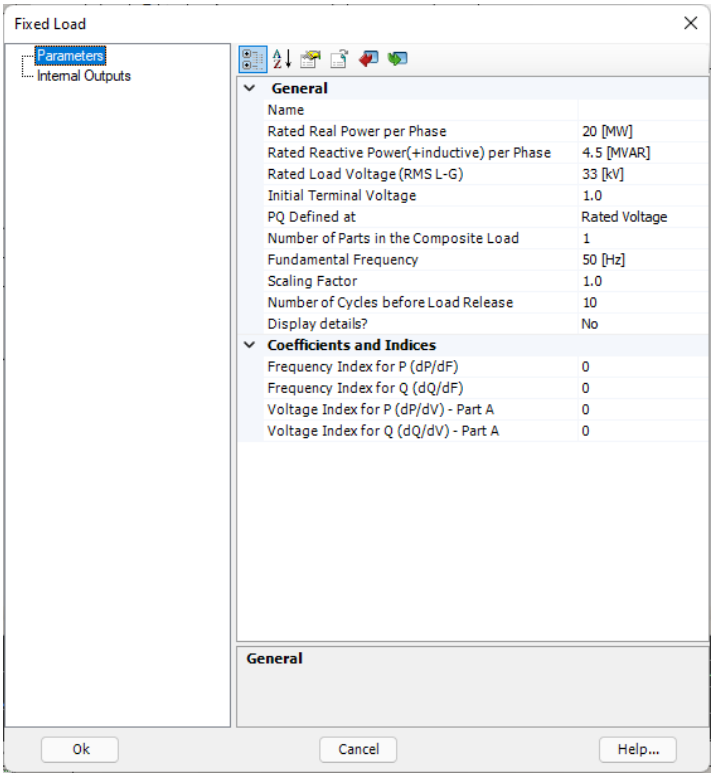

Figure 61. Load parameters on the load connected to Bus 3.

However, after the simulations, I started to notice that the load in the microgrid was lower than expected. The fixed load component took into account hidden default parameters, which should not be used when the number of parts in the composite load is set to 1. These parameters appear when the number of parts is set to 3. The settings are shown in **Figure 62**. It appeared to be taking into account the voltage index for part C. In the component settings, it is possible to disable or enable (0 or 1) the contribution of each part. However, concerning part C, this setting seems to be missing, and from the results, it can be deduced that it is active and contributes to the model characteristics.

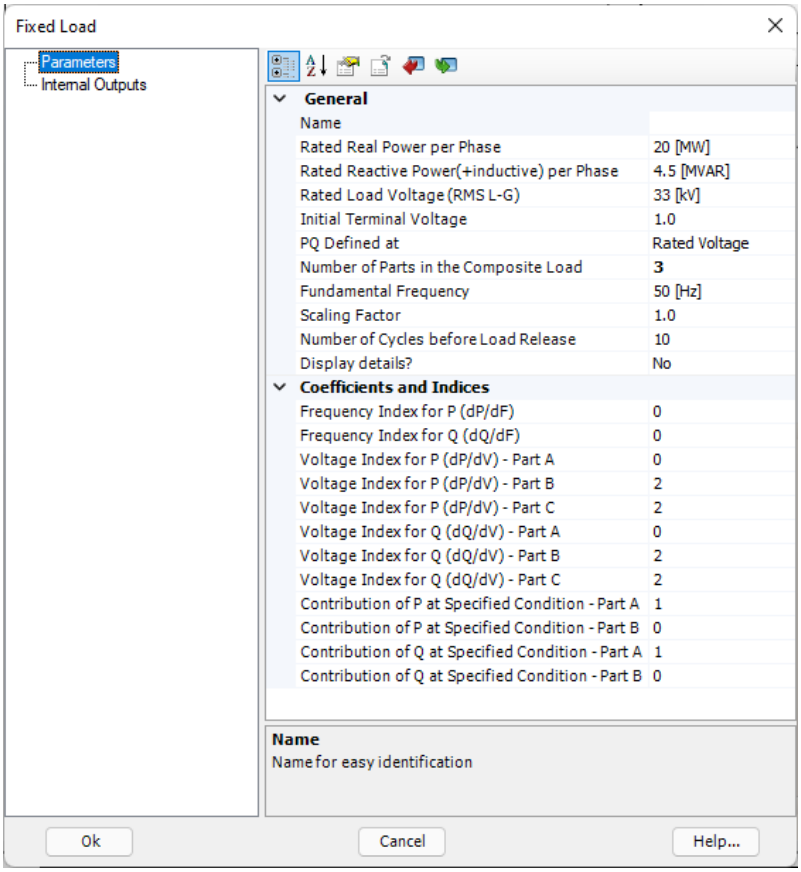

Figure 62. Load parameters on the load connected to Bus 3 with three parts in composite load.

If these parameters are inserted into the equation (15), it can be seen how it affects the voltage-dependency:

$$P = 1 * P_0(1 + 0 * dF) * \left(1\left(\frac{V}{V_0}\right)^0 + 0\left(\frac{V}{V_0}\right)^2 + 1\left(\frac{V}{V_0}\right)^2\right) \quad (17)$$

Under-voltage situation in the microgrid will decrease the amount of connected load and this ways affect the frequency value to which the system will stabilize. This affects the results especially in the cases with severe unbalance between the generation and demand. This will be especially noticeable in the cases without photovoltaic energy in Case 3.

7 Conclusions

This chapter concludes the findings of the thesis and discusses possible future studies. When inertia in the power system is decreased, the expectation is that frequency variations in load imbalance situations are more significant than in a traditional power system with a high share of synchronous generation. However, from these studies, it can be seen that this challenge can be addressed by using the inverters operated in grid forming mode. They provide significant frequency support for the power system because of their fast-acting dynamics. In regard to the control of engine power plants in the microgrid, droop control was chosen to be the best option because of its capability to constantly offer the best frequency response. The largest improvement on frequency response is gained from the addition of BESS.

However, it also becomes evident that when an increasing number of inverter-based generations is implemented in the power systems, it is essential to focus on having a sufficient amount of spinning reserve for the primary control to utilize in under-frequency situations. This study also showed that in the microgrid, or any other power system, with a high share of inverter-based generation, it is necessary to have the matching capacity of traditional generation unit or battery storage as a backup in case photovoltaic and wind energy are not available.

One of this study's main goals was to create a modular tool for Wärtsilä to study the microgrid’s frequency behavior and to test the usability of the IEEE 14 bus system for this kind of usage. As a template, the IEEE 14 bus system works well for studying microgrids. Its simple structure provides a functional base that can be used to model various configurations.

The choice of the tool used was to use the PSCAD. However, this choice turned out to be unsuccessful during this thesis work. For this kind of study involving large power system models with the inverter-based generation, PSCAD's electromagnetic transient (EMT) calculation is too slow, making it nearly unusable. For this model to be utilized in business

use for potential future projects, it must be migrated to some other simulation software. One good option is the DIgSILENT Power Factory tool (DIgSILENT, n.d.), which can be used for RMS calculation and significantly reduce simulation times. OPAL-RT has also introduced a functionality to convert PSCAD models into a HYPERSIM models (OPAL-RT, n.d.), which promises one thousand times faster simulation times on a same model.

This study can be extended in the future in many ways. As said before in this thesis the frequency stability is only one of three main stability concerns in the microgrid with the high share of inverter-based generation and they are as important as the frequency stability. More concerning the frequency stability, one of the ways could be adding different case studies with an even higher share of inverter-based generation to study the effects of low inertia more widely. The addition of a larger scale of different control methods and topologies would also give a better understanding of the possibilities in microgrid frequency control since this thesis is only capable of covering a few of them. More detailed modelling of the loads with voltage- and frequency dependent static loads, and dynamic loads would also give more accurate results concerning the frequency behavior. Also, a sufficient load shedding plan could be implemented into the microgrid for the severe under-frequency situations.

Another way to extend this study in the future is to study the microgrid frequency behavior in modular network where multiple microgrids are interconnected. Also, the validity of the results from this MV microgrid frequency study could be studied further concerning their applicability on more sensitive LV microgrids and also for larger transmission networks.

References

Abu-Rub, H., Malinowski, M., & Al-Haddad, K. (2014). *Power electronics for renewable energy systems, transportation and industrial applications*. IEEE Press and John Wiley & Sons Ltd.

Bevrani, H., Francois, B., & Ise, T. (2017). *Microgrid dynamics and control*. John Wiley &Sons Inc.

Bouzid, A. M., Guerrero, J. M., Cheriti, A., Bouhamida, M., Sicard, P., & Benghanem, M. (2015). A survey on control of electric power distributed generation systems for microgrid applications. *Renewable and Sustainable Energy Reviews*, *44*, 751–766. https://doi.org/10.1016/J.RSER.2015.01.016

DIgSILENT. (n.d.). *Stability Analysis Functions (RMS)*. Retrieved March 18, 2022, from https://www.digsilent.de/en/stability-analysis.html

Dudurych, I. M. (2021). The impact of renewables on operational security: Operating power systems that have extremely high penetrations of nonsynchronous renewable sources. *IEEE Power and Energy Magazine*, *19*(2), 37–45. https://doi.org/10.1109/MPE.2020.3043614

Dutta, S., Li, Y., Venkataraman, A., Costa, L. M., Jiang, T., Plana, R., Tordjman, P., Choo, F. H., Foo, C. F., & Puttgen, H. B. (2017). Load and renewable energy forecasting for a microgrid using persistence technique. *Energy Procedia*, *143*, 617–622. https://doi.org/10.1016/j.egypro.2017.12.736

entso-e. (2016). *Frequency Stability Evaluation Criteria for the Synchronous Zone of Continental Europe-Requirements and impacting factors-RG-CE System Protection & Dynamics Sub Group*.

Entso-E. (2016). Establishing a network code on requirements for grid connection of generators. *Official Journal of the European Union*, 112/1-112/68.

Entso-E. (2020). *Inertia and Rate of Change of Frequency (RoCoF)*.

European Union. (2017). COMMISSION REGULATION (EU) 2017/1485 of August 2017 establishing a guideline on electricity transmission system operation. *Official Journal of the European Union*.

Fernández-Guillamón, A., Gómez-Lázaro, E., Muljadi, E., & Molina-Garcia, Á. (2020). A Review of Virtual Inertia Techniques for Renewable Energy-Based Generators. In *Renewable Energy - Technologies and Applications*. https://doi.org/http://dx.doi.org/10.5772/intechopen.92651

FINGRID. (2018). *Voimalaitosten järjestelmätekniset vaatimukset - Fingrid*. VJV2018. https://www.fingrid.fi/kantaverkko/liitynta-kantaverkkoon/tekniset-vaatimukset/voimalaitosten-jarjestelmatekniset-vaatimukset/#vjv2018-dokumenttia-tasmentavat-lisaohjeet-ja-dokumentit

Gao, D. W. (2015). *Energy Storage for Sustainable Microgrid*. Academic Press, Elsevier Ltd.

Hatziargyriou, N. (2014). *Microgrids: Architectures and Control*. John Wiley & Sons, Incorporated. http://ebookcentral.proquest.com/lib/tritonia-ebooks/detail.action?docID=1578390

IEEE. (2017). IEEE standard for the specification of microgrid controllers. In *IEEE Std 2030.7-2017*. The Institute of Electrical and Electronics Engineers, Inc. https://doi.org/10.1109/IEEESTD.2018.8340204

Jenkins, P., Sonar, A. C., Jenkins, P., & Sonar, A. C. (2020). Feasibility Analysis of an Islanded Microgrid in Tohatchi, New Mexico Using HOMER Pro. *Energy and Power Engineering*, *12*(6), 357–374. https://doi.org/10.4236/EPE.2020.126022

Kontis, E. O., Skondrianos, I. S., Papadopoulos, T. A., Chrysochos, A. I., & Papagiannis, G. K. (2017). Generic dynamic load models using artificial neural networks. *2017 52nd International Universities Power Engineering Conference, UPEC 2017*, *2017-January*, 1–6. https://doi.org/10.1109/UPEC.2017.8231937

Kundur, P. (1994). *Power system stability and control* (N. J. Balu & M. G. Lauby, Eds.). McGraw-Hill,Inc.

Machowski, J., Bialek, J. W., & Bumby, J. R. (2008). *Power system dynamics: Stability and control* (Second edition). John Wiley & Sons Ltd. www.EngineeringEbooksPdf.com

Mohammadi, F. D., Vanashi, H. K., & Feliachi, A. (2018). State-Space Modeling, Analysis, and Distributed Secondary Frequency Control of Isolated Microgrids. *IEEE*

Transactions on Energy Conversion, *33*(1), 155–165. https://doi.org/10.1109/TEC.2017.2757012

Nazaripouya, H., Chung, Y.-W., & Akhil, A. (2019). Energy storage in microgrids: Challenges, applications and research need. *International Journal of Energy and Smart Grid*, *3*(2), 60–70. https://doi.org/10.23884/IJESG.2018.3.2.02

Nemsi, S., Belfedhal, S., & Barazane, L. (2016). Role of flywheel energy storage system in microgrid. *Journal of Engineering Research and Technology*, *3*(3), 44–50. https://www.researchgate.net/publication/312230643

OPAL-RT. (n.d.). *Power system simulation | Power system Analysis | HYPERSIM*. Retrieved April 28, 2022, from https://www.opal-rt.com/systems-hypersim/

Pattabiraman, D., Tan, J., Gevorgian, V., Hoke, A., Antonio, C., & Arakawa, D. (2018). Impact of frequency-watt control on the dynamics of a high DER penetration power system. *IEEE Power and Energy Society General Meeting*, *2018-August*. https://doi.org/10.1109/PESGM.2018.8586562

PSCAD. (n.d.-a). *Overview | PSCAD*. Retrieved November 1, 2021, from https://www.pscad.com/software/pscad/overview

PSCAD. (n.d.-b). *PSCAD V5 Application Help*. Retrieved April 28, 2022, from https://www.pscad.com/webhelp-v5-ol/ol-help.htm

PSCAD. (2018a). *IEEE 14 Bus System*.

PSCAD. (2018b). *Type 4 wind turbine generators*. https://www.pscad.com/knowledge-base/article/227

PSCAD. (2021). *Simple Solar Farm | PSCAD*. https://www.pscad.com/knowledge-base/article/521

Rahmann, C., & Castillo, A. (2014). Fast frequency response capability of photovoltaic power plants: The necessity of new grid requirements and definitions. *Energies*, *7*(10), 6306–6322. https://doi.org/10.3390/en7106306

Ravikumar, K. G., Bosley, B., Clark, T., & Garcia, J. (2017). Isochronous load sharing principles for an islanded system with steam and gas turbine generators. *2017 Petroleum and Chemical Industry Technical Conference, PCIC 2017*, *2017-December*, 405–412. https://doi.org/10.1109/PCICON.2017.8188761

Reliability Panel AEMC. (2020). *Frequency Operating Standard | AEMC*. https://www.aemc.gov.au/australias-energy-market/market-legislation/electricity-guidelines-and-standards/frequency-0

Rocabert, J., Luna, A., Blaabjerg, F., & Rodríguez, P. (2012). Control of power converters in AC microgrids. *IEEE Transactions on Power Electronics*, *27*(11), 4734–4749. https://doi.org/10.1109/TPEL.2012.2199334

Sharma, B., Anwar, T., Chakraborty, K., & Sirohia, H. (2018). Introduction to load forecasting. *Article in International Journal of Pure and Applied Mathematics*, *119*(15), 1527–1538.

UCTE. (2014). A1-Appendix 1: Load-Frequency Control and Performance [E]. *UCTE Operational Handbook*.

Unruh, P., Nuschke, M., Strauß, P., & Welck, F. (2020). Overview on Grid-Forming Inverter Control Methods. *Energies 2020, Vol. 13, Page 2589*, *13*(10), 2589. https://doi.org/10.3390/EN13102589

Wood, E. (2020). *What is a Microgrid?* https://microgridknowledge.com/microgrid-defined/

Zahraoui, Y., Alhamrouni, I., Mekhilef, S., Reyasudin Basir Khan, M., Seyedmahmoudian, M., Stojcevski, A., & Horan, B. (2021). Energy management system in microgrids: A comprehensive review. *Sustainability (Switzerland)*, *13*(19). https://doi.org/10.3390/su131910492

Appendices

Appendix 1. Case 1 results

Case	Event	Control	Condition	Freq peak/nadir (Hz)	Max freq deviation (Hz)	Freq peak/nadir reached (s)
Case1	**Gen**	**Droop**	**Ideal**	48,95	-1,05	120,75
Case1	**Gen**	**Droop**	**No BESS**	48,31	-1,69	121,38
Case1	**Gen**	**Isochro.**	**Ideal**	48,90	-1,10	120,76
Case1	**Gen**	**Isochro.**	**No BESS**	47,85	-2,15	121,69
Case1	**Load**	**Droop**	**Ideal**	50,97	0,97	121,04
Case1	**Load**	**Droop**	**No BESS**	51,47	1,47	121,38
Case1	**Load**	**Isochro.**	**Ideal**	51,03	1,03	121,05
Case1	**Load**	**Isochro.**	**No BESS**	51,70	1,70	121,71
Case1	**Net**	**Droop**	**Ideal**	50,01	0,01	121,41
Case1	**Net**	**Droop**	**No BESS**	50,01	0,01	121,42

Appendix 2. Case 2 results

Case	Event	Control	Condition	Freq peak/nadir (Hz)	Max freq deviation (Hz)	Freq peak/nadir reached (s)
Case2	**Gen**	**Droop**	**Ideal**	48,74	-1,26	120,70
Case2	**Gen**	**Droop**	**No BESS**	47,31	-2,69	121,39
Case2	**Gen**	**Droop**	**No PV**	47,89	-2,11	121,01
Case2	**Gen**	**Droop**	**No WT**	48,84	-1,16	120,72
Case2	**Load**	**Droop**	**Ideal**	51,38	1,38	121,05
Case2	**Load**	**Droop**	**No BESS**	52,06	2,06	121,30
Case2	**Load**	**Droop**	**No PV**	51,46	1,46	121,04
Case2	**Load**	**Droop**	**No WT**	51,14	1,14	120,75
Case2	**Load**	**Isochro.**	**Ideal**	51,39	1,39	121,03
Case2	**Inv**	**Droop**	**Ideal**	48,96	-1,04	120,75
Case2	**Inv**	**Droop**	**No BESS**	48,26	-1,74	121,33
Case2	**Inv**	**Droop**	**No PV**	48,66	-1,34	120,76
Case2	**Inv (PV)**	**Droop**	**No WT**	48,80	-1,20	120,73
Case2	**Net**	**Droop**	**Ideal**	49,75	-0,25	121,52
Case2	**Net**	**Droop**	**No BESS**	49,76	-0,24	121,60
Case2	**Net**	**Droop**	**No PV**	49,82	-0,18	121,91
Case2	**Net**	**Droop**	**No WT**	49,95	-0,05	120,94

Appendix 3. Case 3 results

Case	Event	Control	Condition	Freq peak/nadir (Hz)	Max freq deviation (Hz)	Freq peak/nadir reached (s)
Case3	**Gen**	**Droop**	**Ideal**	49,01	-0,99	120,87
Case3	**Gen**	**Droop**	**No BESS**	46,97	-3,03	121,53
Case3	**Gen**	**Droop**	**No PV**	UNSTABLE		
Case3	**Gen**	**Droop**	**No WT**	48,97	-1,03	120,42
Case3	**Load**	**Droop**	**Ideal**	51,34	1,34	120,69
Case3	**Load**	**Droop**	**No BESS**	52,42	2,42	121,14
Case3	**Load**	**Droop**	**No PV**	48,66	-1,34	120,47
Case3	**Load**	**Droop**	**No WT**	50,94	0,94	120,45
Case3	**Load**	**Isochro.**	**Ideal**	51,36	1,36	120,72
Case3	**Inv**	**Droop**	**Ideal**	49,25	-0,75	120,99
Case3	**Inv**	**Droop**	**No BESS**	49,13	-0,87	121,60
Case3	**Inv**	**Droop**	**No PV**	UNSTABLE		
Case3	**Inv (PV)**	**Droop**	**No WT**	48,84	-1,16	120,44
Case3	**Net**	**Droop**	**Ideal**	50,39	0,39	121,01
Case3	**Net**	**Droop**	**No BESS**	50,48	0,48	121,43
Case3	**Net**	**Droop**	**No PV**	47,51	0,09	120,02
Case3	**Net**	**Droop**	**No WT**	50,13	0,13	121,04

Appendix 4. Fixed load component characteristics

PSCAD fixed load characteristics according to PSCAD Application Help (PSCAD, n.d.-b).

$$P = Scale * P_0(1 + K_{PF} * dF) * \left(K_A \left(\frac{V}{V_0}\right)^{NPA} + K_B \left(\frac{V}{V_0}\right)^{NPB} + K_C \left(\frac{V}{V_0}\right)^{NPC}\right) \quad (15)$$

Where:

P =Equivalent load real power

$Scale$ =Load scaling factor

P_0=Real power at specified condition (Rated or Initial terminal)

V=Load voltage

V_0=Voltage at specified condition (Rated or Initial terminal)

K_{PF} =dP/dF Frequency index for real power

K_A =Portion of the load specified by the first term

NPA=dP/dV voltage index for real power in the first term

K_B =Portion of the load specified by the second term

NPB =dP/dV voltage index for real power in the second term

K_C =Portion of the load specified by the third term

NPC =dP/dV voltage index for real power in the third term